12-16-2014 12:00 AM

Star Cluster Populations in Compact Groups of Galaxies

Konstantin Fedotov, *The University of Western Ontario*

Supervisor: Dr. S. C. Gallagher, *The University of Western Ontario*

A thesis submitted in partial fulfillment of the requirements for the Doctor of Philosophy degree in Astronomy

STAR CLUSTER POPULATIONS IN COMPACT GROUPS OF GALAXIES

(Thesis format: Integrated Article)

by

Konstantin Fedotov

Graduate Program in Department of Physics and Astronomy

A thesis submitted in partial fulfillment
of the requirements for the degree of
Doctor of Philosophy

The School of Graduate and Postdoctoral Studies
The University of Western Ontario
London, Ontario, Canada

Abstract

In this thesis, I have explored the star cluster populations of several compact groups of galaxies, based on observations with the Advanced Camera for Surveys and the Wide Field Camera 3 on the *Hubble Space Telescope*. Low velocity dispersions and high galaxy number densities, the conditions of compact groups (in particular Hickson Compact Groups), represent an environment with frequent and prolonged interactions. Such environment can trigger the formation of star cluster populations associated with specific events. The *BVI* study has shown that star clusters can be used as a powerful tool for studying such events triggered by mergers and tidal interactions between galaxies. The study compares the basic properties between cluster populations in compact groups at distinct evolutionary stages. The information on star clusters in compact groups of galaxies that has been presented in a number of papers is consolidated and presented it in a single catalogue, with the goal of further assisting researchers in star cluster-related studies.

For my next study I concentrate on one of the compact groups, HCG 92, also known as Stephan's Quintet. To the initial *BVI* observations I add observations in U_{336} and V_{547} filters, with the Wide Field Camera 3 on the *Hubble Space Telescope*. The addition of these filters, specifically U_{336}, breaks the age-extinction degeneracy of the *BVI* photometry and allows to shift from a qualitative description of cluster ages to a more quantitative analysis, along with determinations of intrinsic reddening and masses.

Keywords: galaxies: groups: general – galaxies: groups: individual: HCG 07, HCG 31, HCG 42, HCG 59, HCG 92; – galaxies: evolution – galaxies: interactions – star clusters: general

Co-Authorship Statement

"A Comprehensive HST BVI Catalogue Of Star Clusters In Five Hickson Compact Groups Of Galaxies"

Dr. Sarah C. Gallagher outlined the general case for the paper, supplied the original code and provided useful advice during the work on the paper. Dr. Patrick R. Durrell provided some results on the globular clusters. In particular, he determined the values for specific frequencies as well as the expected total number of globular clusters for some galaxies the sample. Dr. Nate Bastian helped to interpreted the results for luminosity functions. Drs. Iraklis S. Konstantopoulos, Jane Charlton, Kelsey E. Johnson, and Rupali Chandar provided useful feedback. I modified the supplied code and streamlined the selection procedure. I prepared the final catalogue for the five HCGs and carried out the analysis. I also was responsible for the writing of the paper and preparation of all of the figures.

"UBVI Study of Star Cluster Populations In Tidal Features Of Stephan's Quintet"

The study is based, in part, on the data obtained through *HST* observation, PI of which was Dr. Sarah C. Gallagher (*HST* Proposal 12301), and as such, provided the initial idea for the project as well as helpful advice and discussions. The images were calibrated and reprocessed by Dr. Tyler D. Desjardins. The clusters masses and ages for this study were provided by Dr. Rupali Chandar, based on *UBVI* catalogue of point sources in SQ prepared by author. Dr. Nate Bastian provided an insight into the analysis of the mass and age functions. Drs. Iraklis S. Konstantopoulos, Phil Appleton, Jane Charlton provided useful feedback. For this paper I updated the selection algorithm. As with previous work, I prepared the final catalogue of sources in HCG 92, carried out the analysis, wrote the paper and made all of the figures.

Contents

List of Figures

List of Tables

List of Appendices

Chapter 1

Introduction

In the introduction to this thesis, I am going to briefly discuss the current state of knowledge on the topics of star clusters, compact galaxy groups, and galaxy interactions. The goal of this introduction is to show how these seemingly unconnected topics come together to reveal the interaction history of compact galaxy groups through the study of their star cluster populations.

Star Clusters **(SCs)** – gravitationally bound groups of thousands to millions of stars born at the same time in a giant molecular cloud – possess a number of properties that make them useful tracers of star formation history as discussed in more detail in § 1.1. With the resolving power and light gathering capacity of ground-based and space telescopes, it is possible to differentiate individual star clusters from the overall stellar populations of distant galaxies. More particularly relevant to this project is our ability to determine the approximate age of a star cluster. Thus, if a group of star clusters formed due to some dynamical event in the history of the host galaxy, I can estimate the approximate date of that event based on the derived ages of those SCs.

Galaxy interactions are also relevant to the theme of this thesis. Observations and theoretical studies support the idea that interactions between galaxies are an important process in galactic formation and evolution. Moreover, there is strong evidence that present day elliptical galaxies were formed through multiple interactions and mergers (e.g., Becker et al., 1991). In the context of the current study, the most interesting feature of galaxy interactions is their likelihood of triggering a significant increase in the star formation rate of the galaxies involved. An increasing star formation rate translates into a corresponding increase in the star cluster population in those galaxies. Hence, an in-depth study of star cluster populations in galaxies could potentially provide us with that galaxy's history of star formation and interactions. By studying the star cluster populations of different types of galaxies, in different stages of interaction, and in various environments, astronomers can build a statistically significant archive of star cluster data. This archive can then be used to investigate the influence of the environment on the evolution of galaxies.

The specific environment for my research into the star cluster populations of galaxies is compact galaxy groups, in particular Hickson compact groups **(HCGs)**. Due to their rather unusual properties, in particular the small projected galaxy separations and relatively low velocity dispersions (for further discussion see § 1.3), galaxies in these groups may be subjected to multiple, prolonged interactions. Because of that, compact groups are prime subjects for studies of star cluster populations formed in galaxies as a result of those (often complex and

recurring) interactions.

1.1 Star Clusters

1.1.1 Star Cluster Flavours

In "Star Formation In Clusters" by Larsen (2004), the author notes that there are a number of problems related to star clusters that make them "interesting in their own right". These include topics such as cluster formation, evolution and their ultimate fate. Additionally, because most stars were formed in the cluster environment (e.g., Fall, 2004; Lada & Lada, 2003), our understanding of star formation in general is intimately linked with star cluster formation. An advantage to studying star clusters as a proxy for star formation is that clusters are much brighter than individual stars and can be identified and studied at much greater distances. SCs also tend to consist of stars that were formed more or less at the same time and out of the same material. Because of this, star clusters can be well approximated by a simple stellar population, and can be very useful as evolutionary tracers of their host galaxies.

A SC is defined as a group of stars consisting of anywhere between a few hundreds and a few million members that are gravitationally stable against the random motions of the stars and the tidal field of the host galaxy. Based on the observations of the SC population in the Milky Way, SCs are divided into two types, *globular* and *open* clusters (Figure 1.1).

Globular Clusters (**GCs**) were first observed and catalogued by Charles Messier in 1774, who did not realize the nature of these objects. With advances in telescope construction, it became possible to resolve individual stars in the closest clusters. Sir William Herschel performed a systematic study of clusters known at that time and he first introduced the term *globular cluster* to describe the largest and most concentrated clusters (Herschel 1789). Based on modern data, globular clusters, on average, are shown to have masses of $\sim 10^6$ $M_\odot$ with no detectable dust and gas. Most of the GCs observed in our Galaxy are very old (e.g., Marín-Franch et al., 2009, $\gtrsim 10^{10}$ year;), and show a bimodal metallicity distribution with values of [Fe/H] ≈ -1.5 dex and -0.5 dex (Zinn 1985), containing mainly Population II stars. GCs are also found to be distributed spherically around the centre of the Galaxy (Figure 1.2).

The term Open Cluster first appeared in Shapley (1916) as a description of nonglobular clusters. Based on observations, open clusters appear to be less massive than GCs (usually $\sim 10^4$ $M_\odot$), although with higher metallicity, consistent with their Population I status (Friel et al. 2002). Most of the Galactic open clusters are young (e.g., Wielen, 1971, a few 10^8 years;) and distributed in the disc of the Galaxy, preferentially in the spiral arms (Figure 1.2).

A good visual example of the differences between open and globular clusters is presented in Figure 1.1. On the right hand side, we see globular cluster M4 (NGC 6121) which is centrally concentrated and consists of mostly evolved stars. It is these evolved stars that give M4 a yellow colour. On the left is M25 (IC 4725), a young open cluster in the Sagittarius constellation. Most stars in that cluster are blue, which reflects their young age. M25 also does not have as strong a central concentration as M4. Overall, the integrated colour of a star cluster is dominated by the most massive, the most luminous stars that are present at a given age.

Figure 1.2 represents the spatial distribution of globular and open clusters in the Milky Way projected onto the Galactic plane. In this figure, we can see that the distribution of GCs is more

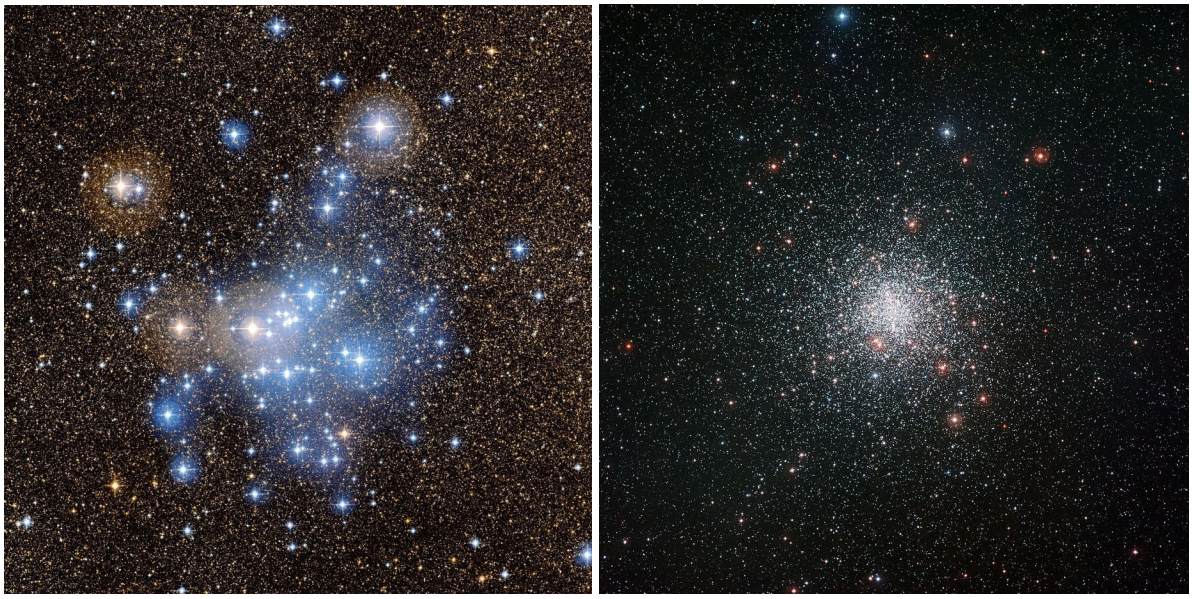

Figure 1.1: On the left hand side is the open cluster M25 (IC 4725) with an estimated age of ∼ 90 Myr and at a distance of ∼ 600 pc (Tadross et al. 2003). On the right side is the globular cluster M4 (NGC 6121), a ∼ 12.2 Gyr old cluster (Caputo et al. 1985) which is located ∼ 1.7 kpc away from the Sun (Peterson et al. 1995). Image credits: Jean-Charles Cuillandre (CFHT) & Giovanni Anselmi (Coelum).

or less spherical with respect to the center of the Galaxy. However, virtually all detected open clusters are located within a sphere of a radius of less than 2 kpc, with the Sun in the center. There are several reasons for this observational fact which arises largely from selection effects. First, SCs form from giant molecular clouds **(GMCs)** (see Section 1.1.2), and for the first ∼ 10 Myr they are embedded in that progenitor cloud, which makes them challenging to detect, particularly with optical surveys (Lada & Lada, 2003). Second, GMCs are mostly located in the Galactic plane, which has higher extinction values. This makes the detection of clusters in the optical regime even more difficult. Third, open clusters have a lower surface brightness compared to GCs.

Combined with stellar crowding in the Galactic disc, it is not surprising to find that open clusters are detected only in the nearby field. However, recent advances in infrared astronomy such as the Galactic Legacy Infrared Mid-Plane Survey Extraordinaire (GLIMPSE) by *Spitzer* and NASA's *Wide-field Infrared Survey Explorer* (WISE) mission promise new and exciting discoveries of clusters that are otherwise obscured in the visible region of the spectrum by gas and dust.

One should note, however, that the classification of clusters as *globular* and *open* is rather artificial and has historical roots. In reality, the boundaries between these two types of clusters are fuzzy as they represent different extremes of a continuum spanned by the Initial Cluster Mass Function (**ICMF**; Section 1.1.2). If we assume a continuous star formation history in the Milky Way, then we expect the mass-age plane to be populated with clusters of all masses (within a range that is appropriate for SCs) and all ages. However, due to the disruptive processes discussed in Section 1.1.3 only the most massive clusters will survive for a significant

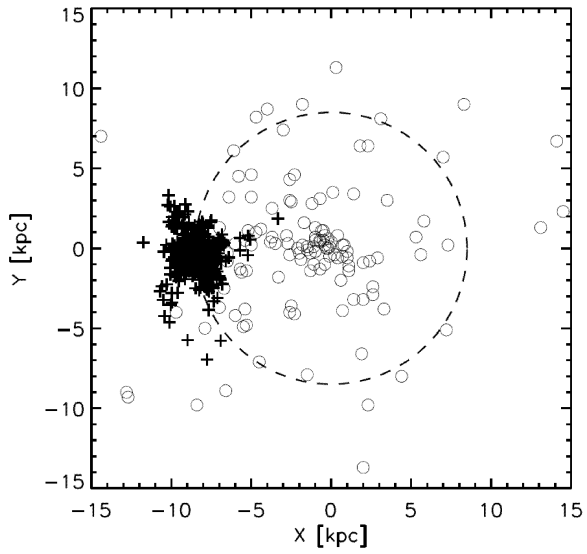

Figure 1.2: The spatial distribution of catalogued open clusters (plus markers) and globular clusters (open circles) in the Milky Way. The data for this plot were obtained from Kharchenko et al. (2005) and Harris (1996) catalogues. The Sun is at (X,Y) = (-8.5, 0) kpc. (Kharchenko et al. 2005).

period of time. Thus, a distribution of clusters we expect to detect in our Milky Way starts with a large number of young clusters with masses in a given range (usually 10^4 $M_\odot$– 10^6 $M_\odot$), with cluster numbers getting smaller as the ages and masses of the clusters that survive are increasing. The upper end of such a distribution will be populated with old, massive clusters.

However, we do not observe this distribution. The missing links here are the intermediate-age and massive young clusters, which have not yet been detected in the Milky Way (with perhaps the single exception of the Westerlund 1 cluster: mass $\sim$ few $\times 10^5$ $M_\odot$, age 3 to 5 Myr; Brandner et al. 2008). On the other hand, such massive, young clusters have been found in abundance in other galaxies, primarily outside of the local group, and particularly in interacting galaxies (Bastian et al., 2006, 2009; Fedotov et al., 2011; Gallagher et al., 2001; Whitmore et al., 2010, e.g., The Antenae galaxies, The Mice galaxies, Stephan's Quintet;). Therefore, until we detect a statistically significant number of such clusters in our Milky Way, we must study extragalactic equivalents to learn more about these populations.

1.1.2 Star Cluster Formation

SC formation is closely related to star formation, and although there are still a number of unresolved issues, the overall process of cluster formation is generally understood.

As previously stated, SCs are formed within giant molecular clouds. Initially, GMCs must cool to appropriate temperatures (few tens of Kelvin) after which the process of collapsing and fragmentation occurs. The presence of shocks, turbulence and magnetic fields can influence SC formation rate, both positively and negatively, depending on the environment (e.g., Ostriker, 2006; Price & Bate, 2008). There are two major paths for the formation of star clusters that depend on the star formation efficiency. In general, the star formation process is rather in-

efficient with only a few percent of the available mass directly transformed into stars (Williams & McKee, 1997). With this kind of star formation efficiency, the formation of a single massive cluster is somewhat problematic, as it requires massive GMCs (larger by at least an order of magnitude than the resulting cluster) within a volume of only a few pc in diameter. Hierarchical formation, wherein many smaller groups of stars merge together to form a cluster, was proposed as an alternative (e.g., Beasley et al., 2002; Elmegreen et al., 2000). Alternatively, if the star formation rate efficiency is greater than 30%, then enough stars could be formed in the given volume to gravitationally bind together into a young star cluster.

The distribution of cluster masses at formation is characterized by the initial cluster mass function, which is defined as the number of objects per cluster mass interval and can be represented by a power law:

$$\mathrm{d}N(M)/\mathrm{d}M \propto M^{\beta}, \tag{1.1}$$

where $\beta \approx -2$. The value of β has been found empirically based on numerous studies of the ICMF in different galaxies, such as the Large Magellanic Cloud (Hunter et al. 2003; de Grijs & Anders 2006; Chandar et al. 2010a), M51 (Bik et al. 2003; Chandar et al. 2011), and the Antennae (Zhang & Fall 1999; Fall et al. 2009). The range of initial masses described by this function usually spans from 10^3 $M_\odot$ to $\sim 10^7$ $M_\odot$.

There are some issues, however, with determining the precise shape of the initial cluster mass function. The general understanding of the ICMF is that it describes the mass function at the moment of a cluster's "birth". Of course, the moment of birth is rather poorly defined and some very young clusters are difficult to detect because of high extinction caused by their natal gas and dust. Moreover, by the time clusters have expelled all remaining gas and dust, some of them might already be destroyed (Section 1.1.3). Additionally, very massive star clusters are relatively rare and the behaviour of the ICMF at the high-mass end is not well defined due to small-number statistics. In fact, some studies have shown a steep decline of the ICMF for masses over 10^6 $M_\odot$(e.g., Williams & McKee, 1997).

One of the predictions made based on the shape of the ICMF is the existence (or ongoing formation) of massive young star clusters in our Galaxy. In particular, according to the ICMF, there should be at least one massive cluster (10^4 $M_\odot \lesssim M \lesssim 10^5$ $M_\odot$) within a 4-kpc circle around the Sun. The recent detection of the Westerlund 1 cluster at the distance of $\sim$ 3.6 kpc, with a mass of $\sim$ few $\times$ 10^5 $M_\odot$ and an age of 3 to 5 Myr (Brandner et al. 2008) fits nicely with that prediction. However, the ICMF also predicts the existence of intermediate-age-to-young clusters in our Galaxy with masses over 10^6 $M_\odot$. Since we don't see any such clusters (due to their sizes, they are unlikely to be destroyed and should be relatively easy to detect), this fact seems to confirm that the high-mass end of the cluster mass function indeed declines more steeply than a power law with exponent -2 (Portegies Zwart et al. 2010).

Nevertheless, one goal of future work is to try to improve the accuracy of the ICMF as it is key to better understanding the formation of stars and galaxies as over 85% of all stars were formed in a cluster environment (de Wit et al., 2005; Gies, 1987). For example, one might assume that the formation process for open and globular clusters was different (given their observed differences in age, distribution throughout the Galaxy, and mass range). However, studies of the mechanism for cluster formation in the Milky Way (e.g., Elmegreen & Efremov, 1997; Selman & Melnick, 2008) suggest that they have been formed in relatively the same manner. Moreover, studies of extragalactic SCs in nearby galaxies, including starburst galaxies,

do not find overwhelming evidence for large systematic variations in the ICMF (Bastian et al., 2010).

1.1.3 Star Cluster Disruptive Processes

In order for a young massive cluster to become a GC it should survive $\sim$ 10 Gyr. This is not a trivial thing to do considering the number of ways in which young clusters can be destroyed. This is reflected in the infant death rate for star clusters which is in the vicinity of 90% (Lada & Lada 2003). Here is a list of possible mechanisms that would contribute most effectively to the disruption of the young stellar clusters as stated in Ostriker et al. (1972) and Harris (1991):

- **Disruption due to the tidal field of the galaxy**

  There are a number of theoretical and numerical studies that have shown that clusters dissolve over time due to two-body relaxation in a steady tidal field of a host galaxy (e.g., Baumgardt & Makino, 2003; Spitzer, 1987). As stars in a SC are moving along their orbits, they are interacting with each other by exchanging kinetic energy and momentum. Through a number of such interactions some stars will gain enough energy to leave a cluster, or to move away from the center of the cluster far enough to be torn out of a cluster by the tidal field of the host galaxy. Conversely, some stars will lose energy and will sink to the center of a cluster. This results in a decrease in the tidal radius of a cluster, subjecting the outer parts of a cluster to increased gravitational harassment from a galaxy. As a consequence, the tidal field of the host galaxy sets a physical limit to the radii of clusters. In particular, clusters located closer to the center of a galaxy, where the galactic potential well is deeper, would tend to have smaller radii (e.g., Sastry et al., 1988). Also, less massive clusters have a smaller chance of surviving for a significant length of time (Larsen, 2010).

- **Star "evaporation"**

  Due to the internal relaxation some stars will fall to the center if the cluster. That will shrink the tidal radius, leading to evaporation of the stars that are now outside the tidal radius. This in turn leads to further contraction of the tidal radius and to star evaporation, and so on.

- **Disruption due to tidal shock**

  When star clusters pass through the galactic bulge or disk, they experience tidal forces from the material in the disk/bulge. These forces can increase the kinetic energy of the clusters, making them expand and shed some of their outer stars (e.g., Ostriker et al., 1972). The same effect can occur when clusters encounter individual objects of masses over $10^6 M_\odot$, such as GMCs.

- **Dynamical friction**

  On their orbits around the galactic center, star clusters gravitationally interact with surrounding matter in a galaxy (GMCs, SCs, stars, etc), albeit very slightly, causing them to shed some kinetic energy and sink towards the center of a galaxy, where they are

more susceptible to destruction by tidal forces. This process works primarily on massive clusters, effectively removing them from the inner part of a galaxy.

- **Unfavourable orbits**

  Some orbits could take SCs through the galaxy center where they will be destroyed through a combination of the disruptive processes described above (e.g., dynamical friction).

- **Gaseous mass loss**

  Since star formation efficiency is very small ($\sim$ 10%) the largest part of the mass of the new star cluster is in the form of gas and dust. Within the first few million years of star formation the first wave of supernovae explodes, effectively clearing all leftover material. Only clusters that have formed a large number of stars close to their geometric centres are capable of surviving a loss of $\sim$ 90% of their mass and remaining intact.

The last disruptive process, also known as infant mortality, is very important as it happens rather quickly in the early stages of cluster evolution and eliminates anywhere between 50% and 90% of all newly formed SCs. The latter estimate comes from Lada & Lada (2003), who compared the number of observed open clusters in the solar neighbourhood with that expected based on their embedded cluster sample. However, Bastian (2011) have argued that this high mortality estimate strongly depends on how one defines an embedded cluster. The authors have shown that with a more conservative definition of embedded clusters, only 50% of clusters have to be destroyed in order to satisfy the observed number of open clusters.

After the process of gaseous mass loss (during which clusters transition from an embedded to an exposed state), other disruptive processes become dominant. They occur on longer time scales and can be divided into two categories: internal (e.g., internal relaxation, stellar evolution) and external (e.g., dynamical friction, interaction with tidal field of host galaxy). It is with respect to the impact of these disruptive processes that the controversy of mass-dependent destruction exists.

Generally, there are two main disruption models that have been put forward: mass-dependent disruption **(MDD)** and mass-independent disruption **(MID)**. The former (in its present form) was suggested by Boutloukos & Lamers (2003) to explain the observed cluster population properties in a number of galaxies: the Small Magellanic Cloud, M33, M51, and the Milky Way. The model describes the lifespan of the cluster as a function of its initial mass $\tau \propto M^{\gamma}$, where $\gamma \sim 0.62$ was found empirically (Boutloukos & Lamers, 2003, ; i.e., more massive clusters live longer)(i.e., more massive clusters live longer). The other empirical model states that cluster disruption is independent of the cluster mass and the ambient environment. Initially this scenario was considered only for the first tens of Myr of the cluster lifetime, when the gaseous mass loss process is dominant. Indeed, since the loss of gaseous mass is an internal process it is expected to be largely independent of the ambient environment (Bastian, 2011). It is also expected to be independent of mass since the mass loss is driven by violent relaxation (e.g., Goodwin & Bastian, 2006). However, the concept has been expanded up to the age of several 10^8 yr, at which point two-body relaxation should begin to dominate the disruptive processes (Fall et al., 2005). The mass-independent disruption scenario predicts that 90% of clusters are disrupted every decade in age. For example, if 1000 clusters are formed at one time, then there

will be only 100 clusters left after 10 Myr, 10 after 100 Myr, and only one cluster will be left after 1 Gyr. This relation was used to explain observed cluster populations in the Antennae (Fall et al., 2005), the Large Magellanic Cloud (Chandar et al., 2010a), and M83 (Chandar et al., 2010b).

What is even more intriguing in the question of mass-dependent disruption and mass-independent disruption scenarios is that Chandar et al. (2006) and Gieles et al. (2007) used the same set of data for the Small Magellanic Cloud and came to different conclusions: the former advocating for the MID and latter for the MDD. In light of this disagreement, the results of the latest work by Bastian (2011) proves to be very interesting. The author studied the stellar cluster population of M83 in two adjacent regions (one closer to and the other farther from the center of the galaxy) using multi-wavelength WFC3/HST imaging. He have shown that the MID model prediction shows a good agreement with the cluster population observations of the inner part of M83. However, observations of the outer field of M83 show a much lower disruption rate than predicted by that model. The pure MID model could provide a reasonable fit in the outer field if one assumed that the fraction of a cluster disrupted every decade in age is ~ 0.5 (instead of 0.9 as in the MID model used by Chandar et al. 2006). The authors also noted that environment-dependent disruption is required to fit the observations. This is consistent with the Elmegreen & Hunter (2010) model of cluster disruption (the model is mass-independent but the disrupted fraction strongly depends on the environment).

In the case of the MDD model, the prediction showed a good fit to the data in the Antennae galaxies, NGC 6946 and M51 when a Schechter function was used to fit the mass distribution of clusters (Gieles et al., 2006a,b, ; this function has a power-law at the low-mass end with an exponential cutoff at high masses). Further studies by Bastian (2008) and Larsen (2009) also concluded that a Schechter function provided a good fit to the observed data, although studies by Whitmore et al. (2010) and Chandar et al. (2011) (which included M83) did not see a truncation in the mass function of clusters at the high mass end in sample galaxies (i.e., did not confirm that the cluster distribution followed a Schechter function).

Overall, Bastian (2011) concluded that both scenarios of cluster disruption can reproduce the observed results if environment-dependent disruption is taken into account in the case of MID, and if a Schechter initial mass function distribution is used in the case of MDD. Although this study could not definitively confirm the correctness of either disruptive scenario, the authors found evidence of higher mass clusters having a longer lifespan, which is more consistent with an MDD process.

1.1.4 Star Clusters as an Age-Dating Tool

As a star cluster ages, the most massive and luminous stars within that cluster die off first, leaving less massive and less luminous stars. This causes the integrated light from a star cluster to change its colour and fade over time. Figure 1.3, also known as the Hertzsprung-Russell diagram, is a good illustration of how the colour of SCs is changing with age. The most massive and brightest stars of the main sequence are located in the upper part of the plot. A few such stars outshine the rest of the stars in a cluster, dominating its integrated light. For example, O- and B-type stars in the solar neighbourhood have luminosities that are brighter than the Sun by 3–4 orders of magnitude. However, their lifespan is very short (as indicated by the green

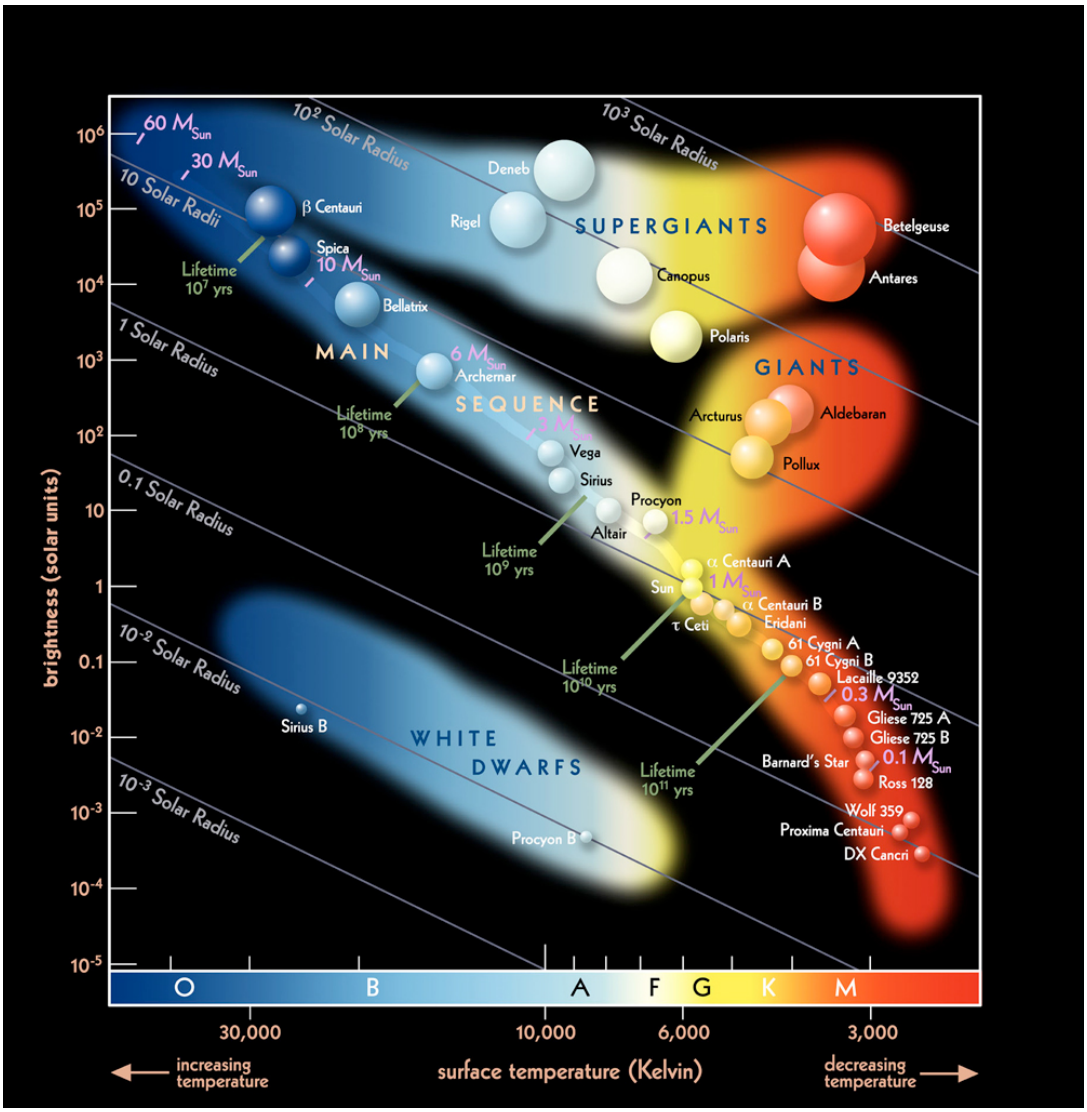

Figure 1.3: A luminosity-temperature plot of stars in the solar neighbourhood. As a cluster with a full mass-range of stars formed at the same time ages, the most massive (and thus most luminous) stars evolve faster than the rest of the stellar population within that cluster. Because the light of a cluster is dominated by the most massive stars still present at any given time, the loss of them causes the integrated light to change colour accordingly, becoming redder and fading over time. Credit: Pearson Education, Inc.

markers in Figure 1.3). When these stars reach the end of their evolution, the remaining most massive stars will dominate the integrated light of a star cluster. Each subsequent generation of such stars will be less bright and have gradually redder colours than the previous one. Thus, the colours of a SC can serve as a good age indicator. However, the age that would be determined by such a method is only an approximation. There are many uncertainties, both observational and theoretical, that are associated with this method of age estimation.

As was mentioned previously (Section 1.1.1), star clusters can be closely approximated by Simple Stellar Populations **(SSPs)**, groups of coeval stars of like chemical composition. Using some stellar initial mass function, the most popular of which are Salpeter (Salpeter, 1955), Kroupa (Kroupa, 2001) and Chabrier (Chabrier, 2003), the SSP is populated by stars with different masses. Because stellar evolution is reasonably well understood, the evolutionary sequence for each star can be determined, and, as a result, the SSP evolution can be followed rather accurately (e.g., Bruzual G. A., 2010). Integrating the light from all of the stars in the SSP (i.e., adding up the theoretical spectral energy distribution of each star contained in the SSP) at any given point in time will yield its wavelength-dependent magnitude, which is associated with that particular age. In turn, tracking the changes of the photometric properties at different wavelengths as the SSP evolves will create an evolutionary track in colour-colour space, which can be used to estimate ages of real star clusters (Figure 1.4).

One of the biggest observational uncertainties associated with age estimation is the inability to determine the precise amount of reddening for the object for which the age estimation is carried out. For example, in Figure 1.4 the reddening vector $A_{\rm V}$, which represents the direction and amount of reddening equivalent to 1 mag in the Hubble Space Telescope V_{606} filter is shown in the upper left corner. In $B-V$ vs. $V-I$ colour-colour space, the reddening vector is approximately parallel to the evolutionary track. There are studies (e.g., Calzetti & Harris, 2002; Dahm & Simon, 2005) that have found that the amount of reddening for young star clusters still embedded in their natal material could reach up to 3 mag in the Johnson V filter. Therefore, the reddening effect can make ages estimate from colours highly inaccurate. An $A_{\rm V}$ of 3 mag would shift a star cluster down and to the right along the evolutionary track, making it appear significantly older than it is.

Chemical abundance is yet another factor that can affect the colours of SCs. As has been established previously (e.g., Padmanabhan, 2002), metal-rich stars appear to be redder than stars of the same age but with lower metallicities. The suite of electronic transitions of heavy ions (in particular iron) leads to absorption preferentially of blue light emitted by a star, making it appear redder; this effect is also known as line blanketing. Thus, a metal-poor stellar population in a star cluster would make the star clusters appear bluer, mimicking the younger age of a more metal-rich cluster. Accurate age estimation thus requires that the metallicity of the star cluster be known reasonably accurately.

Additionally, the initial assumption that star clusters would form from isometallic material (the assumption used for creating SSPs) is rather naïve. Recent studies suggest that star clusters could consist of multiple stellar populations (both in age and/or chemical composition). For example, Piotto et al. (2007) have shown that the main sequence of the globular cluster NGC 2808 splits into three separate branches. This is caused by coeval stellar populations with different chemical abundances.

There are also a number of uncertainties associated with the derivation of the SSP itself. Although (as mentioned earlier), stellar evolution, in general, is well studied, there are some

phases of evolution that are not well understood. Such phases include blue stragglers **(BSs)**, the horizontal branch **(HB)**, the asymptotic giant branch **(AGB)**, and thermally pulsating AGBs **(TP-AGB)**. Some stars in these phases can dominate the red/near-IR light of the whole stellar population (for example AGB stars) and in other cases they can influence the blue and UV end of the population's light (HB stars) (Conroy et al., 2009). For example, blue stragglers are rarely included in the theoretical models of simple stellar populations, although recent studies suggest that they can influence the blue end of the model's spectral energy distribution (e.g., Li & Han, 2008).

Dust (internal to a cluster), which influences observational errors, also adds uncertainties from the theoretical side. For accurate SSP models, an understanding of the mechanism of the attenuation of starlight by dust is required. This is a difficult task however, because it in turn relies on a better understanding of a number of dust grain properties, such as geometry, composition, clumpiness and optical depth of dust clouds (Conroy et al. 2010). Many of those

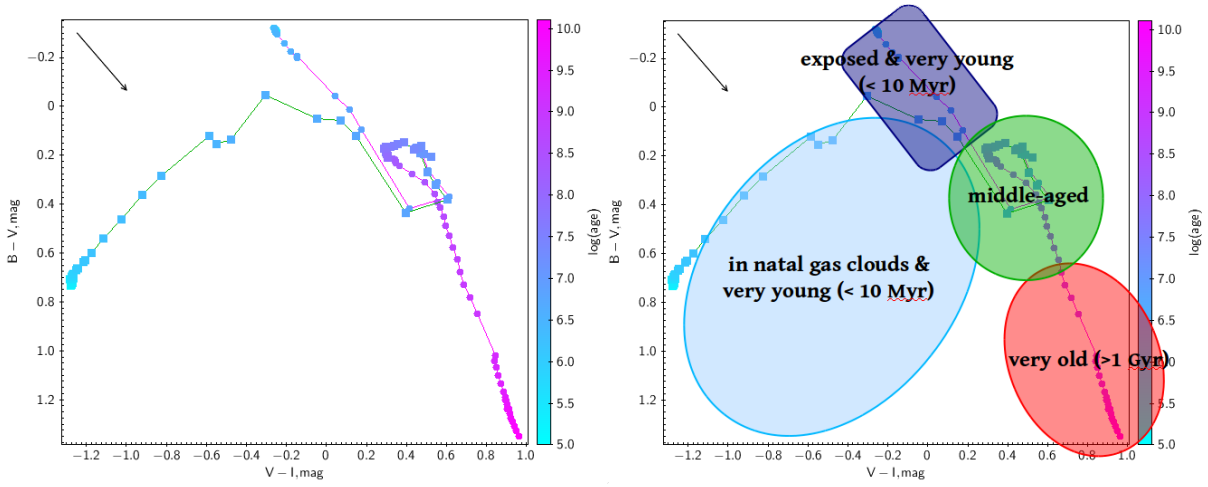

Figure 1.4: **Left:** Graphical representation of how $B_{438} - V_{606}$ and $V_{606} - I_{814}$ colours of a star cluster change with age. Each point on this plot represents colours of a cluster at some specific time, and the color of the point is corresponds to cluster age, according to the colour bar on the right hand side of the plot. The time interval between each point is 0.05 in log(age). Connecting the points as the age of a hypothetical cluster is increasing creates an evolutionary track (points connected by a red line). For a very young star cluster (¡ 10^7 yr), that is still surrounded by the natal gas cloud, the observed colors are going to be different. This is due to absorption of UV light and its re-emission at the longer wavelengths by surrounding material (e.g., Conti et al., 1996; Vacca & Conti, 1992). It is especially noticeable in the V_{606}-band, and the effect of this process on the cluster's colours are outlined by the second evolutionary track (points connected by a green line) that incorporates a model of nebular emission (Starburst99; Leitherer et al., 1999). At $\sim 10^7$ yr, star clusters usually shed their natal gas clouds and the two evolutionary tracks merge. All evolutionary tracks in this work were based on SSP models of Marigo et al. (2008). **Right:** This plot highlights the expected distribution of star clusters and the way we assign their ages. In the top left corner of each panel a reddening vector A_V is shown. It is equivalent to 1 mag in the *HST* V_{606} filter.

properties are not well studied yet.

There are also SSP uncertainties associated with the stellar IMF. The distribution of stars as a function of mass in the SSP happens according to the chosen IMF: the distribution starts with a low number of massive stars and increases in number with decreasing mass until a possible peak at around 1 $M_{\odot}$. It further declines in numbers for stars with lower masses (as in the Kroupa IMF) or simply increases until a cutoff at a certain mass (as in the Salpeter IMF). However, since star formation is a highly stochastic process (Klessen et al. 2011), there is a possibility that the stellar mass distribution is going to be heavily weighted around some specific mass. For example, the colour and luminosity of a relatively small cluster would be substantially different in case if it has one B0 star or in case if it has three B0 stars at a young age. However, in both cases these stars constitute a small fraction of the mass of the cluster. Such a cluster, of course, will not follow the average evolutionary track, and an age estimation based on its colours is not going to be accurate for a few hundred million years. At later stages of the cluster evolution, the colours of moderate mass SCs become more similar to each other, since by that time their stellar populations largely consist of low-mass stars.

As it stands now, most of the IMFs are based on data obtained from stars in the solar neighbourhood (e.g., Kroupa, 2001). Because of that, IMFs at the lower mass end ($M < 1\ M_{\odot}$) are poorly constrained, since stars with such masses are too faint to be observed directly outside of the local Galactic field. However, it might not be as important since less massive stars do not contribute substantially to the integrated colours of SCs (Conroy et al. 2010). Moreover, recent studies suggest that IMF might be dependent on the environment, meaning that each galaxy might have its own IMF (e.g., Meurer et al., 2009; Van Dokkum & Conroy, 2010).

1.2 Galaxy Interactions

The study of galaxies is a relatively new branch of astronomy, merely a hundred years old. With what we know about galaxies today, they can be described as large gravitationally bound systems of stars and gas, whose components interact continually with each other, exchanging matter and energy (Larson 1996). However, at the dawn of galactic studies, they were considered to be some sort of nebulae. With time, based on better observations and the realization of the vast distances that separate galaxies, scientists became aware of the existence of "island universes". It was thought that the shapes (consisting mainly of spiral and elliptical configurations) and evolutionary paths of galaxies were determined by the initial conditions under which those particular galaxies were formed. However, with a growing number of observations, a new class of galaxies started to emerge, which were referred to as peculiar galaxies. The name peculiar came from their unusual appearances (e.g., excess blue integrated colours, prolonged tails protruding from the main galactic bodies, bright plumes). In 1962, Arp created a catalogue of peculiar galaxies, which consisted of 338 entries (two objects from that catalogue, Arp 148 and Arp 256, are presented in Figure 1.5). Many galaxies from Arp's catalogue were studied in great detail (e.g., Ambartsumian, 1961; Arp, 1965; Burbidge et al., 1963; Sandage & Miller, 1964). Furthermore, the number of observed pairs of galaxies at different stages of interaction was also increasing, creating a statistically significant database. All of these observational facts combined with the introduction of computer simulations (e.g., Toomre & Toomre, 1972), which showed that the visual galactic distortions, plumes, and tails

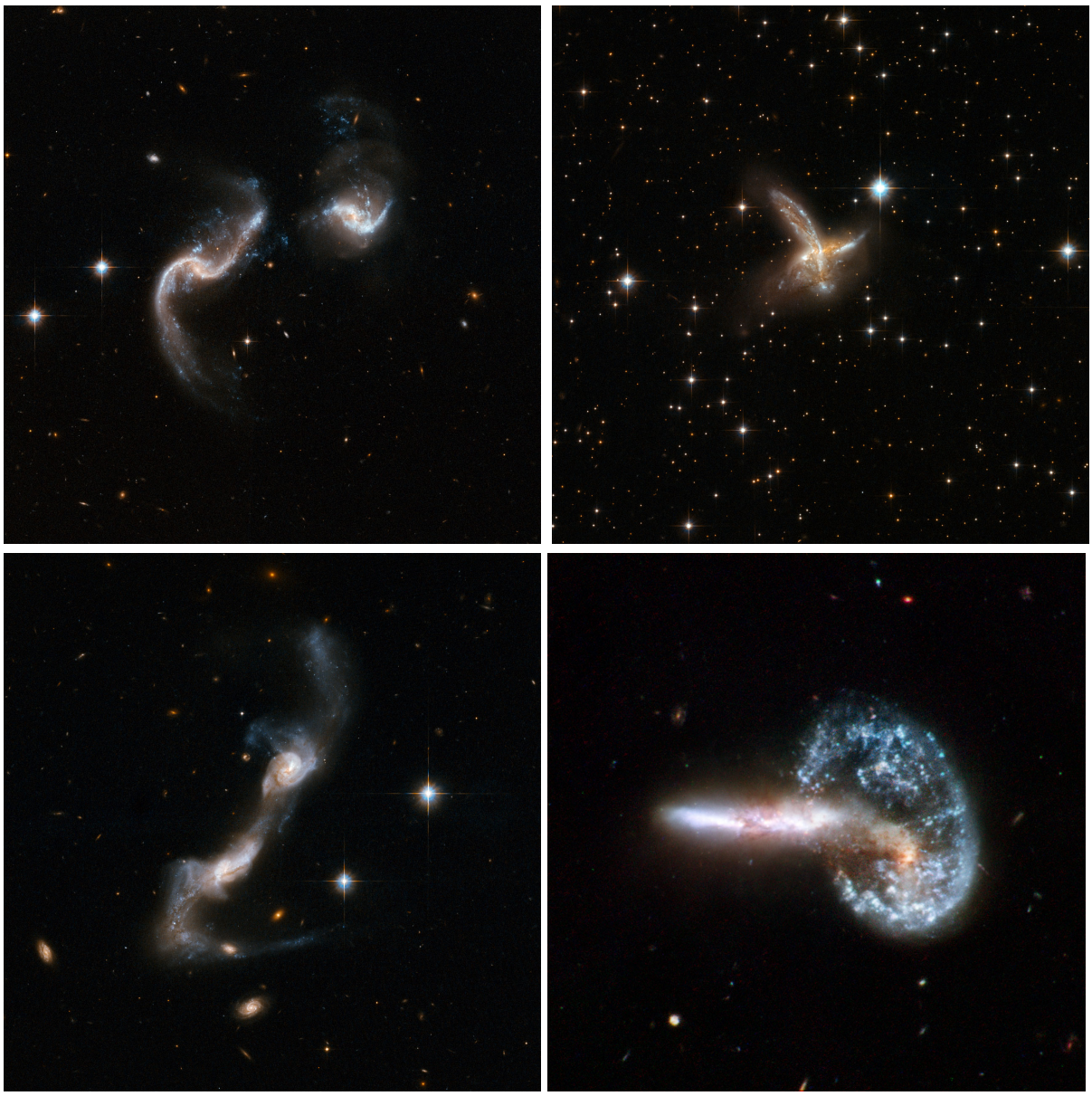

Figure 1.5: Examples of peculiar galaxies. These images display galaxies with strongly disrupted shapes and most of them have an astonishing number of blue knots of star formation. Starting from upper left corner in clockwise direction: Arp 256, ESO 593-8, UGC 8335, Arp 148. Image credits: NASA, ESA, the Hubble Heritage (STScI/AURA)-ESA/Hubble Collaboration, and A. Evans (University of Virginia, Charlottesville/NRAO/Stony Brook University)

could be explained by interactions between galaxies, gave rise to the idea that galactic gravitational encounters and mergers were not only a common event in the life of a galaxy but also a driving force in galactic evolution and diversification (e.g., Moore et al., 1996).

It is now accepted that galaxy interactions can be responsible for drastic increases in star formation rates (e.g., Sanders et al., 1988). One should keep in mind, however, that although mergers and interactions seem to be necessary for enhanced star formation, they are not a sufficient condition (Bergvall et al., 2003). Enhanced star formation requires fuel, molecular gas and dust, which is also referred to as part of the interstellar medium. Moreover, stars start forming only when the density of the interstellar medium reaches a certain threshold ($n_H > 10^5$ cm^{-3}; Larsen, 2010) and the rate of star formation increases with the volume density of the interstellar medium. Most galaxies (except, perhaps, for ellipticals) contain a certain amount of that fuel and there is usually a base star formation rate that is associated with a normal galaxy. Then, the question is what mechanisms would allow an interacting galaxy to dramatically increase the density of its interstellar medium in specific regions?

As was established by previous studies (e.g., Rubin & Ford, 1970; Zwicky, 1933), most of the mass of galaxies comes from the dark matter halo in which those galaxies are embedded. During an interaction, stars act like collisionless particles, whereas clouds and dust are colliding. Through dynamical friction of dark matter halos and direct collisions between gas and dust clouds, the colliding material will lose or transfer orbital energy and angular momentum. That triggers the infall of giant molecular gas and dust clouds towards the central regions of galaxies (increasing cloud densities along the way) and puffing up dark matter halos. Moreover, the gas and dust are highly compressible and gravitational disturbances (e.g., tidal shocks) could also increase the densities of some regions to the levels that are required for high star formation rates. As a consequence of boosted star formation rates, populations of star clusters form.

The Antennae galaxies (NGC 4038/39), presented in Figure 1.6, are a nearby, well-studied example of galaxy-wide star cluster formation that was triggered by a strong interaction. During the last two decades, extensive studies of this early-stage merger have been conducted (e.g., Martín-Hernández et al., 2002; Neff & Ulvestad, 2000; Teyssier et al., 2010; Whitmore et al., 2010)). Many of these studies were carried out with the *Hubble Space Telescope*, which allowed researchers to resolve some of the young massive star clusters in that system (e.g., Whitmore et al., 2007). These studies have confirmed the ideas that galaxy collisions can result in the formation of a large number of young star clusters and that most of the starburst activity occurs in giant H II regions. In areas with particularly high star-formation efficiency, young star clusters form dense groups – cluster complexes (Figure 1.6). The areas with bright blue colours, in the zoomed-in part of the image (right hand side), represents the areas of recent and ongoing star formation. In particular, star-like blue objects are actually young massive star clusters, and more extended objects of the same colour are cluster complexes, some of which can be as massive as a few $\times 10^7$ M$_\odot$ (Bastian et al., 2006). Thus, the population of star clusters that was formed due to the galaxy interaction is effectively a tracer of that interaction, and can potentially be used to determine how long ago that event happened (e.g., Gallagher et al., 2001).

The signs of star formation (both ambient and triggered by galaxy interactions) can be traced across all wavelengths of the spectrum, from X-ray to radio (e.g., Bell, 2003; Calzetti et al., 2007; Kennicutt, 1998; Ranalli et al., 2003). However, the most common ways of tracing star formation have been through the study of the following wavelength regimes: ultraviolet

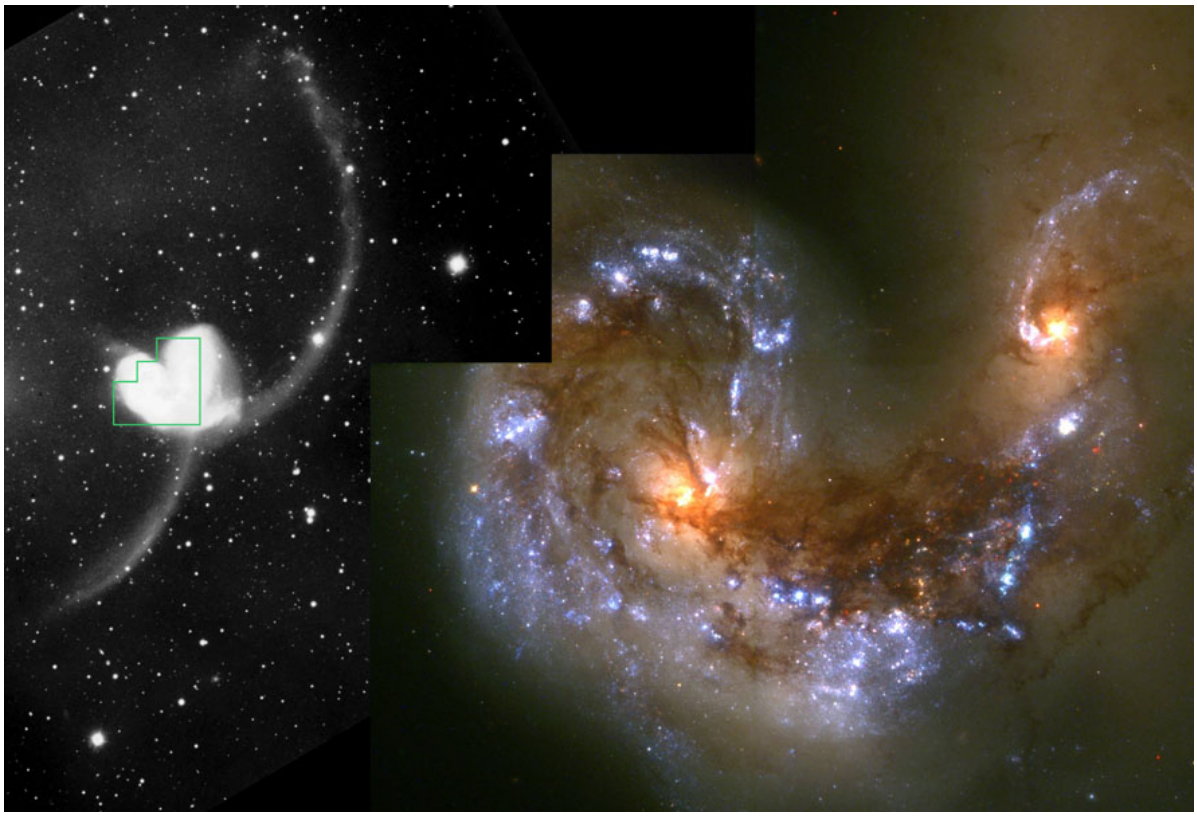

Figure 1.6: The Antennae galaxies: a relatively near-by system (~ 22 Mpc away; Schweizer et al., 2008) that is a very well-studied example of galaxy-wide star cluster formation triggered by a strong interaction (251 publications as of 2011). Compact, star-like objects with blue colours are young massive star clusters, ranging from 10^4 $M_\odot$ to 10^6 $M_\odot$ with median effective radii, R_{eff} = 4 ± 1 pc (Whitmore et al., 1999). Extended objects of the same colour are cluster complexes, with masses reaching a few $\times 10^7$ $M_\odot$and with sizes up to a few hundred pc (Bastian et al., 2006; Whitmore et al., 2010). Image credit: B. Whitmore, *HST*.

(UV), optical/near-infrared, and infrared **(IR)**. Each of these regimes has its advantages and disadvantages, depending on a number of things, such as the redshift of the observed galaxy, intrinsic reddening, or the time scale of star formation.

The amount of flux in the UV regime directly corresponds to the emission from young, massive stars (O- through later-type B-stars). Those stars, on average, have masses above 3 $M_\odot$ and have lifespans on the order of 10^8 yrs. The measurement of the UV continuum as the SFR tracer is very useful since it is probing the emission from the young, massive stars, and it can be used for galaxies with a wide range of redshifts $z \sim 1$–5 (Kennicutt, 1998).

In the optical and near-infrared regime, the star formation rate can be estimated by the strength of hydrogen recombination lines, e.g., H_α, H_β, etc. These lines come from the recombination of ionized gas that surrounds newly formed, massive O- and early-type B- stars. Those stars, in general, have masses over 10 $M_\odot$ and short lifespans, a few Myr. This implies that the strength of recombination lines is a great tracers of current star formation. However, as studies show (e.g., Kennicutt, 1992), mainly H_α is used as an SFR marker, since the strength of the other recombination lines are significantly weaker and interstellar absorption influences them more strongly. Beyond the redshift of 0.5, when the H_α line shifts outside of the optical window, there are some forbidden metal lines generated in the same nebulae that can be used as SFR tracers ([O II]; e.g., Gallagher et al., 1989). However, they are sensitive to metallicity.

The measurements in the UV and optical regimes can be severely affected by dust extinction. For example, a star-forming region with reddening of $A_V = 1$ mag will have 3 mag attenuation in the UV (Calzetti et al., 2007). For optical measurements of generic samples of galaxies, the dust will affect the blue lines more that the red ones, which translates into SFR underestimation by a factor ~ 3 if using H_α, and twice as much if using [O II], if extinction corrections are neglected (Calzetti, 2008; Rosa-González et al., 2002).

Star-forming regions are dusty environments and dust absorbs most efficiently in the UV regime, where young, massive stars exhibit the peak of their emission. Because of this, the IR emission (as a result of processing of the stellar UV light by the dust) can also serve as a tracer of the SFR. However, there are some caveats. The IR and optical regimes are known to be influenced by active galactic nuclei, which can be responsible for significant contributions to the IR continuum as well as recombination lines (H_α in particular; Kennicutt 1998). Furthermore, IR emission can be affected by interstellar dust that was heated up by the general stellar radiation field, including the emission in the optical region from older stars (Walterbos & Greenawalt 1996). As a result, the obtained SFR will be overestimated.

The measurements of the continuum, for UV and IR regimes, and the strength of recombination/forbidden lines, for optical/near-infrared regime, are compared to each other and to the output of the synthesis models of galaxies to derive an estimate of the SFR. With most of the stars being formed in the star cluster environment, a high SFR should be evident in the higher number of SCs. Theoretically, the total number of young star clusters detected in a galaxy could serve as an indicator of the SFR. It seems plausible to create a calibration that would relate the star formation rate to a number of SCs of the certain age range. However, this can not be implemented just yet because at the present moment there is only one galaxy (M31) for which we have a comprehensive demography of star clusters.

As we can see from the above discussion, galaxy interaction is a very important process, both for galaxy formation and evolution. Interactions are capable of increasing the star for-

mation rate, and consequently, the number of star clusters. However, in the local universe the distances between galaxies, on average, are much larger than their sizes. It makes a galaxy interaction a rather rare event in the Galactic neighbourhood. Nevertheless, there are still a number of ongoing smaller acquisitions of dwarf satellites by bigger galaxies in the Local Group. Moreover, some studies (e.g., Purcell et al., 2011) have suggested that some features that are characteristic of our Milky Way, such as spiral arms or the central bar, are a product of such acquisitions.

At early epochs, our universe was smaller and denser, and galaxies interacted with each other at a much higher rate. However, currently we cannot study clusters in those environments as the telescopes that are available to us are not powerful enough to give us the needed resolution and light-gathering power. Nevertheless, there are some objects which are located relatively close to us and which are believed to have similar conditions to those of the intermediate-redshift universe, making them prime targets for galactic evolution investigations. Those objects are compact galaxy groups that are discussed in detail in the next section.

1.3 Compact Group Environment

A compact group **(CG)** is a small system of galaxies, usually 4–8 of them, in close proximity to each other and, at the same time, in relative isolation from other surrounding galaxies. Such an environment is especially interesting scientifically because it closely resembles the environment of the early universe ($z \sim 4$). During that epoch, galaxies assembled through mergers of smaller parts, i.e, via hierarchical formation (Baron & White 1987). The results of such interactions in a compact group at higher redshift could be either the formation of the seeds of galaxy clusters (or protoclusters; Rudick et al. 2006), the formation of the isolated, giant elliptical galaxies that are observed in the field today (White et al. 2003), or, possibly, formation of fossil groups (Mulchaey & Zabludoff 1999), which are systems dominated by a single, giant elliptical galaxy, embedded in a luminous envelope of X-ray-emitting gas (Jones et al. 2003).

One intriguing aspect of the overall compact group population is its number. Numerical simulations have shown that structures like compact groups (with high spatial densities and correspondingly frequent dynamical interactions) are expected to evolve rather quickly and merge (e.g., Barnes, 1989; Diaferio et al., 1994; Mamon, 1987). So, the number of observed CGs is actually higher than predicted by the simulations. To fix this mismatch between theory and observations, a secondary infall scenario was suggested by Gunn & Gott (1972), and then revised by Mamon in a series of studies (Mamon, 1996, 2000, 2007). According to this picture, a secondary collapse of galaxies is occurring around already formed structures. In essence, this implies that compact groups are forming continuously within rich loose groups of galaxies, which is a common environment in the local universe (Diaferio et al. 1994).

The very first compact group was discovered by Stephan in 1877. However, it took 100 years for the first catalogue of compact groups to be published (Rose, 1977). This catalogue covered only 7.5% of the sky and listed groups with galaxies that were brighter than a limiting magnitude of 17.5 and have a projected surface density enhancement of a factor of 1000 compared to the surrounding background galaxy surface density. The follow-up study by Sulentic (1983) revealed that most of the groups in that catalogue actually did not satisfy the selection criteria. In 1982, Hickson created a new catalogue that would follow more robust

constraints during the selection process. According to Hickson (1982), a group of galaxies will be identified as compact group if it satisfies the following selection criteria:

- $N \geq 4$

  The total number of galaxies N within 3 magnitudes of the brightest galaxy (m_1) in the group must be four or more. This is a population criterion. In later work, (Hickson et al. 1992) modified this criterion such that $N \geq 3$, where N now refers to the number of galaxies within 1000 km s^{-1}of the median velocity of the group.

- $\theta_N \geq 3\theta_G$

  This is an isolation criterion. If the centres of all members of the group are located within a circle of angular radius θ_G, then θ_N is the minimal radius of a concentric circle that contains no galaxies with $m < m_1 + 3$.

- $\mu_G < 26$

  This is a compactness criterion. The total magnitude of all galaxies in the group in the R (μ_G) band averaged over the smallest circle that contains their geometrical centres must be less than 26 mag per arcsec^2. That is, the galaxies in a group should have a compact distribution to achieve that level of surface brightness.

As with many selection processes, this one is not free of biases. In particular, the Hickson selection criteria suffer from kinematic and geometric biases (Hickson 1997). Since galaxies are moving with respect to each other, some of the selected systems could be chance projections or transient configurations within a loose group (Mamon 1986), thus producing kinematic bias. Additionally, a non- spherical system oriented with its long axis along the line of sight to the observer could be preferentially chosen, resulting in geometric bias. Both of these biases would influence the compactness and isolation criteria. Another bias introduced by the selection criteria is the distance bias. For example, a nearby system with large angular scale most likely would not be classified as a compact group. The same is true for distant groups, where some galaxies could be too faint to be detected or, conversely, some groups could be falsely identified due to misidentification of members (stars, nebulae, artifacts, etc). As an example, from an initial 100 compact groups identified by Hickson only 86 turned out to be true compact groups following spectroscopy to measure radial velocities (Hickson 1997). These spectroscopic observations revealed that some of the galaxies assigned to groups had radial velocities that were not characteristic of the core galaxies of those groups, and were thus chance projections.

There are a number of other compact group catalogues in existence. The largest one is by Shakhbazyan (Shakhbazyan 1973), based on visual analysis of the Palomar Observatory Sky Survey prints. The catalogue was revised and updated a number of times subsequently (e.g., Baier & Tiersch, 1979; Shakhbazyan & Petrosyan, 1974). In its present form, it contains a total of 377 groups, nearly all of which are true dynamical systems and not chance alignments (Oleak et al. 1995). However, this catalogue received little attention in further studies of compact groups.

Barton et al. (1996) have worked with a complete magnitude-limited redshift survey, using a friends-of-friends algorithm to find 89 local compact groups. These findings formed the Redshift Survey Compact Group (RSCG) catalogue. The selection criteria for the RSCG catalogue

Figure 1.7: **Left:** HCG 92 (Stephan's Quintet) exhibits multiple signs of past and present interactions. As a result, it is a host to a great number of young massive star clusters (Gallagher et al. 2001; Fedotov et al. 2011). **Right:** HCG 07 does not have visible signs of past or present interactions. However, there is a high number of recently formed star clusters, suggesting that galaxies still affect each other dynamically (Konstantopoulos et al., 2010).

found groups very similar to Hickson's Compact Groups, but with relaxed isolation criterion. Because of that, the RSCG catalogue includes CGs that are near to or in the middle of large-scale structures, such as clusters of galaxies (Pompei & Iovino, 2010). The environment in such systems is somewhat different from the isolated CGs, such as HCGs.

Hickson CGs, as a result of the applied selection criteria described earlier, occupy a unique place in the distribution of hierarchical structures of matter in the universe. They possess number densities that are observed in the cores of galaxy clusters, although the total number of galaxies in the groups is relatively low: only 69% of groups originally identified by Hickson have $N \geq 4$ (Hickson et al., 1992). At the same time, the measured velocity dispersions of HCGs on average are $\sim 250\,\mathrm{km\,s^{-1}}$ (Cox et al., 2000; Tago et al., 2008), whereas dispersions of $\sim 750\,\mathrm{km\,s^{-1}}$ have been measured for galaxy clusters (Binggeli et al., 1987; Cox et al., 2000; The & White, 1986). It therefore follows that interactions between members of a compact group are going to be more frequent (because of the high number density) and substantially extended in time (because of the low relative velocity) compared to those of field galaxies or galaxies in the cluster environment.

A great example of a compact group that would support the above statements is HCG 92, shown in Figure 1.7. HCG 92 exhibits multiple signs of past and present interactions, such as galaxy distortions, tidal tails, and a number of young star clusters (< 10 Myr) detected both in intergalactic regions as well as in the galaxies themselves (Fedotov et al., 2011; Gallagher et al., 2001). It is a perfect illustration of how a high number density translates into multiple interactions among group members, which, in turn, leads to global onset of star formation in the interacting galaxies and in the inter-galactic medium.

One of the interesting features of HCGs is that they are deficient in H I gas as a class. Verdes-Montenegro et al. (2001) have shown that HCGs on average have 40% less gas by mass

than similar galaxies in the field. This implies that the compact group environment could be responsible for accelerated gas consumption by member galaxies. Indeed, as can be seen in Figure 1.7, HCG 07 does not present any signs of direct interactions, past or present. At the same time, a high number of recently formed star clusters is detected in this group (Konstantopoulos et al., 2010). It appears that even without direct collisions, the gravitational potentials of galaxies in this group are still influencing each other. This group can also serve as a reminder that the history of strong collisions alone does not provide the whole story for the system.

1.4 Conclusion

In this brief introduction to my thesis, I have highlighted the main areas of my current and future research.

The central object of my research is star clusters. There is strong evidence that galaxy interactions are capable of triggering star-burst events. Since most stars in the universe are formed in star clusters, those star-burst events will increase star cluster populations in interacting galaxies. Thus, star clusters can be used as tracers of the interactions during which they were formed. Additionally, star clusters can be well approximated by simple stellar populations, which in turn can be modelled with population synthesis evolutionary codes such as that of Marigo et al. (2008). These give us a handle on estimating the ages of those star clusters. Thus, combining the spatial distribution of clusters in interacting systems with their estimated ages can potentially allow us to reconstruct the history of events that led to the current system configuration.

One of the main goals of astronomy as a science is understanding the formation and evolution of the universe and its constituents. One particular aspect of that goal is to study the conditions of the process of formation of galaxies and their evolution. Ideally, we would like to examine the earlier universe in greater detail. However, the current state of our technology does not allow us to do that with the desired level of detail.

Compact groups, and in particular Hickson compact groups, are excellent proxies of the earlier universe, a characteristic of which (in dense environments) is multiple prolonged interactions between galaxies. Thus, by studying Hickson compact groups in the nearby universe, in particular their SC populations, we can have a better understanding of the processes of galaxy formation and evolution.

Chapter 2

A Comprehensive HST BVI Catalogue of Star Clusters in Five Hickson Compact Groups of Galaxies.

K. Fedotov, S. C. Gallagher, P. R. Durrell, N. Bastian, I. S. Konstantopoulos, J. Charlton, K. E. Johnson, and R. Chandar
Submitted to the Monthly Notices of the Royal Astronomical Society

Abstract

We present a photometric catalogue of star cluster candidates in Hickson compact groups (HCGs) 7, 31, 42, 59, and 92, based on observations with the Advanced Camera for Surveys and the Wide Field Camera 3 on the *Hubble Space Telescope*. The catalogue contains precise cluster positions (right ascension and declination), magnitudes, and colours in the *BVI* filters. The number of detected sources ranges from 2200 to 5600 per group, from which we construct the high-confidence sample by applying a number of criteria designed to reduce foreground and background contaminants. Furthermore, the high-confidence cluster candidates for each of the 16 galaxies in our sample are split into two sub-populations: one that may contain young star clusters and one that is dominated by globular older clusters. The ratio of young star cluster to globular cluster candidates varies from group to group, from equal numbers to the extreme of HCG 31 which has a ratio of 8 to 1, due to a recent starburst induced by interactions in the group. We find that the number of blue clusters with $M_{\rm V} < -9$ correlates well with the current star formation rate in an individual galaxy, while the number of globular cluster candidates with $M_{\rm V} < -7.8$ correlates well (though with large scatter) with the stellar mass. Analyses of the high- confidence sample presented in this paper show that star clusters can be successfully used to infer the gross star formation history of the host groups and therefore determine their placement in a proposed evolutionary sequence for compact galaxy groups.

2.1 Introduction

It is widely accepted that interactions and mergers between gas-rich galaxies lead to star formation (e.g., Barton Gillespie et al., 2003; Kennicutt et al., 1987; Mihos & Hernquist, 1996; Springel et al., 2005), and that the majority of stars form in clusters and associations (Bressert et al., 2010; Lada & Lada, 2003). It therefore follows that a detailed analysis of star cluster populations in a galaxy can reveal its history of interaction events (e.g., Bastian et al., 2005a; Gallagher et al., 2001; Whitmore et al., 1999; Wilson et al., 2006).

In that light, star clusters are a powerful tool for studying star formation events triggered by mergers and tidal interactions between galaxies. In particular, star clusters could could prove useful for studying compact groups (CGs), specifically Hickson Compact Groups (Hickson, 1982, 1997; Hickson et al., 1989, 1992). By virtue of their selection criteria (low velocity dispersions and high galaxy number densities), HCGs represent an environment with frequent and prolonged interactions, that can trigger the formation of star cluster populations associated with specific events.

Initially motivated by the work of Verdes-Montenegro et al. (2001), Johnson et al. (2007) proposed an evolutionary sequence of HCGs by separating them into three types based on the ratio of their H I content (a proxy for the available reservoir of cool gas for star formation) and the dynamical mass, with Type I being the gas-rich groups and Type III the gas-poor ones. Johnson et al. (2007) also report – based on *Spitzer* mid-infrared colours – that galaxies in Type I groups are more actively star-forming than galaxies in Type II groups while galaxies in Type III groups are relatively quiescent. Konstantopoulos et al. (2010) expanded on this classification by splitting group types into two parallel sequences according to their gas distributions: sequence A groups maintain the bulk of their cold gas inside galaxies, whereas sequence B groups have gas dispersed throughout the intra-group medium (IGM) (Konstantopoulos et al., 2010, their fig. 1). The gas distribution of sequence B groups likely results from strong interactions that occur while disk galaxies are still gas-rich. The initial conditions of the positions and relative velocities of Sequence A group galaxies are such that only softer interactions occur, and while secular evolution may be enhanced and lead to a boost in star formation rates in individual galaxies, the bulk of the cold gas is not pulled into the IGM. As a consequence, the groups in Sequence A are expected to ultimately lead to the formation of a single elliptical galaxy with little to no X-ray envelope, as gas is consumed within galaxies before late-stage dry mergers. Groups in Sequence B – where galaxies interact strongly before gas is consumed – would be more likely to form ellipticals with a strong X-ray envelope (heated by star-formation triggered by one or more gas-rich mergers), as can be seen around some massive elliptical galaxies or so-called 'fossil' groups (Jones et al., 2003). The differences in star-forming histories, which vary depending on gas content and distribution and advance along the evolutionary path, must be reflected in the star cluster populations of the groups. Thus, star cluster populations can potentially be used to infer their hosts' placement on the CG evolutionary sequence proposed by Konstantopoulos et al. (2010).

In this paper, we consolidate the information on star clusters in compact groups of galaxies that has been presented in a number of projects (Fedotov et al., 2011; Gallagher et al., 2010; Konstantopoulos et al., 2010, 2012, 2013) and present it in a consistent, coherent catalogue, with the goal of further assisting researchers in star cluster-related studies. We also take this opportunity to compare the basic properties between cluster populations in compact groups at

distinct evolutionary stages.

This paper is organized in the following way: in Section 2, we describe the samples and data sets. We outline the procedure for constructing the catalogue in Section 3, and present our results and discuss them in Section 4. Lastly, we summarize the main conclusions in Section 5. Throughout, we use the cosmology $H_0 = 73.0\,\mathrm{km\,s^{-1}\,Mpc^{-1}}$, $\Omega_{\mathrm{matter}} = 0.27$, and $\Omega_{\mathrm{vacuum}} = 0.73$ to determine distances and physical sizes.

2.2 Data

The data for this project were obtained with the *Hubble Space Telescope* (*HST*) Advanced Camera for Surveys (ACS) and Wide Field Camera 3 (WFC3). These observations are part of two programs: ID 10787 (PI J. Charlton) and ID 11502 (PI K. Noll). The former program was design to study 12 nearby ($v_{\mathrm{r}} < 4500\ \mathrm{km\,s^{-1}}$) compact groups covering the full range of the group types in the evolutionary sequence. Within each type of the evolutionary sequence there is a large variety in group properties. Thus, covering the whole range is essential for understanding the dependence of star formation and galaxy transformation on group properties. Unfortunately, only 4 groups were observed with the ACS (HCG 07, 31, 59, and 42 partially) before it stopped working due to electrical short in 2007. HCG 92 was a target for the WFC3 Early Release Science Program and a perfect addition (albeit a bit more distant than the rest of the groups) to our truncated sample. Combined, these 5 groups cover the full range for the evolutionary Sequence B (groups with the gas dispersed throughout the IGM) and 2 out of 3 types for Sequence A (groups with gas contained inside galaxies).

The observations were carried out in the F435W (F438W for WFC3), F606W, and F814W filters, which are similar to the Johnson *BVI*-bands. Hereafter, we refer to the *HST* filters as B_{435}, B_{438}, V_{606}, and I_{814}, although we did not make transformations to the Johnson-Cousins system.

Table 2.1 contains an observation log. The last column in the table lists publications related to those observations. Table 2.2 presents properties of the 16 individual galaxies within the five compact groups included in this sample.

2.3 Data Analysis

Before we go into the detailed description of selecting and sorting the detected sources, here are a few words about our terminology to clarify the differences between samples.

Our catalogue consists of all detected point sources that passed the criteria described below. However, the high-confidence portion of the catalogue is divided into two subcategories that we denote as star cluster candidates (SCCs) and globular cluster candidates (GCCs). The major difference between these two subcategories is that the selection criteria for the SCCs do not discriminate against sources with significant nebular emission. In contrast, the selection criteria for GCCs filter out objects with nebular emission (both in terms of their colours and their spatial extent), while being less strict about the lower luminosity limit (see Fig. 2.1). These two subcategories are not mutually exclusive, i.e., the same cluster may be present in both categories. Many GCCs can be labelled as SCCs (since the more luminous ones will

Table 2.1: Details of observations.

Group	Galaxy	Instrument	Program ID	t_{exp} (s)			Date	References
				F435W*	F606W	F814W		
HCG 07	A, B, D	ACS/WFC	10787	1710	1230	1065	Sept 2006	K10
	C	ACS/WFC		1710	1230	1065	Sept 2006	
HCG 31	A–C, E–H	ACS/WFC	10787	1710	1230	1065	Aug 2006	G10
HCG 42	A, C	ACS/WFC	10787	1710	1230	1080	Dec 2007	K13
HCG 59	A, C	ACS/WFC	10787	1710	1230	1065	Dec 2007	K12
	B, I	ACS/WFC		1710	1230	1065	Nov 2006	
HCG 92	B, D	WFC3	11502	3410	1395	1860	Aug 2009	F11, T12
	C, B	WFC3		3410	1395	1860	Aug 2009	
	E	WFC3		3410	1395	1860	July 2009	

Notes. * For HCG 92 B filter is F438W of WCF3 camera. In the last column we reference star cluster studies that used the associated observations.
G10: Gallagher et al. 2010
F11: Fedotov et al. 2011
K10: Konstantopoulos et al. 2010
K12: Konstantopoulos et al. 2012
K13: Konstantopoulos et al. 2013
T12: Trancho et al. 2012

satisfy the SCC criteria), however, virtually no young SCCs will be in the GCCs subcategory (unless the young SCs are severely reddened). Hence, we use the SCC sample primarily to study the young star cluster populations and GCCs to study globular cluster populations.

Throughout the paper we use the terms young, intermediate, and old when we talk about star clusters. These are general terms without standard definitions in the literature. For this paper, when we talk about young star clusters we mean clusters that are younger (according to their location in *BVI* colour space) than 10 Myr. For intermediate clusters the age range is between a low hundreds Myrs and a few Gyrs, and for the old clusters the range is from $\sim$ 5 Gyr to 14 Gyr. The intervals not covered by our definitions are grey areas, and star clusters in those intervals are labelled according to context. For example, if we are talking about intermediate age clusters (750 Myr old), clusters less than 50 Myr old could be referred to as young/younger SCs. For most of the cases, whenever we are using these terms (young, intermediate, old) we are specifying the time intervals within the parentheses following the term.

2.3.1 Star Cluster Selection

For the ACS observations, the closest group is HCG 07 at a distance of 56.6 Mpc (from the initial radial velocity measurement by Hickson (1982) modified based on the velocity field model of Mould et al. (2000)), equivalent to a distance modulus of $(m - M)_0 = 33.76$ mag. At this distance, the $0\farcs049$ pixel size of the ACS corresponds to 13.7 pc. The distance to Stephan's Quintet which was observed with the WFC3, is adopted to be 88.6 Mpc (Hickson,

Table 2.2: Information on HCG Galaxies.

Galaxy	Name	RA (2000)	Dec (2000)	Type	v_r km s^{-1}	M_* log($M_\odot$)	SFR ($M_\odot$ yr^{-1})
07A	NGC0192	00h 39m 13.4s	+ 00d 51m 52s	Sb	4133	11.28	3.88±0.47
07B	NGC0196	00h 39m 17.8s	+ 00d 54m 46s	SB0	4255	10.76	0.23±0.02
07C	NGC0201	00h 39m 34.8s	+ 00d 51m 36s	SBc	4415	10.89	2.06±0.17
07D	NGC0197	00h 39m 18.8s	+ 00d 53m 31s	SBc[a]	4121	10.15	0.43±0.04
31A	NGC1741	05h 01m 38.7s	– 04d 15m 34s	Sdm	4074[b]	10.32[c]	8.11±0.74[c]
31B		05h 01m 36.2s	– 04d 15m 43s	Sm	4136[b]	9.51	0.78±0.07
31C	M1089	05h 01m 37.7s	– 04d 15m 28s	Im	4019[b]	[c]	[d]
31E		05h 01m 37.5s	– 04d 15m 57s	Sdm	4009[e]	...	[d]
31F		05h 01m 40.0s	– 04d 16m 22s	Sbc	3969[e]	...	0.19±0.02
31G	IC 0399	05h 01m 44.0s	– 04d 17m 20s	Sbc	3991	10.04	1.47±0.12
42A	NGC3091	10h 00m 14.3s	– 19d 38m 13s	E3	3964	11.53	0.44±0.04
42C		10h 00m 10.3s	– 19d 37m 19s	E2	4005	10.70	0.09±0.02
59A	IC 0737	11h 48m 27.5s	+ 12d 43m 39s	Sa[f]	4109	10.19	4.99±0.67
59B	IC 0736	11h 48m 20.1s	+ 12d 43m 00s	E0[g]	4004	10.14	0.02±0.01
59C	KUG 1145+129	11h 48m 32.4s	+ 12d 42m 19s	Sb	4394	9.82	0.16±0.03
59D	KUG 1145+130	11h 48m 30.6s	+ 12d 43m 47s	Im	3635	9.38	0.48±0.04
92B	NGC7318B	22h 35m 58.4s	+ 33d 57m 57s	Sbc	5774	10.89	0.52[h]
92C	NGC7319	22h 36m 03.5s	+ 33d 58m 33s	SBc	6747	11.35	0.08[h]
92D	NGC7318A	22h 35m 56.7s	+ 33d 57m 56s	E2	6630	11.19	0.05[h]
92E	NGC7317	22h 35m 51.9s	+ 33d 56m 42s	E4	6599	10.83	0.03[h]

Notes. Unless indicated otherwise stellar masses are taken from Desjardins et al. (2014), SFR values listed are from Tzanavaris et al. 2010, velocity values are from de Vaucouleurs et al. 1991, and morphology types are from Hickson et al. 1989.

[a] In RC3 galaxy listed as SB0.

[b] Nishiura et al. 2000.

[c] Stellar mass value listed is measured as the total mass of galaxies 31A and -C.

[d] SFR value listed is combined value of galaxies 31A, -C, and -E.

[e] Mendes de Oliveira et al. 2006.

[f] In RC3 galaxy listed as E?.

[g] In RC3 galaxy listed as S0.

[h] Bitsakis et al. 2014.

1982; Mould et al., 2000), equivalent to $(m - M)_0 = 34.74$ mag. Thus, one 0.″04 pixel on WFC3 corresponds to ∼ 17.2 pc. With the average star cluster half-light radius of ∼ 4 pc (e.g., Barmby et al., 2006; Larsen, 2004; Scheepmaker et al., 2007), the majority of the detected clusters in all observations are expected to be unresolved or marginally resolved in the case of the closest groups (e.g., Harris, 2009). Therefore, for this catalogue we used point spread function (PSF) fitting as the preferred method of obtaining photometry. This methodology for unresolved star clusters is widely accepted, and has been used previously in a number of CG studies (e.g., Fedotov et al., 2011; Gallagher et al., 2010; Konstantopoulos et al., 2010, 2012, 2013). Additionally, PSF-fitting delivers more accurate photometry with varying backgrounds and crowded fields, conditions commonly found in HCGs.

For point source detection we used the V_{606} images, as they offer the faintest limiting magnitudes at 50% completeness level among the observations (see Table 2.5). To detect point sources, we run the `DAOFIND` (Stetson, 1987) task in `IRAF`[1] on median-divided images, obtained by division of the original images by median boxcar-smoothed ones (with a 13×13 pixel smoothing window). The coordinates of point sources detected in V_{606} were transformed into the $B_{435/438}$ and I_{814} coordinate systems. PSF photometry was performed on each image independently, and the results were cross-matched (with matching radius of 1.5 pixels) to yield point sources that were present in all three frames.

PSF models for each filter of each group were constructed from bright, isolated, and unsaturated stars with smooth radial curves of growth. The aperture correction was calculated as an average of the difference between magnitudes obtained from aperture photometry (with a 10-pixel aperture) and PSF-magnitudes (calculated at 3 pixels). The aperture corrections between 10 pixels and infinity in the case of ACS observations were taken from Sirianni et al. (2005), and in the case of WFC3 observation were calculated from the enclosed energy curves as the difference between unity and the enclosed energy in the given aperture and wavelength (B. Whitmore, priv. comm.). The foreground extinctions were obtained from Schlafly & Finkbeiner (2011), published in the NASA/IPAC Extragalactic Database (NED)[2]. Table 2.3 gives overall information on the number of stars used in the PSF constructions, the aperture correction values, and foreground extinctions for different filters and targets.

At this stage, we had an unfiltered point source list for each group, which we call the extended sample.

2.3.2 Star Cluster Candidate Selection

To create a catalogue of high confidence star cluster candidates we applied to our extended samples the following selection criteria:

1. **Magnitude cut at $M_{V_{606}} < -9$ mag (S1)**
   To eliminate the contamination from individual luminous supergiants, which can reach $M_{V_{606}} \simeq -8$ mag, we only considered sources with $M_{V_{606}} < -9$ mag. This roughly corresponds to a cluster mass of a few $\times 10^4$ $M_\odot$ at 10 Myr and $\sim 10^6$ $M_\odot$ at 10 Gyr (depending

[1] `IRAF` is distributed by the National Optical Astronomy Observatory, which is operated by the Association of Universities for Research in Astronomy (AURA) under cooperative agreement with the National Science Foundation.

[2] http://ned.ipac.caltech. edu/ngi/

Table 2.3: Information on number of stars used to create a PSF model, aperture corrections, and foreground extinctions in *BVI* filters for every pointing.

Group	Pointing	# of PSF stars			Foreground extinction			Aperture correction					
		B_{435}	V_{606}	I_{814}	B_{435}	V_{606}	I_{814}	B_{435}		V_{606}		I_{814}	
					mag	mag	mag	$3 \rightarrow 10$ mag	$10 \rightarrow \infty$ mag	$3 \rightarrow 10$ mag	$10 \rightarrow \infty$ mag	$3 \rightarrow 10$ mag	$10 \rightarrow \infty$ mag
HCG 07	1	8	8	6	0.081	0.056	0.036	0.144	0.107	0.209	0.088	0.213	0.087
	2	10	12	12	0.081	0.056	0.036	0.223	0.107	0.139	0.088	0.224	0.087
HCG 31	1	13	13	18	0.210	0.144	0.093	0.161	0.107	0.121	0.088	0.211	0.087
HCG 42	1	24	41	55	0.174	0.119	0.078	0.107	0.107	0.113	0.088	0.030	0.087
HCG 59	1	8	11	9	0.151	0.104	0.066	0.137	0.107	0.162	0.088	0.203	0.087
	2	11	8	16	0.151	0.104	0.066	0.160	0.107	0.174	0.088	0.221	0.087
HCG 92	1	27	14	48	0.32	0.22	0.14	0.207	0.110	0.258	0.103	0.342	0.108

Notes. Foreground extinction coefficients in this table were obtained with Schlegel et al. 1998, published on NED. $3 \rightarrow 10$ aperture corrections were calculated as the mean brightness difference of the stars we used to construct the PSF, between the 3 pixel PSF photometry and brightness measured in a 10 pixel aperture. $10 \rightarrow \infty$ aperture corrections for ACS observations were taken from Sirianni et al. 2005. $10 \rightarrow \infty$ aperture corrections for WFC3 observations were calculated as the difference between unity and the enclosed energy in the given aperture.

on metallicity and distance modulus).

2. **Photometric error $\sigma < 0.3$ mag in all three filters (S2)**
   To maintain photometric quality of magnitudes and colours, all point sources that had photometric errors larger than 0.3 mag in any of the $B_{435/438}$, V_{606}, or I_{814} filters were discarded.

3. **Sharpness between −2 and 2 in all bands (S3)**
   To further minimize contamination from cosmic rays and background galaxies, we applied a sharpness filter which, essentially, is a constraint on the intrinsic angular size of the detected objects. Sharpness is measured as the difference between the square of the width of the object and the square of the width of the PSF, and for our purposes should be between −2 and 2: large positive values of sharpness are indicative of blended sources and partially resolved galaxies, whereas large negative numbers are flags for cosmic rays and blemishes. For a well-matched width the sharpness is zero.

4. **$\chi < 3$ in the I_{814}-band (S4)**
   The `DAOPHOT` goodness of fit factor χ from PSF-fitting in the I_{814}-band should be less than 3. The use of I_{814}-band for the χ parameter is twofold: (a) the PSF model is typically best determined in that band because we have the most PSF stars; and (b) no contamination

from nebular emission lines (e.g., Hα) is expected (nebular emission around a young star cluster may cause them to be marginally resolved in the V_{606}-band images).

5. **Colour cuts (S5)**
   In order to minimize the contamination from foreground Galactic stars, we applied colour cuts, where all sources that had colours $B_{435/438} - V_{606} > 1.5$ mag or $V_{606} - I_{814} > 1.0$ mag were discarded (e.g., see fig. 8 of Trancho et al. 2012).

2.3.3 Globular Cluster Candidate Selection

In a similar manner we created a catalogue of Globular Cluster Candidates, with the following (generally stricter) criteria (based on Rejkuba et al. (2005)):

1. **Hyperbolic filters in photometric error (G1)**
   The hyperbolic filter in the photometric error was defined in such a manner as to retain $\sim 97\%$ of all recovered artificial sources (these are the sources that were used in determining the completeness level, see Section 2.3.4). The application effect of this filter on detected sources can be observed in Fig. 2.1, panels b_0 and b_1.

2. **Hyperbolic filters in `DAOPHOT` sharpness parameter (G2)**
   We defined the hyperbolic filter in the V_{606} `DAOPHOT` sharpness parameter in the same manner as the photometric error filter. That is, the sharpness filter is tuned so that it retains $\sim 97\%$ of all recovered artificial sources. However, there is a possibility that for the closest groups (e.g., HCG 07, HCG 42) some of the GCCs might be marginally resolved. In these cases we relax the upper envelope of the sharpness filter to make sure that we do not discard larger GCCs. The example of the application and effect of the sharpness filter on detected sources can be seen in Fig. 2.1, panels c_0 and c_1.

3. **Magnitude cut at $M_{V_{606}} < -7.8$ mag (G3)**
   Because contamination from supergiants is less of a problem for objects with GC-like colours, we relaxed our luminosity cut to $M_{V_{606}} < -7.8$ mag to get closer to the expected peak of the GC luminosity function $M_V \sim -7.4$ (e.g., Ashman & Zepf, 1998; Harris, 2001). The -7.8 magnitude cutoff roughly corresponds to a globular cluster mass of $\sim 5 \times 10^5$ $M_\odot$ (depending on metallicity and distance modulus). The effect of application of this filter is shown on Fig. 2.1, panels d_0 and d_1.

4. **Milky Way Globular Cluster selection parallelogram (G4)**
   We use dereddened GCs from the updated Harris (1996) Milky Way Globular Cluster catalogue to derive a selection parallelogram in $B-V$ vs. $V-I$ colour space. We convert the vertices of the parallelogram from Johnson's B, V, I magnitudes to B_{435}, V_{606}, I_{814} magnitudes via transformations derived from Sirianni et al. (2005). We keep all sources

Table 2.4: Percentage remaining of the initial sources after applying particular criteria.

Group	S1 %	S2 %	S3 %	S4 %	S5 %	G1 %	G2 %	G3 %	G4 %	Number of initial sources
HCG 07	11.6	91.3	100.0	92.3	88.3	84.0	66.1	40.6	28.2	4243
HCG 31	25.5	93.7	99.9	84.1	88.8	64.4	44.7	58.6	22.3	2670
HCG 42	22.1	94.7	99.7	94.2	82.2	92.1	85.2	58.5	67.8	2262
HCG 59	12.9	76.3	99.9	93.5	84.7	78.8	79.6	41.1	39.1	3445
HCG 92	52.9	94.5	99.3	82.9	78.7	92.4	81.4	92.6	23.5	5493

Notes. Criteria S1 through S5 are for star clusters, criteria G1 through G4 are for globular clusters; S1 – Magnitude cut at $M_{V_{606}} < -9$ mag, S2 – Photometric error less than 0.3 mag in all three frames, S3 – Sharpness between −2 and 2 in all bands, S4 – χ in I-filter less than 3, S5 – Color cuts, G1 – Hyperbolic filter in the magnitude errors, G2 – Hyperbolic filter in the sharpness, G3 – Magnitude cut at $M_{V_{606}} < -7.8$ mag, G4 – Colours similar to those of the dereddened Milky Way globular clusters.

that would fall into the selection parallelogram in the $B_{435}-V_{606}$ vs $V_{606}-I_{814}$ colour space or that would overlap the selection region with their 1σ error bars. HCG 92 was observed with WFC3 and there is (to our knowledge) currently no equivalent to the Sirianni et al. (2005) calibration paper for this instrument. Therefore, we apply the same selection box for globular clusters to these data as for the ACS data. Given the similarities between these two instruments and their filter sets, we would not expect a significant change in the number of globular cluster candidates as the result of that action.

Table 2.4 specifies what fraction (in percent) of the initial number of point sources (rightmost column) remains after applying each criterion individually. For example, after applying the S1 criterion (absolute magnitude cut) on 4243 sources detected in HCG 07 only 11.6% (or 493 sources) of the original sample remains, whereas after applying the S2 criterion (photometric error < 0.3 mag in all three filters) on the initial list of 4243 sources 91.3% of the extended sample (or 3874 sources) remain, and so on.

2.3.4 Completeness Levels

To determine completeness of our catalogue we carried out the following routine for each group in our sample. For groups HCG 07, 42, 31 and 59 we used `ADDSTAR` to add 3000 artificial stars to the images (over the entire field, including the galaxies) in the apparent magnitude range 24–28 mag, i.e., absolute magnitudes ranging between −9.99 mag and −5.76 mag (taking into consideration that these groups are located in the range of distances from 56.6 and 62.8 Mpc). For HCG 92 we used `ADDSTAR` to add 5000 artificial stars to the image as the image covers a larger field of view. The apparent magnitude range of artificial stars was the same, i.e., 24–28 mag, which translates into absolute magnitudes range between −10.74 mag and −6.74 mag, given that the distance modulus for HCG 92 is 34.74 mag. After artificial stars were added to the images, we applied the same algorithm for point source detection to determine the recovery

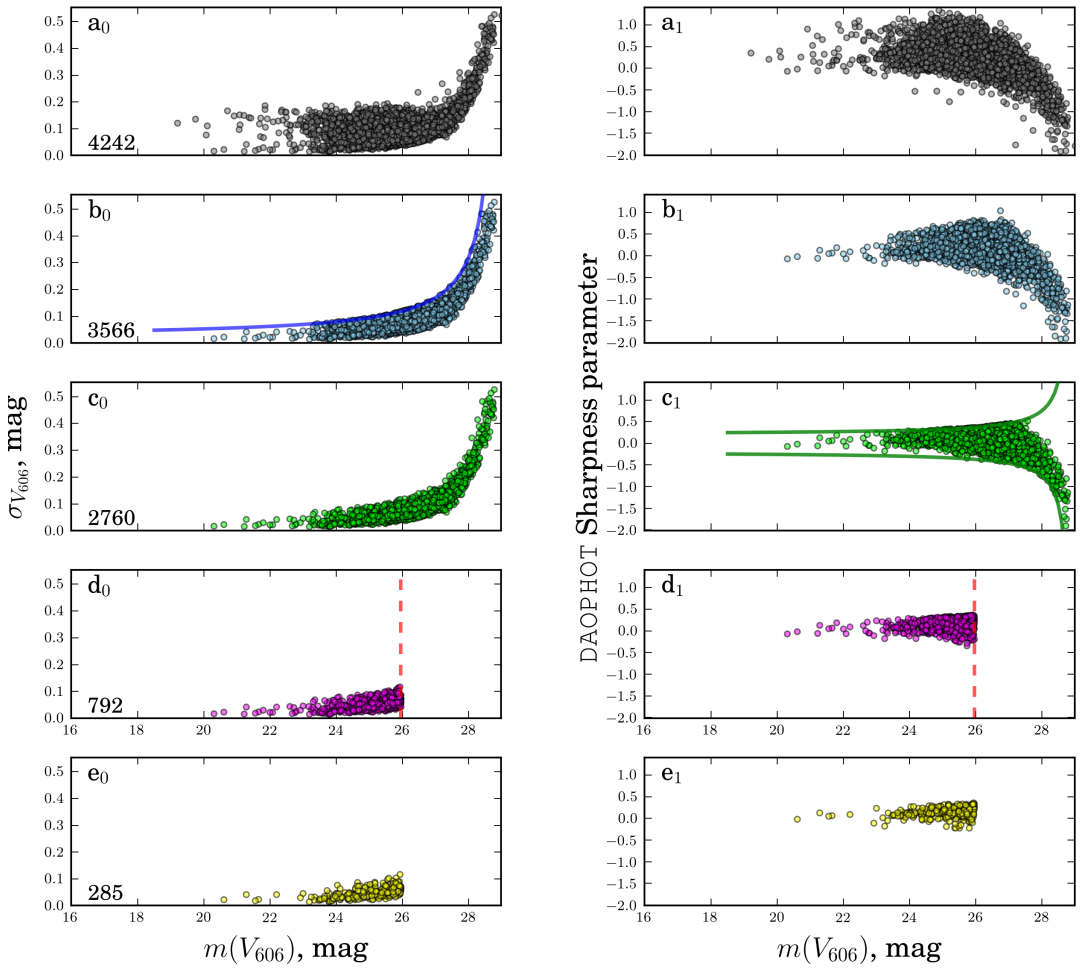

Figure 2.1: Illustration of the criteria applied to the HCG 07 extended point source catalogue to produce the GCC sample for that group. The rows in this figure show the same point sources being plotted in error, $\sigma_{V_{606}}$, vs. V_{606} magnitude (left-hand-side panels with subscript 0) and in DAOPHOT sharpness parameter vs. V_{606} magnitude space (right-hand-side panels with subscript 1). The upper row of panels shows the initial point sources. We apply the hyperbolic filter in magnitude error, as observed in panel b_0, and panel b_1 represents the point sources that satisfy that criterion in sharpness parameter space. Panel c_1 shows the hyperbolic filter that was applied in the sharpness parameter space, and c_0 displays point sources in magnitude error space that pass that filtration. We apply a magnitude cut ($M_{V_{606}} < -7.8$) which is illustrated by panels d_0 and d_1. To obtain the final GCC sample for HCG 07, we select only those sources that have colours similar to those of the Milky Way globulars (see Fig. 2.14, panel (a) for reference). Resulting objects are presented in panels e_0 and e_1. The number in the lower left corner of the left-hand-side panels indicates the number of point sources that remain after application of each criterion (A colour version of this figure is available in the online journal.)

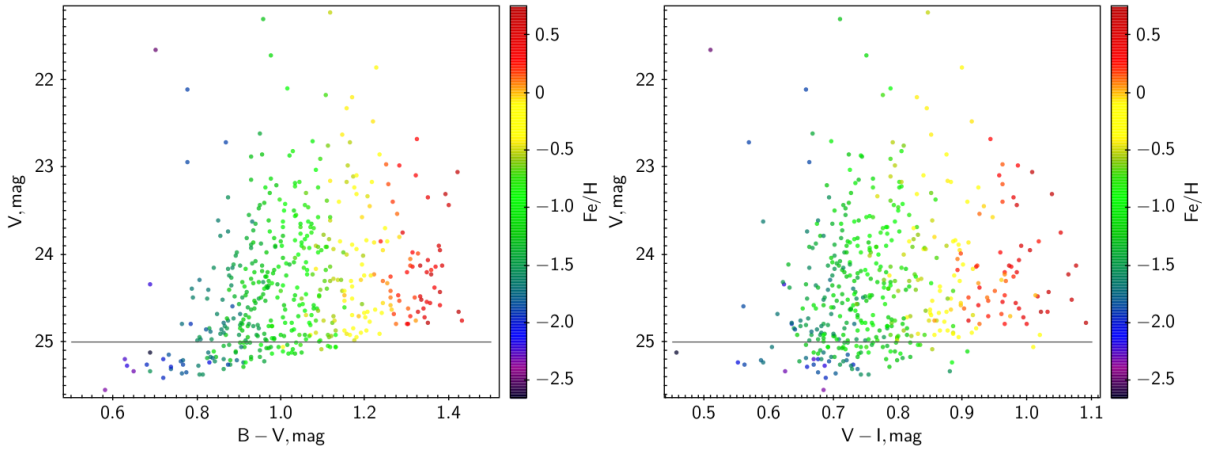

Figure 2.2: $B - V$ and $V - I$ colour-magnitude diagrams for HCG 42. The displayed sources are GCCs at or above 90% completeness level in all three filters. The sources themselves are colour coded according to their metallicities (see §2.3.6), represented with colour bars on the right hand side of each plot. As can be seen from the plots, even at the 90% completeness level we are still missing some of the metal enriched GCCs. To minimise this effect, we are making a magnitude cut at V = 25 mag for this group, and at V = 25.5 mag for HCG 07, 31, and 59. Thus, for obtaining values of the expected total number of GCs in a galaxy, $N_{\rm total}$, the value of specific frequency, S_N, or for the analysis of the metallicity distribution of GCCs we will be using a sub-catalogue with aforementioned magnitude cut. (A colour version of this figure is available in the online journal.)

rates. The average limiting magnitudes for the 50% and 90% recovery rates for each group are presented in Table 2.5. As can be seen, we operate at the slightly higher than 90% completeness level (in V_{606} filter) for GCCs and at even higher completeness level for the SCCs, except for HCG 92 which is the most distant group in our sample. In that case we are at $\gtrsim$ 50% and $\sim$ 90% completeness level for the GCCs and SCCs, respectively. We point out that the method described gives the values for the average completeness level over the entire image. Because of the random distribution of artificial sources and because galaxies (with elevated surface brightness) typically take up a smaller fraction of the field-of-view, our actual completeness levels will generally be lower as star clusters tend to be found in galaxies (with HCG 92 as a notable exception).

The level of completeness becomes especially important when we are dealing with the specific frequencies and metallicity distributions for globular cluster candidates. The $B - V$ colour for GCCs is, on average, about 1 although our selection parallelogram (the G4 criterion, §2.3.3) goes down to $B - V = 1.38$. As an example, consider a hypothetical GCC source in HCG 42. If this source has $m_V = 26$ mag (just above the 90% completeness level in the V filter; Table 2.5), its magnitude in B, according to our G4 criterion, will be between 26.68 and 27.38. However, the 90% completeness level in B is 26.2 mag. Thus, if we force our sources to have 90% completeness level only in the V filter, we will be missing some of the red sources at the faint end. Moreover, even forcing 90% completeness in the limiting filter (in our case it is B filter), we are still risking missing some objects (Fig. 2.2). So, for the calculation of the total number of clusters in the GC system of a host galaxy, the globular cluster specific

frequency, and the metallicity distributions, we will be using a portion of our catalogue, in which all sources are at or above 90% completeness level in all three filters and which also minimises the loss of the faint metal rich GCCs. For our sample of HCGs, that corresponds to V-filter magnitude cutoffs at 25.0 mag for HCG 42, and 25.5 mag for HCG 07, 31, and 59. The only exception is HCG 92, the farthest group in our sample. For this group we went down to 50% completeness level, to maximise the number of GCCs to strengthen the statistical conclusions validity. Unfortunately, even at that completeness level, we are still sampling only about 10% of the GCLF making the derived values of the total number in the GC populations ($N_{\rm total}$) and specific frequencies (S_N) of HCG 92 galaxies highly uncertain. Although we forego determining $N_{\rm total}$ and S_N for HCG 92 (for aforementioned reasons), we are still attempting a GCC population analysis, based on a "face value" GCC catalogue containing sources that are at or above the 50% completeness level with a cutoff at $V = 25.5$ mag (to minimise the loss of the faint metal rich GCCs).

2.3.5 Physical Extent of the SCC and GCC Systems

For each group, we present an image with regions that define the expected extent of the star cluster and globular cluster systems for each galaxy in that group (e.g., panel (b) of Fig. 2.9, panel (c) of Fig. 2.14). We define the extent of the star cluster systems as a brightness contour of $\sim 1.25\sigma$ above the background level in the V_{606} image to trace the stellar light in each galaxy. We successfully applied this criterion in our previous studies, and we enclose areas large enough to include sources that are likely associated with the host galaxies. To define the expected extent for the globular cluster systems (which populate much fainter galaxy halos), we initially use the formula outlined in Rhode et al. (2007):

$$y = [\,(45.7 \pm 9.5)\,x^2\,] - [\,(985 \pm 217)\,x\,] + (5320 \pm 1240), \tag{2.1}$$

where x is the mass of a host galaxy in $\log(M/M_\odot)$ and y is the expected radial extent of a system in kpc. However, given the quadratic nature of the above equation and the low mass of some galaxies in our sample, we needed to modify that expression to get more realistic numbers for the lower range of stellar masses. We made an assumption that for a small galaxy with a mass of $10^9 M_\odot$, the expected radial extent of the GC system would be 9 kpc. This assumption is supported by observed GCC distributions in galaxies in our HCG sample. Combining that with data of the GC systems extent from Rhode et al. (2007) and fitting a power-law function, we obtain the following relation:

$$y = 8.85 + (2.376 \times 10^{-22})\,x^{21.743}, \tag{2.2}$$

with x and y defined as above. This relation is valid for the range of log(mass) values from 9 to 12.5 $M_\odot$. The result (dashed line) can be seen in Fig. 2.3.

2.3.6 Photometric Estimates of Metallicity

We use the Sirianni et al. (2005) synthetic transformations to convert $(B-I)$ colours for GCs to the Johnson photometric system $(B-I)_0$ colours. We estimate the globular cluster metallicities

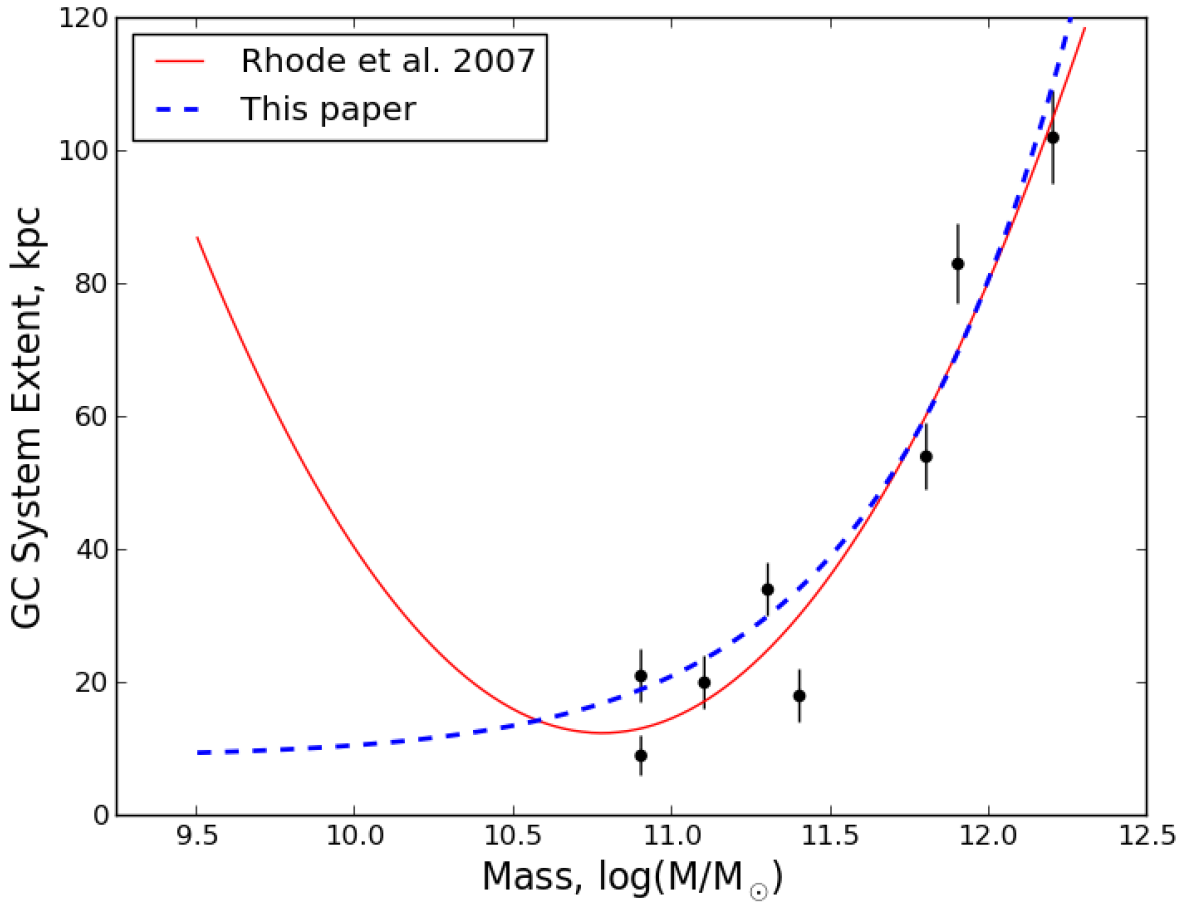

Figure 2.3: The relation between the expected extent of a globular cluster system from Rhode et al. (2007) (solid line) and the modified version used in this paper (dashed line). The modified relation was meant to be used only on the mass range presented in this plot (i.e., from 10^9 to $\sim 10^{12.5}$ $M_\odot$). The black dots are from the sample of Rhode et al. (2007), which consists of the radial extent of the GC system and the galaxy mass in solar masses for nine elliptical, S0, and spiral galaxies from their wide-field GC system survey. (A colour version of this figure is available in the online journal.)

Table 2.5: Completeness levels for our Hickson Compact Group sample. The values for distance moduli were taken from NED with the following cosmology parameters: $H_0 = 73.0$ Mpc km s^{-1}, $\Omega_{\rm matter} = 0.27$, and $\Omega_{\rm vacuum} = 0.73$.

Group	B_{435}		V_{606}		I_{814}		Distance	GCC cutoff	SCC cutoff
	50%	90%	50%	90%	50%	90%	modulus	$M_{V_{606}} < -7.8$ mag	$M_{V_{606}} < -9$ mag
HCG 07	27.4	26.7	27.5	26.3	27.1	26.4	33.76	25.96	24.76
HCG 31	27.3	26.7	27.4	26.4	27.2	26.5	33.68	25.88	24.68
HCG 42	27.2	26.2	27.2	26.1	27.1	26.0	33.86	26.06	24.86
HCG 59	27.2	26.6	27.2	26.5	27.1	26.5	33.99	26.19	24.99
HCG 92	26.9*	25.9*	27.1	26.0	27.0	25.9	34.74	26.94	25.74

* For HCG 92 B filter is B_{438} of WCF3 camera

using the $(B-I)_0$ to [Fe/H] transformation from Harris et al. (2006):

$$(B-I)_0 = 2.158 + 0.375[\mathrm{Fe/H}]. \tag{2.3}$$

For the GC population of our sample galaxies with a sufficient number of clusters (we use populations with 40 or more GCs), we plot the $(B-I)_0$ colour distribution and measure the specific frequency. We also plot $(B-I)_0$ colour distributions of GCs for each galaxy group in our sample. We use the GMM (Gaussian Mixture Modeling) code of Muratov & Gnedin (2010) to probe the bimodality and to determine the peaks and dispersions of these distributions. Because mixture modeling codes are generally sensitive to extended tails we use GMM on the distribution between $-2.5 <$ [Fe/H] < 1.0. The GMM results are recorded in Table 2.6 similarly to table 2 of Blakeslee et al. (2012), where one can find a detailed guide to interpreting the GMM results. The plots of the metallicity distributions for groups and galaxies from Table 2.6 are presented in Figures 2.14 – 2.18, and described on a group-by-group basis in §4 below.

2.3.7 Empirical Estimate of GC System Population

In recent work, Harris et al. (2013) have determined an empirical predictor of the total number of GCs for galaxies of all luminosities as a function of effective radius ($R_{\rm e}$) and velocity dispersion ($\sigma_{\rm e}$), given by equation:

$$N_{GC} = (600 \pm 35)\left[\left(\frac{R_{\rm e}}{10\ \mathrm{kpc}}\right)\left(\frac{\sigma_{\rm e}}{100\ \mathrm{km\ s^{-1}}}\right)\right]^{1.29\pm0.03}. \tag{2.4}$$

For those galaxies in our sample for which we were able to find the values of $R_{\rm e}$ and $\sigma_{\rm e}$ in the literature, we calculate the predicted numbers of GCs and compare them to our estimates (Table 2.7) based on the observed GC luminosity function in each galaxy.

Table 2.6: GMM results of probing modality of metallicity distributions.

Group/Galaxy (1)	N (2)	kurt (3)	p-val (4)	p1 (5)	p2 (6)	D (7)	Frac(2) (8)	Bimodal (9)
HCG 07	165	−0.748	0.115	−1.21 ± 0.23	−0.08 ± 0.26	2.46 ± 0.32	0.21 ± 0.19	No
HCG 07BD	83	−0.576	0.442	−0.86 ± 0.23	0.31 ± 0.27	2.73 ± 0.57	0.07 ± 0.18	No
HCG 42	400	−0.598	0.001	−1.05 ± 0.07	0.15 ± 0.14	3.14 ± 0.33	0.25 ± 0.08	Yes
HCG 42A	393	−0.611	0.001	−1.04 ± 0.07	0.16 ± 0.15	3.14 ± 0.35	0.26 ± 0.08	Yes
HCG 59	198	−0.475	0.592	−1.20 ± 0.46	−0.37 ± 0.33	1.69 ± 0.63	0.20 ± 0.33	No
HCG 59B	112	−0.306	0.803	−1.05 ± 0.36	−0.43 ± 0.28	1.36 ± 0.80	0.38 ± 0.29	No
HCG 92	290	−0.575	0.004	−0.79 ± 0.62	0.63 ± 0.53	2.65 ± 0.39	0.09 ± 0.36	Yes
HCG 92BD	67	−0.541	0.766	−0.46 ± 0.20	0.68 ± 0.32	2.76 ± 0.76	0.07 ± 0.19	No
HCG 92C	46	−0.814	0.010	−0.79 ± 0.34	0.59 ± 0.34	3.24 ± 0.61	0.18 ± 0.22	Yes?
HCG 92E	52	−0.608	0.738	−0.93 ± 0.28	0.09 ± 0.29	2.36 ± 0.67	0.29 ± 0.20	No

Notes. Columns list: (1) group, galaxy or region for which modality is being determined; (2) number of analysed GCs in given distribution; (3) kurtosis of the input distribution; (4) an indicator of the significance of a bimodal Gaussian over a unimodal Gaussian distribution (lower p-values are more significant); (5) mean of the first peak of the proposed bimodal Gaussian distribution; (6) mean of the second peak of the proposed bimodal Gaussian distribution; (7) separation of the peaks; (8) the fraction of GCCs that was assigned to the second peak of bimodal Gaussian distribution; (9) our expectation on bimodality of the given distribution based on the evidences displayed in this table. For the purpose of statistic significance only galaxies/regions with over 40 GCCs were checked for bimodality. The GCCs that were used for this purpose were all at or above 90% completeness level (except for HCG 92, where sources were at or above 50% completeness level). To minimise the loss of the faint metal enriched GCCs, we further apply a $V = 25.5$ magnitude cut ($V = 25.0$ mag for HCG 42). All these manipulations reduces the GCC numbers available for analysis, but at the same time, brings our completeness to 95% level for HCG 07, 31, 42, and 59.

2.4 Results and Discussion

Below, we present a short overview of the star cluster populations in our sample of Hickson Compact Groups. Analyses of the data presented in this catalogue for individual groups have been published in a number of publications. However, most of these analyses were on a case-by-case basis. In this publication, we aim for a systematic approach by applying the same criteria to the catalogue selection as whole. Because of this, there will be some differences between already published results and the numbers obtained in this paper. For example, the total number of GCCs may differ because we apply a different magnitude cut off or use a slightly modified distance modulus. Throughout the paper, we carefully outline all of our steps so the reader can follow them and, if desired, modify them to apply their own criteria.

Furthermore, we examine the star cluster populations of compact groups through the prism of the formation history and evolution of those groups. As mentioned previously, Konstantopoulos et al. (2010) outlined a proposed evolutionary sequence of CGs with respect to the amount and spatial distribution of cold gas in these groups. Our sample represents all three types of groups in terms of gas content, and so we can trace differences between the group

types through the lens of their star cluster populations.

To check the general properties of galaxies in our sample we plot two figures. First, we plot thr number of detected GCCs in galaxies as a function of stellar masses of those galaxies, Fig. 2.4. On average, the numbers of GCCs in a host galaxy are proportional to the stellar mass of that galaxy. However, galaxy 59B, and as the result the whole HCG 59, appears to have an excess of GCs given its stellar mass. This is discussed in §2.4.4 in more detail.

The second plot represents the number of "blue" star clusters (young SCs with ages $\lesssim$ 10 Myr) in each galaxy as a function of star formation rate of the host galaxies, Fig. 2.5. The young SCs were selected by applying the colour cut of $V - I < 0.1$. This generous colour cut enables us to keep the maximum number of young clusters, even those that may have significant reddening, avoiding both the evolutionary track loop around ages of 10 and 100 Myr and the old globular cluster region (see Fig. 2.9 for reference). The numbers of young SCs behave in a predictable manner as well: the galaxies with higher SFR have a larger number of young SCs. Notably, the large irregular 59d has a very high number of young SCs given its mass and SFR.

In the subsections below, we discuss the star and globular cluster populations of each group individually.

2.4.1 HCG 07

Star Cluster Candidates

This group is classified as a Type II group in the evolutionary sequence, with an intermediate amount of gas contained within the individual galaxies. As first presented in Konstantopoulos et al. (2010), although we do not observe strong signs of interactions between the galaxies in this group, the large number of young star clusters indicates that star formation rates are at an elevated level (see Fig. 2.5). From the distribution of clusters within the colour-colour diagrams compared to the simple stellar population models of Marigo et al. (2008), galaxies A, C, and D appear to have the youngest SCCs, while B has a more mature population. Most of the youngest SCCs are located down and to the right of the dashed evolutionary track of nebular emission for < 10 Myr clusters along the direction of the reddening vector, consistent with the hypothesis that these clusters have $A_V = 1$ to 3 mag. Similarly, Whitmore & Zhang (2002) found that the median extinction value for optically selected very young clusters ($\lesssim$ 4 Myr) in the Antennae galaxies is 2.6 mag. Moreover, from the distribution of SCCs it would appear that the star formation in galaxy C has a more extended history, whereas galaxies A and D exhibit an onset of more recent star formation (Fig. 2.9), as shown by lower cluster densities between the ages of 100 Myr and 1 Gyr.

Globular Cluster Candidates

The colour-colour plots of the GCC population for galaxies in HCG 07 are presented in Fig. 2.14 and their properties are presented in Table 2.7. Because galaxies A, C, and D are spiral galaxies (with C and D being face-on galaxies), the number of GCCs in them should be taken with caution. The GCCs located in the central regions and spiral arms may be contaminated by reddened young star clusters. For the GCCs of galaxies B and D, we considered the pair as a single object because of the difficulty of distinguishing cluster ownership given the overlap

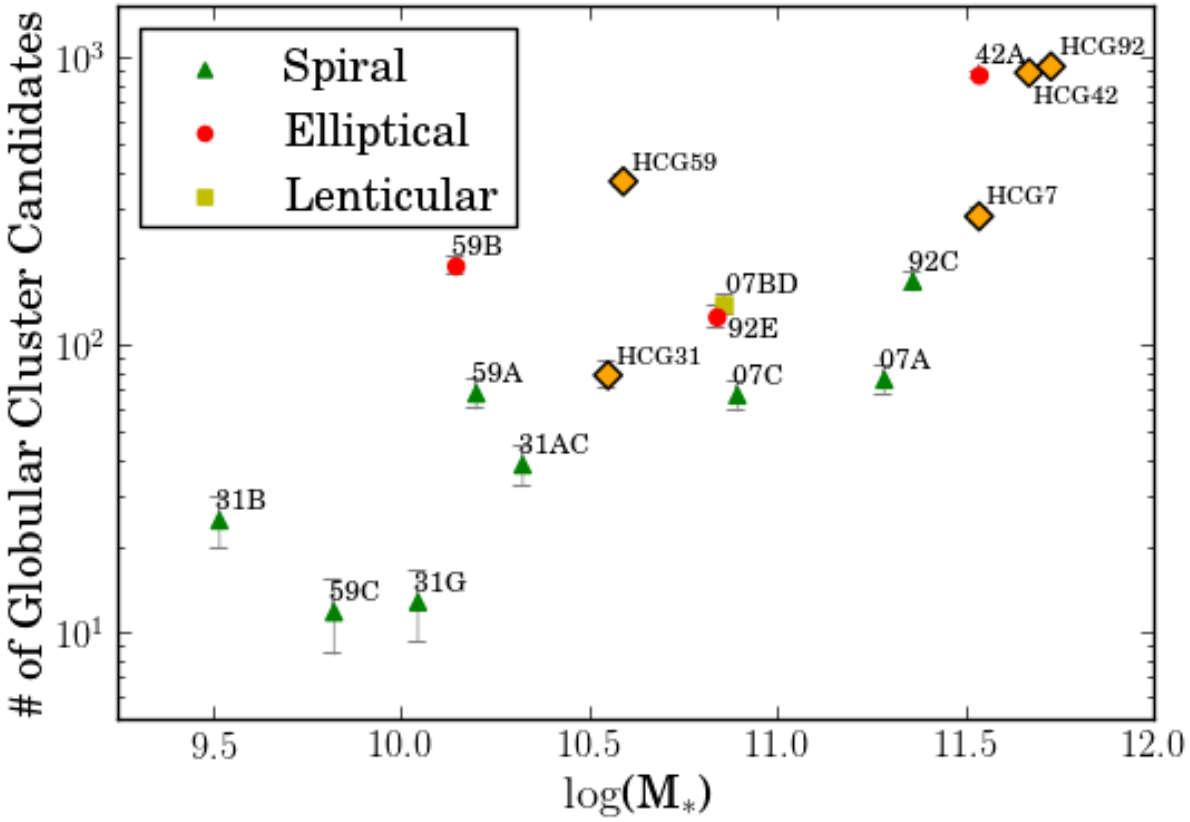

Figure 2.4: Plot of the number of GCCs ($M_{V_{606}} < -7.8$) in a galaxy vs. its stellar mass. Large diamonds represent HCGs, where the total number of globular clusters in each group is the summation of globular clusters of its individual galaxies. Similarly, the mass of a group is the summation of the stellar masses of all galaxies in that group from Desjardins et al. (2014). The masses were determined by SED fitting and the reported errors (T. Desjardins, private communication, Apr. 30, 2014) are not derived from the photometric uncertainties but rather from the fitting, and are very small (not visible behind the symbols). From this plot we can see that 59B has a very large globular cluster population, on a par with the total numbers for some individual groups. The region 07BD is presented here as a lenticular galaxy because the dominant galaxy B – expected to have the most GCCs of the two – is lenticular. (A colour version of this figure is available in the online journal.)

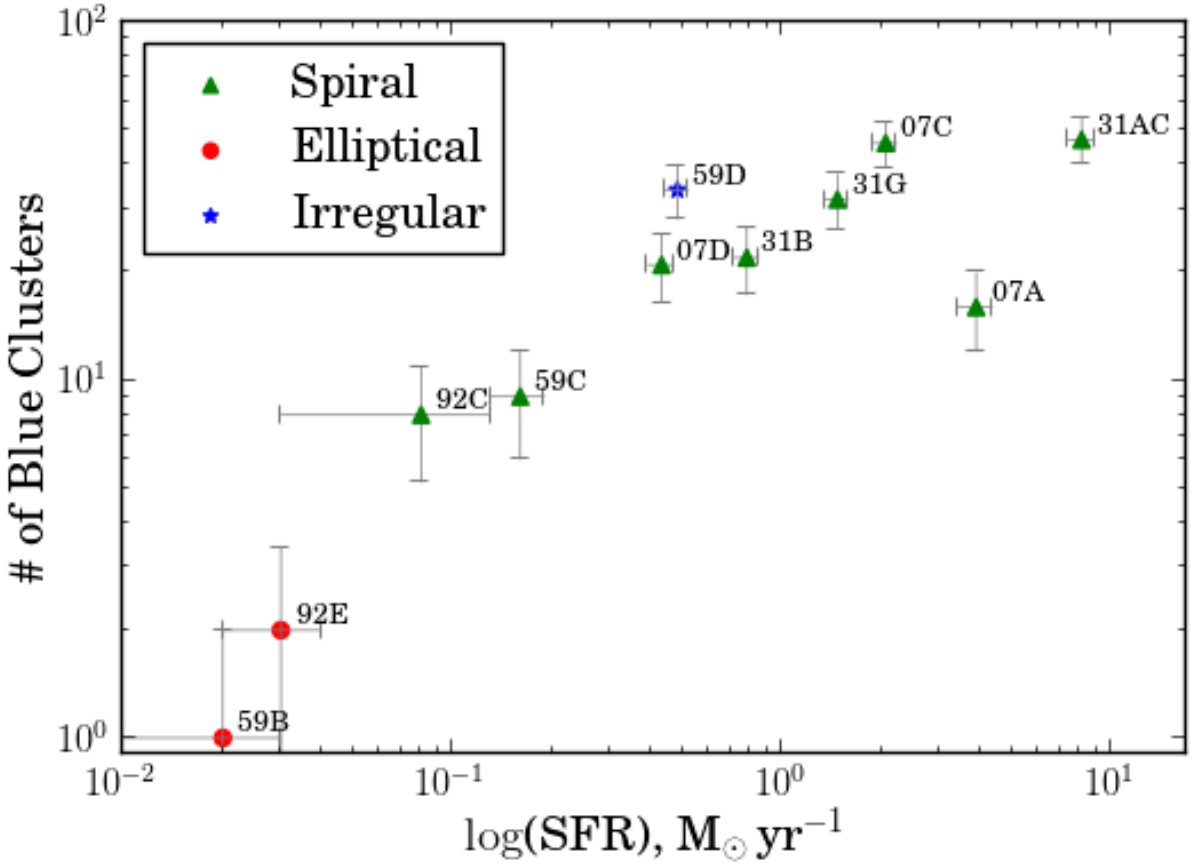

Figure 2.5: Plot of the number of "blue" clusters (with colour $V-I < 0.1$) in a galaxy versus its star formation rate. On average, the elliptical galaxies have low SFR with correspondingly low number of "blue" clusters; spirals have higher number of young clusters and higher SFRs. The relatively high number of young clusters and relatively low SFRs of galaxies 92C and 59C are consistent with a recent end to a star formation phase in these galaxies. However, the young clusters are still numerous and bright enough to be detected. Also, as was noted earlier, galaxies in HCG 07 exhibit elevated SFR, and correspondingly large numbers of young blue clusters, without visible signs of interactions. 59B has only one, 92E has two, and 07B has none of the blue clusters. This is expected given that these are elliptical/lenticular galaxies. The region 31AC is marked as a spiral because the largest of the two interacting galaxies, galaxy A, is classified as spiral. (A colour version of this figure is available in the online journal.)

of the expected extent of the GC systems in these galaxies. As derived from the $B - I$ colour, the average metallicities of the globular clusters in galaxy A (spiral) and the BD (B is lenticular, D is spiral) system are below Solar metallicity and comparable to metallicities of galaxies of comparable luminosity (e.g., Barmby et al., 2000; Chandar et al., 2004; Goudfrooij et al., 2003; Kundu & Whitmore, 2001; Peng et al., 2006). Galaxy A has 43 ± 7 observed GCCs with $V < 25.5$ mag. Compensating for the missing portion of GC system extent, and assuming a circular symmetry, we estimate the total number of observed GCCs as 62 ± 14 (taking in consideration the foreground sources, Table 2.7). At the given $V = 25.5$ mag cutoff, assuming the GCLF turnover at -7.4 ± 0.2 mag and width $\sigma = 1.2 \pm 0.2$ mag, we sample 28% ± 6% of the GCLF. Taking our completeness fraction as 0.95 ± 0.05, we conclude that for galaxy A ($M_V = -21.31$ mag) the total number of GCCs in the system is $N_{\rm total} = 226 \pm 73$ and specific frequency is $S_N = 0.7 \pm 0.2$. Applying the same approach to other galaxies in the group we find that for the BD region ($M_V = -20.9$ mag for B, $M_V = -19.7$ mag for D) $N_{\rm total} = 580 \pm 150$ and $S_N = 2.5 \pm 0.8$, for C ($M_V = -20.85$) $N_{\rm total} = 140 \pm 39$ and $S_N = 0.6 \pm 0.2$. We note that because galaxies A and C are spiral (A is highly inclined and C is a face-on), a significant number of objects with GC-like colours could, potentially, be reddened young star clusters.

2.4.2 HCG 31

Star Cluster Candidates

This group – classified as Type I with a cold gas-rich intra-group medium – consists of a number of small galaxies apparently coming together for the first time. The colour-colour plot of all detected SCCs, including those in the intra-group medium, paints a picture of a group that is actively forming stars for the last tens of Myrs (panel (a) of Fig. 2.10). Simultaneous interactions (e.g., galaxies AC and B) have triggered a very high star formation rate of 8.11 $M_\odot\,yr^{-1}$ (Tzanavaris et al., 2010), as shown by the large number of very young SCCs on the colour-colour plots. Virtually all of the SCCs in regions E and F (24 SCCs combined) are younger than 10 Myr. These regions are tidal features connecting spiral galaxy G, interacting pair AC and B, placing a time constraint on the interaction between those galaxies. There is a high concentration of SCCs around the region where the evolutionary track makes a backward loop, essentially making it impossible in this colour-space to distinguish between SCs of 10 to 100 Myr old (panels (c) and (d) of Fig. 2.10). However, given the low density of SCs older than 300 Myr ($\log(t) \sim 8.5$ yr) and the large number of young SCs ($\lesssim 10$ Myr), we consider it likely that most of the SCs in the vicinity of evolutionary track loop are closer to being a few tens of Myr old rather than 100 Myr.

Globular Cluster Candidates

The globular cluster population of HCG 31 as expected is rather small, with only 77 sources with colours similar to the Milky Way's GCs. Most of the clusters are situated within the boundaries of the major galaxies AC, B, and G, and, in all likelihood, are reddened young SCs (especially for galaxies B and G). Additionally, we do not expect a large GC population in this group as the galaxies are not massive enough to host a significant number of GCs with masses (and hence luminosities) large enough to be detectable at such distances. Furthermore,

we observe a lack of old (> 1 Gyr) star clusters in the colour-colour plot for SCCs of HCG 31 (panel (a) of Fig. 2.10).

Determining the total number of GCCs and GC specific frequencies in the galaxies of HCG 31 is more straightforward – there is no reason to extrapolate to areas outside the ACS field of view. At the $V < 25.5$ mag cutoff we observe 30% ± 7% of the GCLF, assuming the GCLF turnover is at -7.4 ± 0.2 mag and $\sigma = 1.2 \pm 0.2$ mag. Taking the completeness fraction as 0.95 ± 0.05, we obtain $N_{\rm total} = 67 \pm 23$ and $S_N = 0.6 \pm 0.2$ for 31AC ($M_V = -20.5$), $N_{\rm total} = 35 \pm 14$ and $S_N = 1.0 \pm 0.4$ for 31B ($M_V = -18.9$), and $N_{\rm total} = 28 \pm 13$ and $S_N = 0.7 \pm 0.3$ for 31G ($M_V = -19.0$).

2.4.3 HCG 42

Globular Cluster Candidates

The HCG 42 group consists of four large galaxies, three of which are elliptical and one lenticular, with low overall H I content. In the evolutionary sequence scheme this group qualifies as Type III. More details on this group configuration including the dwarf galaxy population can be found in Konstantopoulos et al. (2013). Because of the predominance of elliptical galaxies in the group and the low content of the cold gas we do not expect to find young and intermediate-age star clusters, as illustrated by Fig. 2.11 panel (c). Thus, we start our star cluster population analysis by looking at the GCCs. The ACS observations of this group consist of only one pointing that covers the two elliptical galaxies, 42A and C (panel (b) of Fig. 2.11). The brightest of these two galaxies, 42A, has an optical luminosity comparable to M87 ($M_{\rm V,42a} = -22.8$ and $M_{\rm V,M87} = -22.77$; Misgeld & Hilker, 2011). The extent of the globular cluster system for this galaxy covers most of the field of view and overlaps the extent of the globular cluster system of the neighbouring galaxy 42C. From the magnitude difference of these two galaxies ($M_{\rm V,42c} - M_{\rm V,42a} = 2.11$ mag), most of the detected globular cluster candidates in this image are expected to belong to 42A. Additionally, northward of 42A lies a dwarf galaxy [VC94] 095753−1922.2, which has been identified as a member of HCG 42 (Carrasco et al., 2006; Konstantopoulos et al., 2013). We observe a slight overdensity of globular clusters in that region (panel (c) of Fig. 2.16). However, following the same line of argument as above, we consider those clusters to be part of the 42A globular cluster system. Altogether, there are 878 detected GCCs that located inside the GC system extent. The photometric metallicity distribution as probed by $B_{435} - I_{814}$ was determined for 393 of them (for reasons mentioned in §2.3.4). The distribution has a very well defined bimodality with peaks at [Fe/H] $= -1.04 \pm 0.07$ and [Fe/H] $= 0.16 \pm 0.15$, for the 'blue' and 'red' peaks, respectively. Both peaks appear to be more metal rich by ~ 0.4 as compared to the average peaks of GC metallicity distributions of approximately −1.5 and −0.5 measured for different types of galaxies (VanDalfsen & Harris, 2004, and references within).

From RC3, we find that the effective radius is 32.″9 (estimated from a Johnson B image and corresponding to ~ 9.4 kpc); the value for the velocity dispersion of 321.4 ± 9.3 was obtained from HyperLeda[3]. Using the above numbers and equation 2.4, we find that the predicted population of the GC system for 42A is 2498 ± 146 GCs. At the cutoff magnitude of $M_V = 25.0$ and with the assumption for GCLF turnover at -7.4 ± 0.2 mag and $\sigma = 1.2 \pm 0.2$ mag, we

[3] http://leda.univ-lyon1.fr

probe 14% ± 7% of the GCLF. Taking a completeness fraction as 0.95 ± 0.05 we estimate $N_{\rm total} = 3420 \pm 1710$ and $S_N = 2.6 \pm 1.3$. Although the $N_{\rm total}$ number is $\sim 50\%$ larger that one predicted by equation 2.4, it is still within reasonable uncertainties. Given the large number of GCCs in a luminous, central dominant group elliptical, it seems likely that 42A is the product of a gas-rich merger from several Gyr ago.

2.4.4 HCG 59

Star Cluster Candidates

According to Konstantopoulos et al. (2012), HCG 59 belongs to the Type III groups, with low H I content relative to its apparent dynamical mass. However, a number of young SCCs are found in this group, located in the smaller galaxies 59C and D (panels (f) and (g) of Fig. 2.12). The SCC population of the spiral 59C is somewhat small, with only 16 SCCs detected in the disc of the galaxy. These clusters span a range of ages between a few Myr and 1 Gyr, similar to clusters in the large irregular 59D. The difference between the SCC populations of those galaxies is that 59D has a larger population of clusters detected and there is also a number of very young clusters present ($\sim 1 Myr$). Given that these two galaxies have approximately the same stellar mass (Table 2.2) we can compare their sSFRs and see that 59D is forming stars over 8 times more efficiently than 59C (sSFRs are 0.024 $\rm Gyr^{-1}$ and 0.200 $\rm Gyr^{-1}$ for 59C and 59D, respectively), which can be seen clearly in the colour-colour plots for each galaxy. The irregular galaxy 59D has a higher sSFR likely because of the larger amount of available cold gas. Star formation in 59D may also be enhanced dynamically because of its proximity to 59A.

Globular Cluster Candidates

The majority of GCCs in HCG 59 are part of the globular cluster system of the elliptical galaxy 59B (IC 0736) (panels (d) and (g) of Fig. 2.17). Intriguingly, it appears that the GCC population is much richer than would be expected of a galaxy of its luminosity ($M_B = -18.5$; Sabater et al., 2012). We use the SDSS (York et al., 2005) values for the velocity dispersion, $\sigma = 99.9\ \rm km\,s^{-1}$ and the value of the effective radius $R_{\rm e} = 3\farcs18$ (as determined from a deVaucouleurs profile) which corresponds to 0.96 kpc. Substituting these numbers into equation 2.4, we find that the predicted number of GCs for this galaxy $N_{GC,\rm pred} = 29 \pm 2$ is significantly smaller than the number of GCs estimated from the observed bright end of the GCLF ($N_{\rm total} = 507 \pm 150$, details to follow), and is in fact even smaller than the number of detected GCCs ($N_{\rm All\ GCCs} = 191 \pm 14$ or $N_{95\%} = 112 \pm 11$ for sources with 95% completeness level). However, we note that the velocity dispersion value taken from SDSS appears to be rather low for a galaxy with this mass (see Table 2.2). In addition, we point out the unusually dense population of extragalactic star clusters located to the south-west of 59B (panel (d) of Fig. 2.17), away from the visual center of the group and along the stellar stream that appears to connect galaxies A and B Konstantopoulos et al. (2012). One of the possible explanations for this population of clusters is that they are possibility a remnant of a prior interaction between the A and B galaxies, approximately 1 Gyr ago (see Konstantopoulos et al. (2012) for further discussion).

At the cutoff magnitude of $M_V = 25.5$ and with the assumption of a GCLF turnover at -7.4 ± 0.2 mag and width $\sigma = 1.2 \pm 0.2$ mag, we probe 22% ± 6% of the GCLF of galaxies in

Table 2.7: General properties of GCC systems in galaxies in our sample.

Galaxy (1)	$N_{\rm GCC}$ (2)	$N_{\rm contam}$ (3)	$N_{\rm total}$ (4)	S_N (5)
HCG 07A	62 ± 14	2 ± 1	226 ± 73	0.7 ± 0.2
HCG 07BD	155 ± 22	2 ± 1	580 ± 150	2.5 ± 0.8
HCG 07C	38 ± 6	2 ± 1	140 ± 39	0.6 ± 0.2
HCG 31AC	19 ± 5	1 ± 1	67 ± 23	0.6 ± 0.2
HCG 31B	10 ± 3	1 ± 1	35 ± 14	1.0 ± 0.4
HCG 31G	8 ± 3	1 ± 1	28 ± 13	0.7 ± 0.3
HCG 42A	465 ± 26	4 ± 2	3420 ± 1710	2.6 ± 1.3
HCG 59A	18 ± 5 *	1 ± 1 **	86 ± 33	0.7 ± 0.3
HCG 59B	106 ± 11	1 ± 1 **	507 ± 150	8.7 ± 2.6
HCG 59C	≤ 2	1 ± 1 **	< 10	< 0.1

Notes. Columns list: (1) galaxy id; (2) number of GCCs in the system's full extent (detected numbers of GCCs are scaled if full system extent is not visible; foreground contamination is also taken into account); (3) estimated number of contamination sources from Besançon Milky Way stellar population model (Robin et al., 2003) in the direction of the group up to the distance of 100 kpc, with colours similar to MW GC colours and in the visible area of GC system extent; (4) estimated total number of GC population based on GC luminosity function; (5) specific frequency. * Because the extent of 59A GC system overlaps sources from 59D (which are, most likely, reddened young star clusters), the predicted number of GCCs for 59A galaxy was obtained by subtraction of 59D sources from all detected sources in that region. ** For HCG 59, the background contamination is much higher (4 ± 2), due to the close proximity of the Sagittarius dwarf galaxy (Konstantopoulos et al., 2012).

this group. Taking the completeness fraction as 0.95 ± 0.05 we estimate $N_{\rm total} = 86 \pm 33$ and $S_N = 0.7 \pm 0.3$ for 59A ($M_V = -20.1$; after removing clusters around the irregular 59D that are within the expected 59A GC system extent, but are most likely reddened young star clusters), and $N_{\rm total} = 507 \pm 105$ and $S_N = 8.7 \pm 2.6$ for 59B ($M_V = -19.4$). For galaxy 59C, the number of detected GCCs from the 95% completeness sub-catalogue, is on a par with the number of contaminating sources, $N_{obs} \leq 2$. That gives us the upper limits for $N_{\rm total} < 10$ and $S_N < 0.1$. We did not estimated $N_{\rm total}$ and S_N for 59D because the detected objects may well be reddened bluer objects, rather than GCCs.

Being the only elliptical with sufficient number of GCCs in this group, 59B was checked for bimodality in its metallicity distribution. The GMM statistical results do not support the idea of bimodality, rather, it would appear that the distribution is unimodal with a peak at [Fe/H] = −1.04 ± 0.05.

In all, the population of old clusters in HCG 59 is intriguing enough to warrant further study.

2.4.5 HCG 92

Star Cluster Candidates

HGC 92, which also known as Stephan's Quintet and which classified as Type II in the proposed CG evolutionary sequence (Konstantopoulos et al., 2010), is a group of four galaxies (the fifth of the Quintet is the foreground interloper NGC 7320) with numerous signs of past and ongoing interactions. As a result, this group exhibits the largest number of detected star clusters in our sample. There are a number of interesting features singular to this group which are explored in depth in Fedotov et al. (2011). For example, we were able to detect star clusters in two tidal tails, the Old Tail (OT) and Young Tail (YT) (Fig. 2.13). Because tidal tails typically have low gas and dust content ($A_V \lesssim 0.5$ mag; e.g., Temporin et al., 2005), star clusters in tails usually suffer minimal reddening and their ages estimated from *BVI* colour-colour plots are more accurate than in galaxy discs. In our case, star clusters detected in these tails have compact distributions in the colour-colour plane, supporting the idea that SCCs within each tidal tail were formed coevally (Trancho et al., 2012), presumably during the interactions that caused the formation of those features. Thus, from overdensities of star clusters in colour-colour plots and supplemental information from the literature, we were able to estimate the ages for the young and old tidal tails to be 150–200 Myr and 400–500 Myr, respectively (Fedotov et al., 2011).

HCG 92 is an ideal system to study populations of star clusters forming outside of galaxies. In particular, there are two areas of extragalactic clusters labelled as the Northern Star Burst Region (NSBR) and the Southern Debris Region (SDR). The NSBR has a SCC population that spans a wide range of ages, from young SCCs of a few Myr to very old globular clusters of over 10 Gyr old. This region includes two intersecting tidal arcs, a byproduct of the interaction between 92B (NGC 7318B) and 92D (NGC 7318A). The young SCs detected in the region were likely formed during that interaction. The presence of a significant number of intermediate-age SCCs (ranging from 100 to 500 Myr old) could be indicative of earlier interactions involving 92C (NGC 7319), NGC 7320C, and perhaps 92D (Moles et al., 1997; Xu et al., 1999). And finally, there are a few old star clusters likely deposited into that region through gravitational interactions between the galaxies.

Consideration of the SCC population of the Southern Debris Region, on the other hand, paints a bit different picture. To begin with, there are not as many very young (1 to 8 Myr) SCs in that region. Also, there is a well-defined separation between two groups of SCCs in the colour-colour plane, one group consists of clusters that are approximately 10 to 100 Myr old (unfortunately, it is impossible to establish more precise ages based only on *BVI* photometry) and the second group, a collection of older star clusters ranging in age from 1 to 10 Gyr. Interestingly, there appears to be a concentration of clusters with ages between 6 and 8 Gyr. Since it is highly unlikely that a galaxy interaction would specifically launch into this extragalactic region star clusters of such a limited age range, we speculate that these clusters (with ages 6 to 8 Gyr) were formed together at some location, and the population of the younger SCCs is either the latest addition or a chance projection. We consider the former as more likely explanation, and as such, SDR could potentially be the remnants of a dwarf galaxy that used up its last reservoir of gas to form these younger population of clusters. However, there are a few reasons why this might not be true. For example, the SDR region appears to extend over

a large area for a dwarf galaxy, and there is no detection of extended, diffuse light consistent with a dwarf galaxy.

The spiral galaxy 92C is the largest galaxy in the group. At the same time, it has no detectable H I (Sulentic et al., 2001), which most likely was stripped during previous interactions among the group members (Moles et al., 1998). Unless the galaxy manages to acquire more cold gas, the intermediate age (100 to 500 Myr) population of SCCs is likely the trace of the last epoch of star formation in that galaxy.

Globular Cluster Candidates

For the GCC population in SQ we focus on three regions (panel (c) of Fig. 2.18). One region is associated with the elliptical galaxy 92E (NGC 7317), another one with the spiral galaxy 92C (NGC 7319), and the last one with the interacting pair 92B and D (NGC 7318B and A). For the last system, we expect that a large fraction of GCCs belong to 92D: first, because it is an elliptical galaxy, and, secondly, it is more massive than the spiral 92B (Table 2.2). According to our estimates of the GCC system extent, the GCC systems of 92C and 92BD overlap. Moreover, the overlap adds virtually no GCCs to 92BD region, whereas the expected system extent of 92C adds an appreciable part of the eastern tidal feature of 92BD.

According to GMM statistics, the distribution of all GCCs in SQ has detectable bimodality (panel (b) of Fig. 2.18). However, the individual distributions for each galaxy/region do not have well defined bimodality, with the possible exception in the case of 92C. However, this galaxy does not have a large enough number of GCCs for statistically significant analysis. If we look at the unimodal peaks of -0.55 ± 0.12, -0.38 ± 0.08, and -0.63 ± 0.10, for the GCC systems in 92C, 92BD, and 92E, respectively, we notice that these values are a bit larger (less negative) compare to the average value of Galactic GCs, the bulk of which have metallicities around [Fe/H] = -1.3 (Murdin, 2001).

2.4.6 Bimodality of GCC Population of Elliptical Galaxies

Above we discussed bimodality in the galaxies from our sample and the results are outlined in Table 2.7. We compare our results with those in the literature, in particular, the bimodality analysis in the sample of 92 elliptical galaxies in the Virgo cluster (Peng et al., 2006). The authors found a relationship between the GCs colour distribution modality and absolute magnitude of the host galaxy. According to their fig. 5, which plots the colour distributions of GCs in seven bins of host galaxy magnitude, for the luminous HCG 42A we expect a well defined bimodality, whereas with the much lower luminosity of HCG 59B, only a weak bimodality is expected. Given that we observe only 22% ± 6% of the total GC population in that galaxy, it is not surprising that we can not confirm bimodality of GC distribution. Thus, our findings compare well with the conclusions of Peng et al. (2006): HCG 42A has a well defined bimodal distribution and the colour distribution of HCG 59B GCCs is unimodal. The question of the nature of colour distribution for HCG 92E is still open. The luminosity of HCG 92E, according to Peng et al. (2006), corresponds with a relatively well defined bimodality. However, we currently do not posses the required number of GCCs to definitively answer that question. As it is, with the currently observed number of GCCs, HCG 92E has a unimodal distribution.

2.4.7 Star Cluster Populations in Compact Groups

Here, we relate the star cluster populations to the CG evolutionary sequence proposed by Konstantopoulos et al. (2010, see their fig. 1). Upon inspection, the SCC populations of different group types have qualitative differences. Specifically, the population of HCG 31 (panel (d) of Fig. 2.6), classified as a Type I group (gas-rich and dynamically young), is distinguished by a large number of young and intermediate-aged SCs. Type II groups, represented in our sample by HCG 07 and 92 (panels (b) and (e), respectively), still have a large number of young and intermediate SCs; however, a population of > 500 Myr – 10 Gyr is also well defined. For compact groups of Type III, which predominantly consist of early type galaxies, we can observe the lack of young SCs, and a significant reduction in the numbers of intermediate-aged SCs (HCG 42, panel (f)). Initially, Johnson et al. (2007) classified HCG 59 (panel (c)) as Type II group. The recent work of Konstantopoulos et al. (2013) has associated five additional dwarf galaxies with that group. The updated information on velocity dispersion and H I mass led to a change of the HCG 59 from Type II to Type III. However, based on the observations outlined above, the SC population of HGC 59 would appear to be more consistent with that of Type II groups.

These discrepancies between type classification based on the SC populations and on the ratio of H I to dynamical mass point to the issue of accuracy in measurements of the dynamical masses. In particular, it is quite difficult to accurately measure a dynamical mass of a group given only a handful of radial velocities and the projected separations between galaxies (McConnachie et al., 2008). It may be more appropriate in this case to classify the groups based on the ratio of H I to total stellar mass, which can be much more reliably measured from near-to-mid infrared photometry (Desjardins et al., 2014).

2.4.8 Cluster Luminosity Function

Figure 2.7 shows the cluster luminosity functions (CLFs) for selected galaxies from our sample. To obtain statistically significant results, only galaxies with more than 40 SCCs were used. In each plot, the CLF is shown as a cumulative distribution function of the absolute magnitude, $M_{V_{606}}$. The solid line represents the best- fitting slope of the distribution that was determined by the least squares fit over the range covered by the line. This range was chosen manually, based on our assessment of the linear region of each CLF starting at the faint-end cutoff. The dashed line represents the best- fitting slope over a common range for all CLFs, from -9 mag to -10.75 mag. The slope is for a power-law distribution index α from $NdL \propto L^{-\alpha}dL$ as $2.5 \times$ slope + 1. The overall range of the indices (from here on we are using slopes fitted to the custom ranges) for CG galaxies in our sample is from -2.13 to -3.24 (see Table 2.8 for all the numbers). Figure 2.8 represents a plot of the LF index as a function of Hubble T-type. For comparison, on the same figure, we overplot the data for 20 nearby star-forming spiral galaxies, which span Hubble T-types from 2 to 9, obtained from Whitmore et al. (2014). As can be seen, our results do not reproduce the shape of the LF index distribution of Whitmore et al. (2014). Moreover, it appears that no significant correlation between α and T can be observed.

Overall, the CLF indices of spirals in our sample of galaxies are in reasonable agreement with the values reported in other works (e.g., Larsen, 2002; Ryon et al., 2014; Whitmore et al., 2014), except for a noticeable outlier 07C, which is a bit more negative than in Gieles et al.

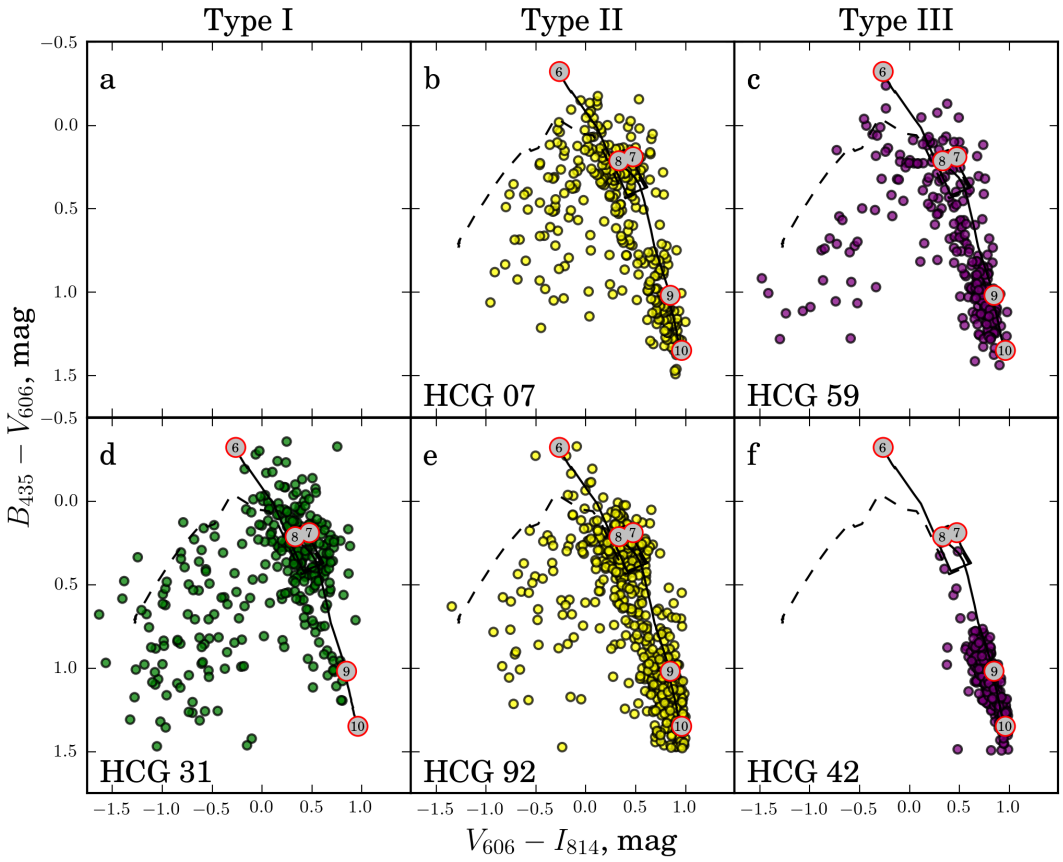

Figure 2.6: Colour-colour plots of the SCC populations of the compact groups in our sample, arranged similarly to Fig. 1 in Konstantopoulos et al. (2010). The upper panels represent groups with the H I gas contained within the member galaxies, whereas the lower panels represent groups with the H I gas stripped from the galaxies. These groups tend to have a rich intra-group medium. Although Konstantopoulos et al. (2013) have classified HCG 59 (panel c) as a Type III group based on its estimated dynamical mass, the SC population is more consistent with a Type II group. (A colour version of this figure is available in the online journal.)

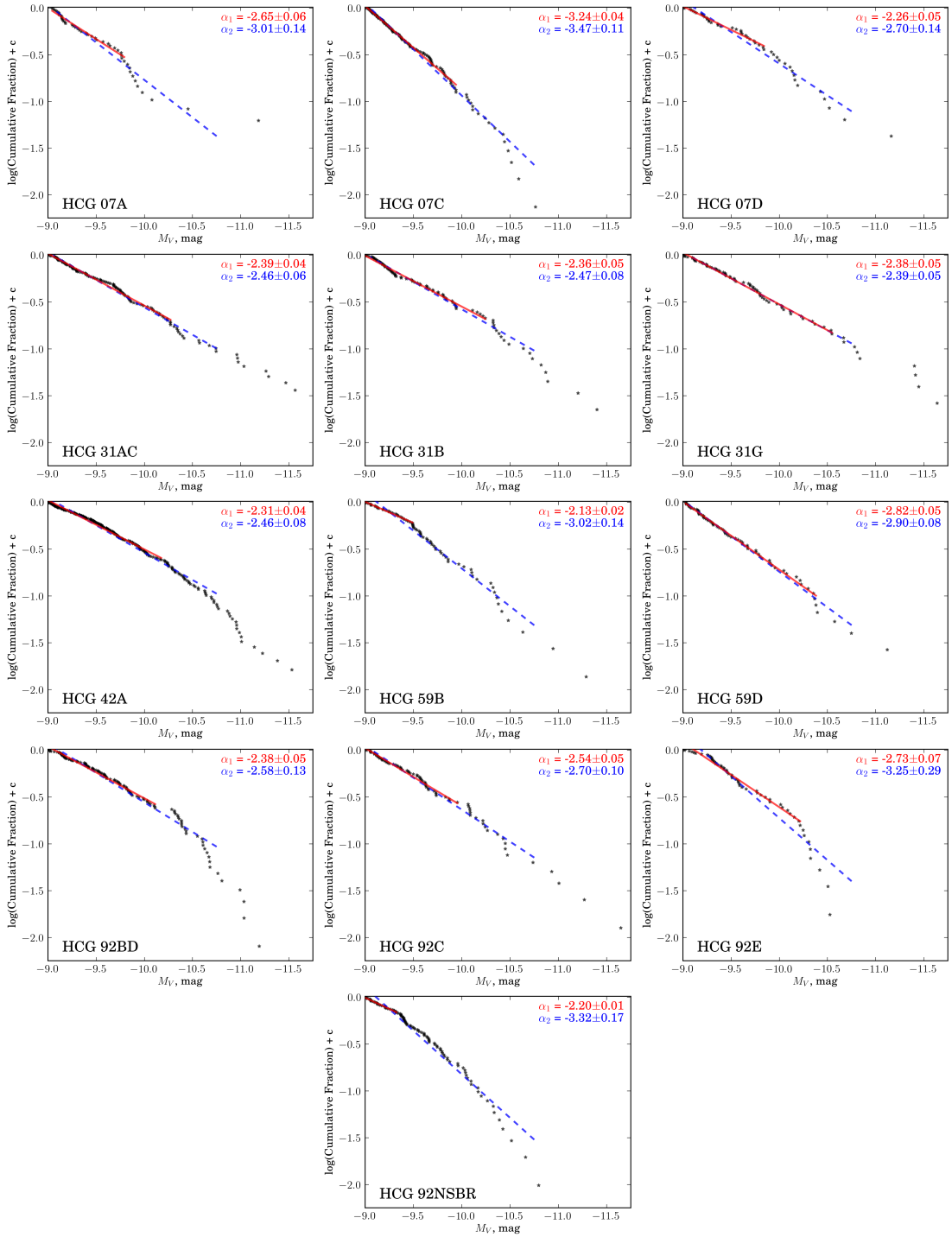

Figure 2.7: Cumulative luminosity functions of galaxies in our sample. For statistically significant results, only galaxies with more than 40 SCCs were used. The slopes were determined by a least squares fit over the range covered by the line. The solid line represents the best-fitting slope over the range that was chosen manually, whereas the dashed line represents the best-fitting slope over a common range for all CLFs, from −9 mag to −10.75 mag. The corresponding α values for each slope are displayed in the upper right corner of each panel. (A colour version of this figure is available in the online journal.)

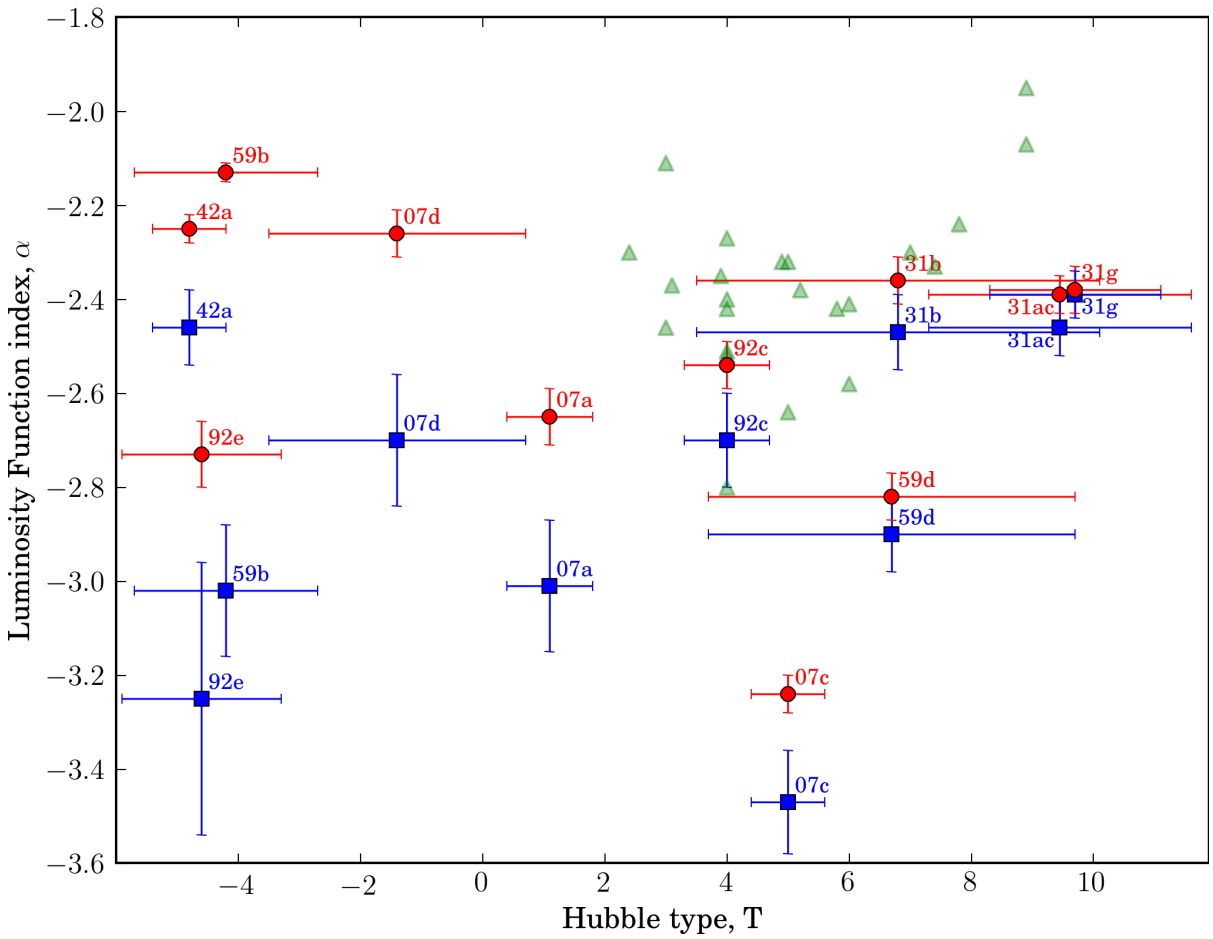

Figure 2.8: Plot of CLF index α as a function of Hubble type (T). Red circles represent indices based on fitting custom ranges of CLFs, and blue squares represent indices of common range fittings. In all cases, extending the fitting range makes the indices more negative. Green triangles are the indices obtained from Whitmore et al. (2014), who studied a sample of 20 nearby star-forming spiral galaxies and found a correlation between α and T, for T ranging from 2 to 9. Based on our sample, it appears that no significant correlation between α and T can be observed. Out of 11 data points in this plot, 1 point does not represent a galaxy itself but rather a pair of close interacting galaxies: 31AC – a combination of spiral and irregular galaxies. Because their Hubble type is very close in value (for 31A T = 8.9 ± 0.9, for 31C T = 10 ± 2), for the T value of 31AC we adopted the value of 9.45 ± 2.15. For another interacting pair, 92BD – a close pair of a spiral and an elliptical, the morphological types are very different and the "average" value would not be meaningful. For this reason, we do not include this data point in our plot. The morphological types are taken from HyperLeda. (A colour version of this figure is available in the online journal.)

Table 2.8: CLF indicies for galaxies in our sample that have over 40 SCCs.

Galax/Region	N_{SCC}	Type	α-index		Magnitude range	
			α_1	α_2	custom	common
HCG 07A	48	Sb	-2.65 ± 0.06	-3.01 ± 0.14	$-9.00 \ldots -9.81$	$-9.00 \ldots -10.75$
HCG 07C	135	SBc	-3.24 ± 0.04	-3.47 ± 0.11	$-9.00 \ldots -9.96$	
HCG 07D	47	SBc	-2.26 ± 0.05	-2.70 ± 0.14	$-9.00 \ldots -9.91$	
HCG 31AC	138	Sdm + Im	-2.39 ± 0.04	-2.46 ± 0.06	$-9.00 \ldots -10.28$	
HCG 31B	89	Sm	-2.36 ± 0.05	-2.47 ± 0.08	$-9.00 \ldots -10.28$	
HCG 31G	76	Sbc	-2.38 ± 0.05	-2.39 ± 0.05	$-9.00 \ldots -10.60$	
HCG 42A	246	E3	-2.31 ± 0.04	-2.46 ± 0.08	$-9.00 \ldots -10.20$	
HCG 59B	73	E0	-2.13 ± 0.02	-3.02 ± 0.14	$-9.00 \ldots -9.49$	
HCG 59D	75	Im	-2.82 ± 0.05	-2.90 ± 0.08	$-9.00 \ldots -10.39$	
HCG 92BD	124	Sbc + E2	-2.38 ± 0.05	-2.58 ± 0.13	$-9.00 \ldots -10.14$	
HCG 92C	79	SBc	-2.54 ± 0.05	-2.70 ± 0.10	$-9.00 \ldots -10.24$	
HCG 92E	57	E4	-2.73 ± 0.07	-3.25 ± 0.29	$-9.00 \ldots -9.91$	
HCG 92NSBR	102	–	-2.20 ± 0.01	-3.32 ± 0.17	$-9.00 \ldots -9.34$	

Notes. Types of galaxies are taken from Hickson et al. (1989). Region 92NSBR represents a collection of intergroup clusters and as such does not have a morphological type. The magnitude range column specifies the range over which the slope was fitted.

(2006b). In addition, the galaxies in HCG 31 have very similar α-values (-2.39 ± 0.04, -2.36 ± 0.05, and -2.38 ± 0.05, for galaxies 31AC, 31B, and 31G, respectively); the irregular 59D has a rather high negative α-value of -2.82 ± 0.05. As in the case of 07A and 07C, recent (and on-going) star formation could be responsible for the steeper value of α in 59D. A sustained star-formation episode could cause a build-up of clusters near the low-luminosity end of the luminosity function as old clusters fade with age.

Some CLFs for the galaxies in our sample exhibit a bend at the bright part of the distribution, with that part of the distribution being steeper, a trend that was also noticed in the aforementioned studies. Gieles et al. (2006b) argues that the bend in the CLF corresponds to the upper mass limit in the cluster initial mass function. For example, their linear fit to the CLF of the Antennae galaxies suggests a bend at $M_V = -10.3$, which corresponds to a maximum mass of $\sim 2.5 \times 10^6$ $M_\odot$(with the assumption that the oldest cluster in the CLF is 3 Gyr). In our sample, the galaxies 42A, 92BD, 92E display a bend at magnitudes of approximately $-10.2, -10.4$, and -10.3, respectively. Galaxy 59B exhibits two possible bends, one at -9.5 and the other one at ~ -10.3. Because there is the possibility that the GC system for this galaxy consists of two populations, its own GCs and clusters stripped from 59A (see § 2.4.4), we speculate that each bend is imprinted on the overall CLF by the two constituent cluster populations.

Also worth noting is that the galaxies with active star formation according to the cluster colour-colour plots (in particular galaxies C and D in HCG 07; AC, B, and G in HCG 31, and irregular galaxy D in HCG 59) show the most linear CLFs over a broad range of absolute magnitudes.

2.4.9 Spatial Distribution of Globular Clusters in Elliptical Galaxies

For the three elliptical galaxies in our sample with significant GC systems (HCG 42A, 59B, and 92E), we examined the physical distribution of the globular clusters in those galaxies as a function of metallicity (Fig. 2.19). We divided the clusters in each system into three groups, based on their metallicity distribution plots (e.g., panel (e) of 2.16). Specifically, all clusters to the left of the "blue" peak are considered to be relatively metal-poor. Similarly, all clusters rightward of the "red" peak are considered relatively metal-rich. The clusters between the peaks are tagged as having an intermediate metallicity content. Then we plot the cumulative distribution of the clusters as a function of projected distance from the center of the galaxy. We find that 42A and 59B have more metal-rich clusters concentrated closer to their galaxy centres, clusters with intermediate metal content are distributed throughout the galaxies, and metal-poor clusters tend to have higher concentrations in the outer regions of the galaxies.

A Kolmogorov-Smirnov (KS) statistical test was used to determine if the cumulative radial distributions of the different metallicity clusters are consistent with each other. The results showed that the p-value for comparing the low and high metallicity distributions in 42A was $\sim 10^{-4}$, which allows us to reject the null hypothesis (that they are drawn from the same parent population) with $> 99.9\%$ confidence. Similarly, $p = 4 \times 10^{-4}$ for the rich and poor clusters of 59B, and so their radial distributions are also significantly different. For galaxy 92E the p-values for all combinations of distributions are not rejecting the null hypothesis. From the lower panel of Fig. 2.19 it appears that the GCs of different metallicities are mixed throughout the galaxy. However, we have to note that the statistics of small numbers might be at play here. The way we split the GC population into three groups with the different metallicity content leaves the the metal-rich population of 92E with only 7 GCs (20 and 26 GCs in metal poor and medium metal content populations, respectively). Thus, it is highly speculative to talk about the radial distribution of the metal-rich clusters. To try to avoid this situation, we split GC sample into two roughly equal groups, metal rich and metal poor, at [Fe/H] $= -0.63$ (panel (i), fig. 2.18). The KS test does not reject the null hypothesis, and so it would appear that GCs do not have a preferential distribution based on their metallicities. One of the possible explanations for this apparently well-mixed distribution would be a dry merger between two galaxies of similar mass. An examination of the unsharp-masked image of 92E to look for signs of recent interaction such as shells or streams did not reveal any such features.

2.5 Conclusions

We present a catalogue of star clusters detected in five compact galaxy groups (HCG 07, 31, 42, 59, and 92), based on sensitive, high-resolution multi-colour images from the *Hubble Space Telescope* Advanced Camera for Surveys and Wide Field Camera 3 (in the case of HCG 92) with the goal of examining the properties of the star cluster systems of compact group galaxies overall and further assisting researchers in star cluster-related studies. Altogether, the catalogue consists of 18,292 objects. After applying a number of criteria, we left with 1963 star cluster candidates and 1505 globular cluster candidates detected in 16 galaxies in the high confidence samples. The entirety of the photometric data from this catalogue is presented in the electronic Table 2.9.

Table 2.9: A sample table of the *BVI* catalogue for star clusters in Hickson compact groups. The full catalogue is available online.

RA	Dec	B			V			I			χ_I	S1	S2	S3	S4	S5	G1	G2	G3	G4	SCC	GCC	[Fe/H]	HCG
deg	deg	mag	err	sharp	mag	err	sharp	mag	err	sharp														
(1)	(2)	(3)	(4)	(5)	(6)	(7)	(8)	(9)	(10)	(11)	(12)	(13)	(14)	(15)	(16)	(17)	(18)	(19)	(20)	(21)	(22)	(23)	(24)	(25)
338.9945	33.936701	28.921	0.502	-0.122	27.844	0.203	-0.67	26.716	0.107	0.143	1.35	0	0	1	1	0	1	1	0	1	-	-	0.1232	92
339.04261	33.936755	25.844	0.057	0.112	25.462	0.048	0.224	24.997	0.055	0.218	1.784	1	1	1	1	1	1	1	1	0	yes	-	-3.441	92
339.02544	33.936792	26.918	0.1	0.111	26.642	0.123	-0.615	26.429	0.183	-0.408	2.811	0	1	1	1	1	1	0	1	0	-	-	-4.399	92
338.96391	33.936928	27.076	0.13	-0.348	25.919	0.062	-0.079	25.111	0.054	0.075	1.606	0	1	1	1	1	1	1	1	1	-	yes	-0.499	92
338.97734	33.937033	26.903	0.116	0.033	26.369	0.075	-0.046	25.716	0.158	0.122	3.819	0	1	1	0	1	1	1	1	0	-	-	-2.539	92
339.0115	33.937167	28.51	0.365	0.652	27.192	0.105	-0.22	27.058	0.208	-0.034	2.137	0	0	1	1	1	1	1	0	0	-	-	-1.840	92
339.03373	33.937201	28.678	0.388	-1.17	26.171	0.075	0.168	26.308	0.128	0.439	2.171	0	0	1	1	0	1	1	1	0	-	-	0.5495	92
338.95818	33.937251	27.208	0.144	-0.517	26.064	0.066	-0.137	25.33	0.074	-0.072	2.078	0	1	1	1	1	1	1	1	1	-	yes	-0.725	92
339.00239	33.93731	26.475	0.063	0.313	25.395	0.057	0.369	24.446	0.063	0.386	2.433	1	1	1	1	1	1	1	1	1	yes	yes	-0.333	92
338.96115	33.93742	25.62	0.046	0.182	24.629	0.026	-0.035	23.736	0.042	0.19	1.955	1	1	1	1	1	1	1	1	1	yes	yes	-0.710	92
339.02347	33.93746	28.012	0.228	-1.068	26.94	0.093	0.051	25.747	0.102	0.029	2.271	0	1	1	1	0	1	1	1	1	-	yes	0.2784	92
338.99922	33.937483	27.763	0.155	0.289	25.791	0.051	0.236	24.743	0.064	0.337	2.284	0	1	1	1	0	1	1	1	0	-	-	2.2147	92
...																								

Notes. Columns list: (1) Right Ascension (J2000); (2) Declination (J2000); (3)—(5) Magnitude, error in magnitude, and sharpness values for B-band (F435W; F438W for HCG 92); (6)—(8) Magnitude, error in magnitude, and sharpness values for V-band (F606W); (9)—(11) Magnitude, error in magnitude, and sharpness values for I- band (F814W); (12) Goodness of fit factor χ from PSF-fitting in I-band; (13)—(17) Star cluster candidate selection criteria, see Section 2.3.2 for full description. 1 means that a given criterion is satisfied; (18)—(20) Globular cluster candidate selection criteria, see Section 2.3.3 for full description. 1 means that a given criterion is satisfied; (21) Star cluster candidate flag. If 'yes', all SCC criteria are satisfied; (22) Globular cluster candidate flag. If 'yes', all GCC criteria are satisfied; (23) Metallicity value derived from B–I color, see Section 2.4 for more details; (24) Hickson Compact group number.

In particular, a detailed examination of our catalogue revealed the following:

- Star clusters are powerful tracers of episodes of star formation activity. Careful study of the distribution of cluster colours can lead to a better understanding of the evolutionary state of their hosts and can help to constrain (and in some cases to reconstruct) the sequence of events in the host groups (e.g. Fedotov et al., 2011; Gallagher et al., 2010; Konstantopoulos et al., 2010, 2012, 2013). Thus, the analysis of star cluster populations in CGs allowed us to propose a reclassification of HCG 59 from a Type III to a Type II group. Most galaxies in Type III groups appear to be 'red' and 'dead' (e.g., HCG 42). However, the galaxy morphologies of HCG 59 do not comply with that statement. Moreover, its population of star clusters is more consistent with Type II groups.

- In general, the cluster luminosity functions of the CG spiral galaxies were consistent with spirals studied in the literature (e.g. Larsen, 2002; Whitmore et al., 2014). In particular, their CLF α-values ranged from -2.26 ± 0.05 to -2.54 ± 0.05. A notable exception were the large negative α-values for the spirals HCG 07A and 07C with $\alpha = -2.65 \pm 0.06$ and $\alpha = -3.24 \pm 0.04$, respectively.

- We have examined the metallicity distributions of GCCs in the five groups overall and individually in the elliptical galaxies (nominally elliptical 07BD and 92BD, 42A, 59B, 92C, and 92E) with sufficient numbers of GCCs. Only in galaxy 42A do we detect a metallicity distribution with well-defined bimodality peaking at [Fe/H]= -1.04 ± 0.07 and [Fe/H]= -0.16 ± 0.15. The galaxy 92C may also host a bimodal distribution, but the statistical results were not conclusive.

- The number of GCs in each galaxy is proportional to the total stellar masses of galaxies (Fig. 2.4). Notably, we detect a rather large number GCs in 59B (and its immediate environs) and a small number of GCs in 59A. It is possible that these two galaxies have interacted before given their morphologies (59B is elliptical, 59A is lenticular) and apparent proximity; the GC population distribution may be the only record of that interaction. A low surface brightness stream of material between galaxies 59A and B, reported in Konstantopoulos et al. (2013), as well as their line-of-sight velocities (within 3% of eachother) also support the idea of previous interactions.

- The number of "blue" clusters (with colour $V - I < 0.1$, representing the population of young star clusters) is well correlated with the star formation rate. Two spiral galaxies (92C and 59C) have a large number of "blue" clusters given their relatively lower star formation rates. That likely indicates that a recent bout of star formation triggered by interactions is coming to an end. However, the young star clusters have not been significantly age-dimmed yet, and so a large number of them are still detectable.

- For the three elliptical galaxies in our sample (42A, 59B, and 92E) we looked at the radial distribution of GCs of different metallicities. According to the KS-test, metal rich and metal poor populations of 42A and 59B are drawn from different distributions (with confidence of > 99%). The GCs of different metallicities in 92E appear to be well mixed throughout the galaxy. Dry mergers of galaxies with a similar mass could explain this

last observation. However, the characteristic features for such a merger (such as shells and streams) are not detected.

The star cluster populations of Hickson Compact Group galaxies are particularly interesting given their potential to reveal the history of dynamical interactions that have clearly been so important in shaping the evolution of individual groups as a whole and the current state of their member galaxies. The sensitive *BVI* imaging and photometry presented in this catalogue illustrate this point. However, the advantage of adding U-band to photometric studies of star clusters is considerable. It breaks the age-extinction degeneracy of the *BVI* photometry and allows a shift from a qualitative description of cluster ages to a more quantitative analysis, along with determinations of intrinsic reddening and masses. This additional information adds considerably to the descriptive power of star cluster populations in specific environments.

Our future work on star cluster populations of Stephan's Quintet (HCG 92; Fedotov et al., in prep.) with *UBVI* photometry will illustrate that.

Acknowledgements

K.F. and S.C.G. thank the Natural Sciences and Engineering Research Council of Canada and the Ontario Early Researcher Award Program for support. This research has made use of the NASA/IPAC Extra- galactic Database (NED) which is operated by the Jet Propulsion Laboratory, California Institute of Technology, under contract with the National Aeronautics and Space Administration. Additional support for this work was provided by NASA through grant No. HST-GO-10787.15-A from the Space Telescope Science Institute which is operated by AURA, Inc., under NASA contract NAS 5-26555. We thank Alan McConnachie, John Blakeslee, Pat Côte, and Ruben Sanchez-Janssen for illuminating discussions on the properties of GCs. We also thank Robert Corless, Gretchen Harris, John Landstreet, and Aaron Sigut for a careful read of the manuscript and their valuable suggestions that improved the paper.

Facilities: HST

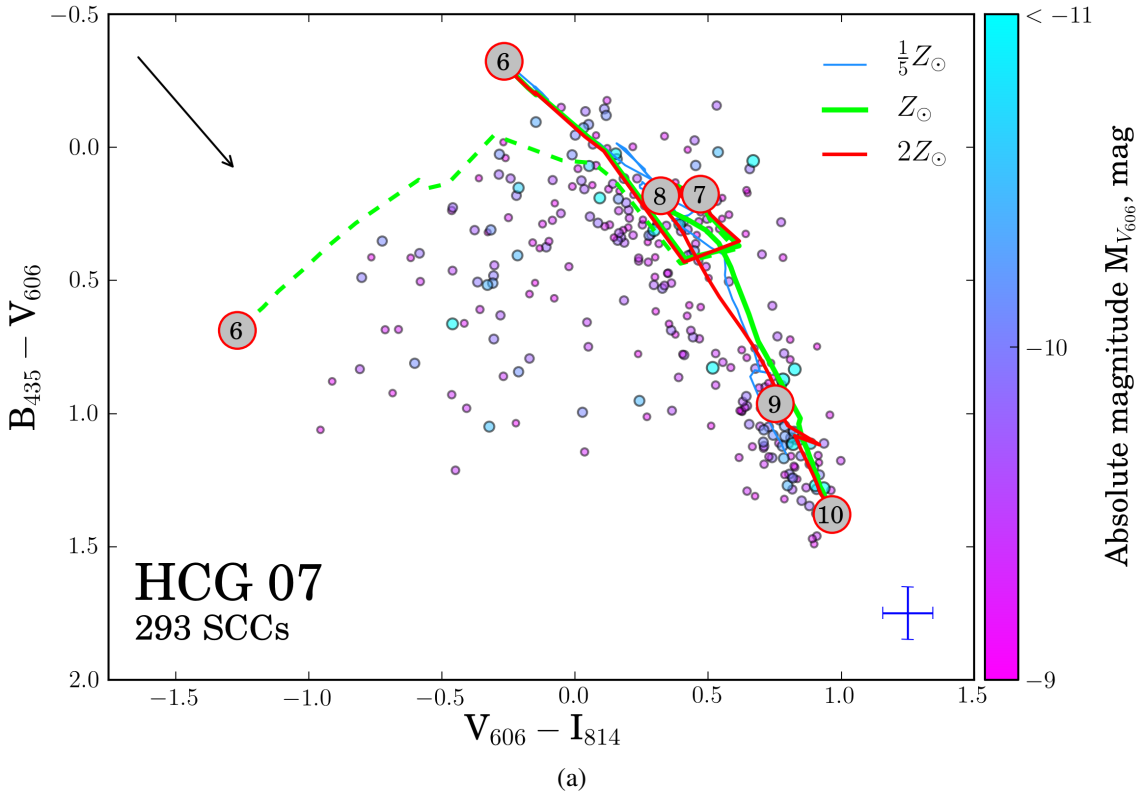

(a)

Figure 2.9: Colour-colour plots of all the star cluster candidates in HCG 07 (a), including clusters located in the IGrM. The thin solid line, solid line, and dashed line trace the evolution of SSP models of [0.2, 1.0, 2.0] Z⊙ (Marigo et al., 2008). The thin dashed line to the left of the main evolutionary track represents a track including nebular emission, common for young star clusters (e.g. Conti et al., 1996; Vacca & Conti, 1992). In the upper left corner one can find a reddening vector with length equivalent to V_{606} = 1 mag. The number of star cluster candidates detected in this group is marked in the lower left corner. A typical photometric error bar, based on the median errors, is located in the lower right corner. A colour bar that represents the absolute magnitude of SCCs is given on the right. For ease of reading the plot, the sizes of SCCs in the plot are linearly proportional to their magnitude: the larger the dot, the brighter the SC. All SCCs on this and following plots have absolute magnitude ≤ −9 mag. This figure is continued on the next page. (A colour version of this figure is available in the online journal.)

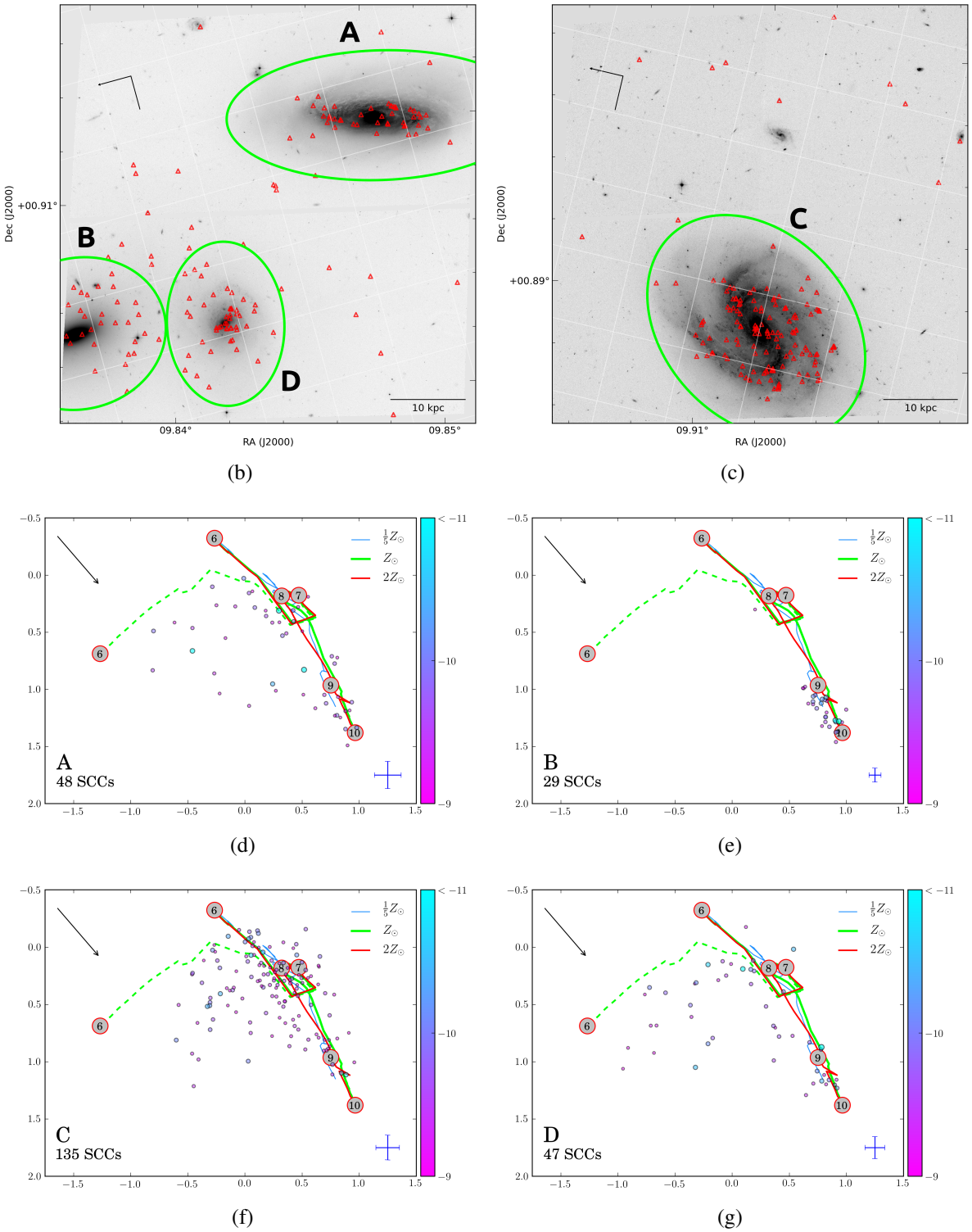

Figure 2.9: Figure continued from the previous page. Panels (b) and (c) are inverted V_{606} images which show the star cluster system extent of each galaxy as defined by a brightness contour in V_{606} of $\sim$ 1.25σ above the background level. Here and in subsequent plots, a compass indicates North (with an arrowhead) and East (without the arrowhead). Panels (d)–(g) are *BVI* colour-colour plots for individual galaxies and regions in the group. The large spiral HCG 7C hosts the greatest number of young clusters, while the quiescent elliptical HCG 7B has only globular clusters. (A colour version of this figure is available in the online journal.)

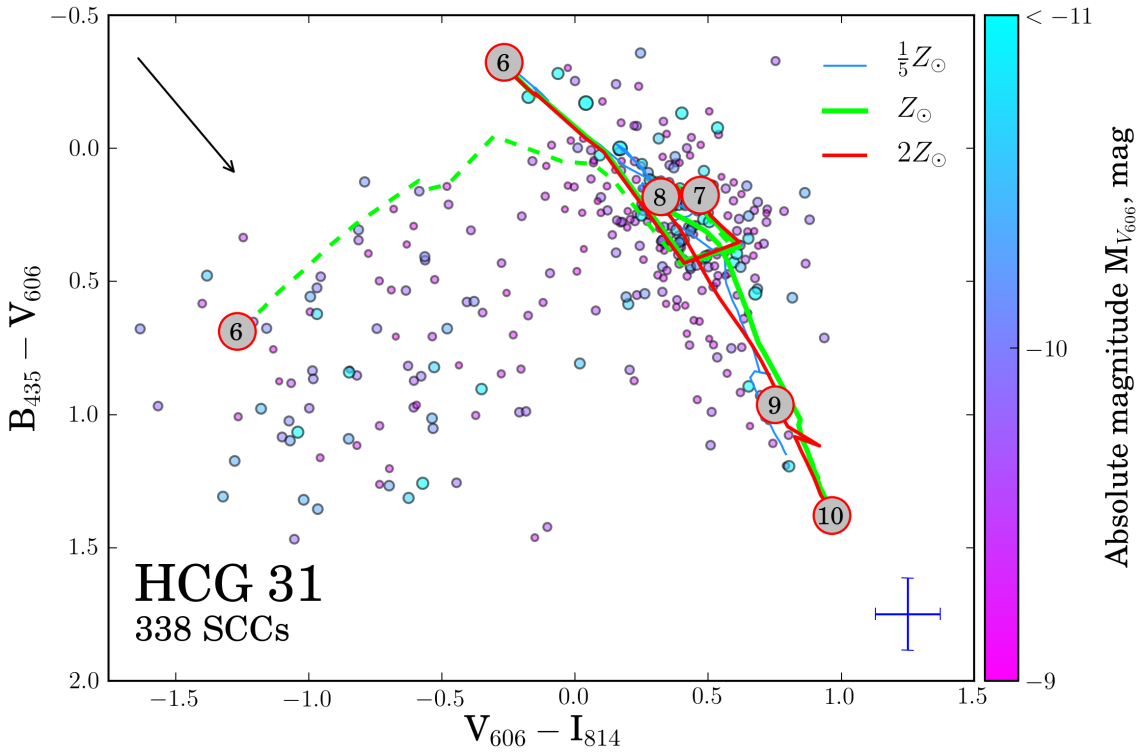

(a)

Figure 2.10: A colour-colour plot of all the star cluster candidates in HCG 31 (a), including clusters located in intragroup medium. Symbols are as in Fig. 2.9. (A colour version of this figure is available in the online journal.)

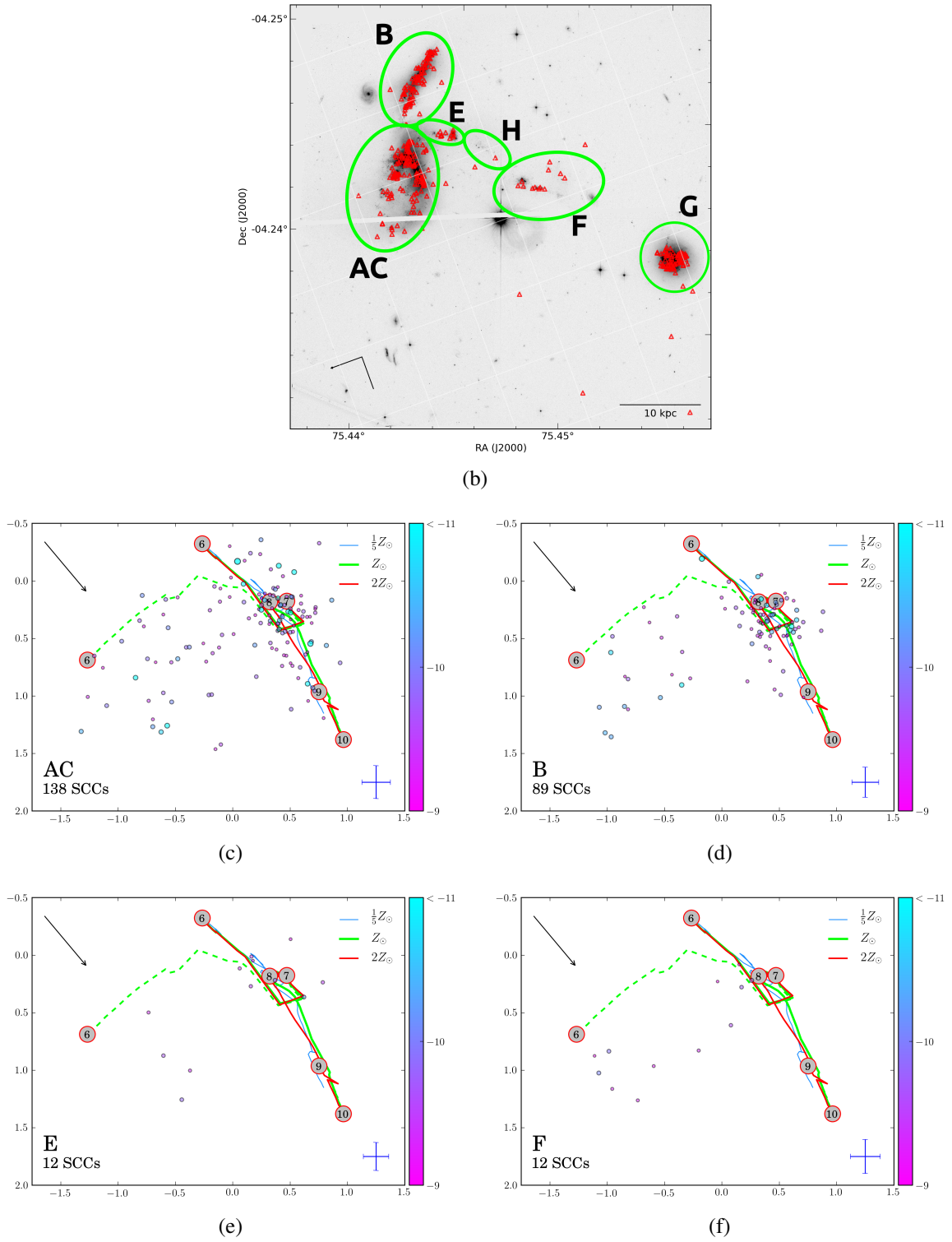

Figure 2.10: Figure continued from the previous page. Image (b) is the inverted V_{606} image which shows the SCC system extent as defined by a brightness contour of $\sim 1.25\sigma$ in V_{606} above the background level. Panels (c)–(f) are colour-colour plots for particular galaxies and regions in the HCG 31 group. All galaxies (31AC, B, and G) and tidal regions (31E and F) in this group host young clusters; the entire system is suffused with star formation triggered by strong, recent galaxy interactions. (A colour version of this figure is available in the online journal.)

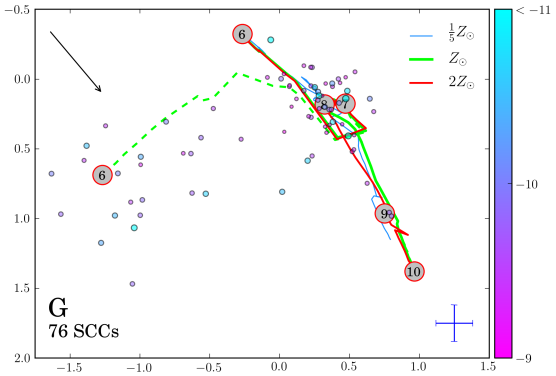

(g)

Figure 2.10: . . . Figure continued from the previous page. A colour-colour plot for the galaxy G. (A colour version of this figure is available in the online journal.)

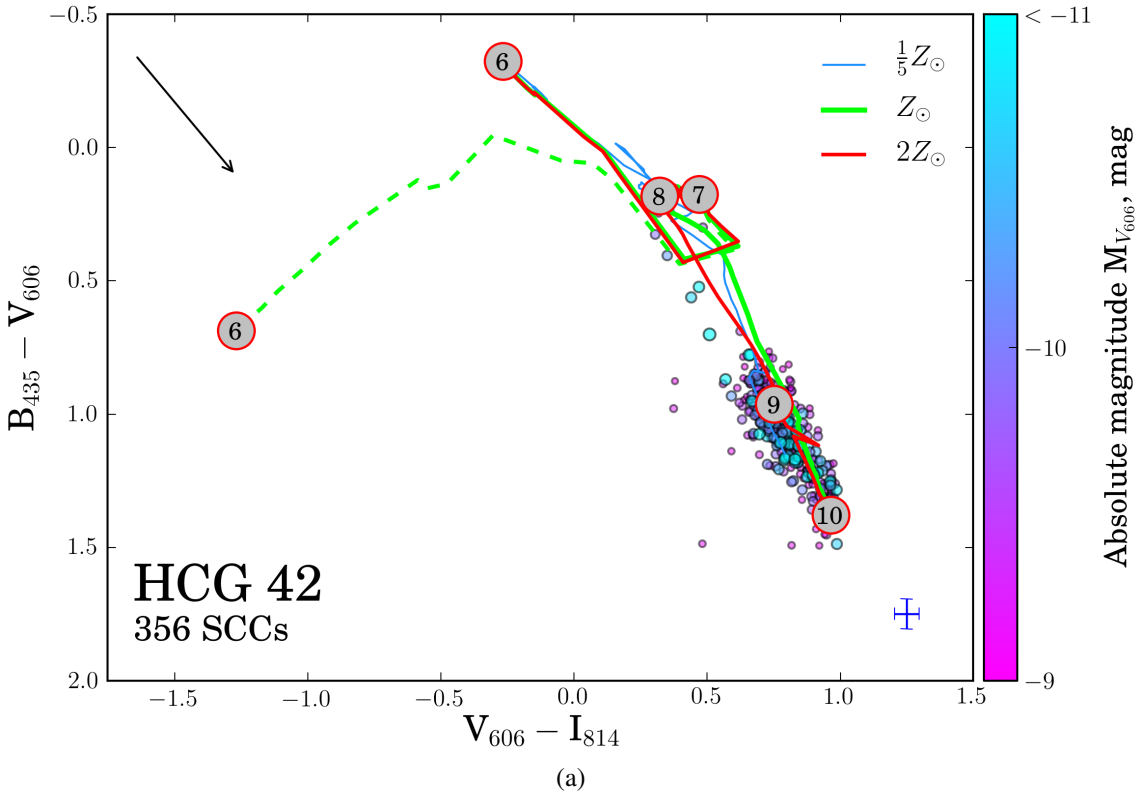

(a)

Figure 2.11: A colour-colour plot of all star clusters candidates in the ACS image of HCG 42 (a), including clusters in intergroup medium, and subplot for a particular galaxy in that group (b), continued on the next page. For more details see caption for Fig. 2.9. (A colour version of this figure is available in the online journal.)

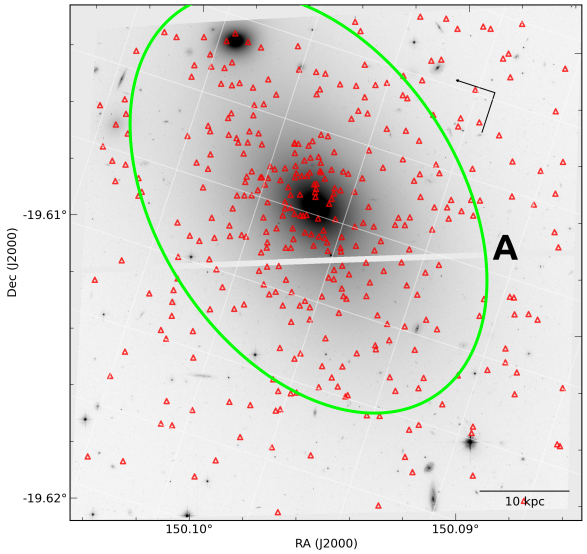

(b)

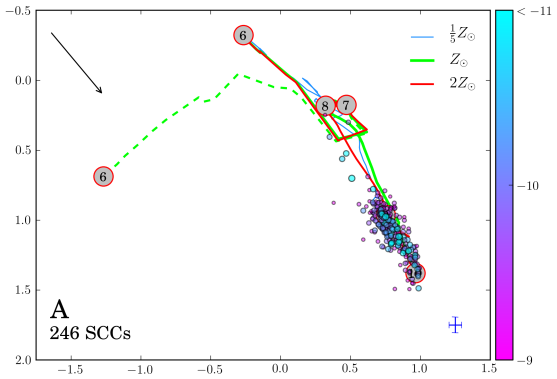

(c)

Figure 2.11: Figure continued from the previous page. Panel (b) is the inverted V_{606} image which shows the SCC system extent as defined by the V_{606} brightness contour of $\sim 1.25\sigma$ above the background level. Panel (c) is a colour-colour plot for the luminous elliptical 42A. In this colour-space, all of the clusters are consistent with being old globular clusters. (A colour version of this figure is available in the online journal.)

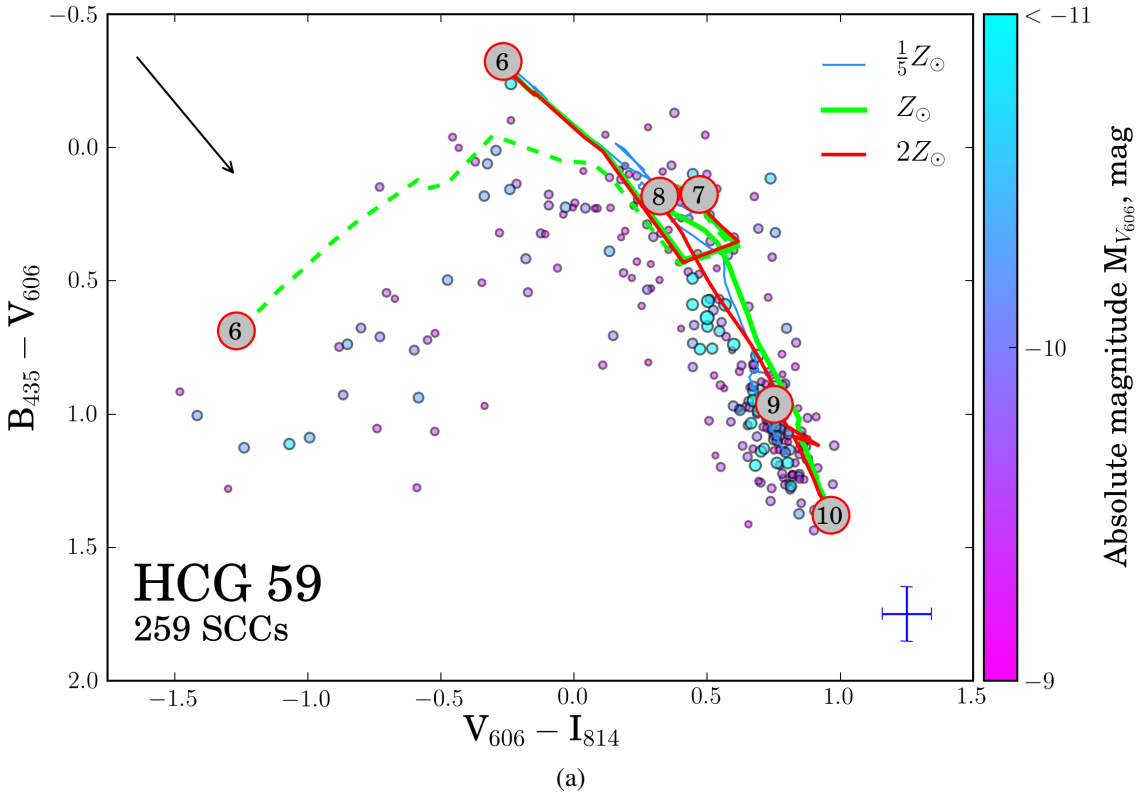

(a)

Figure 2.12: A colour-colour plot of all star clusters candidates in HCG 59 (a), including clusters in the intergroup medium, and subplots for particular galaxies in that group (c)–(f), continued on the next page. For more details see caption for Fig. 2.9. (A colour version of this figure is available in the online journal.)

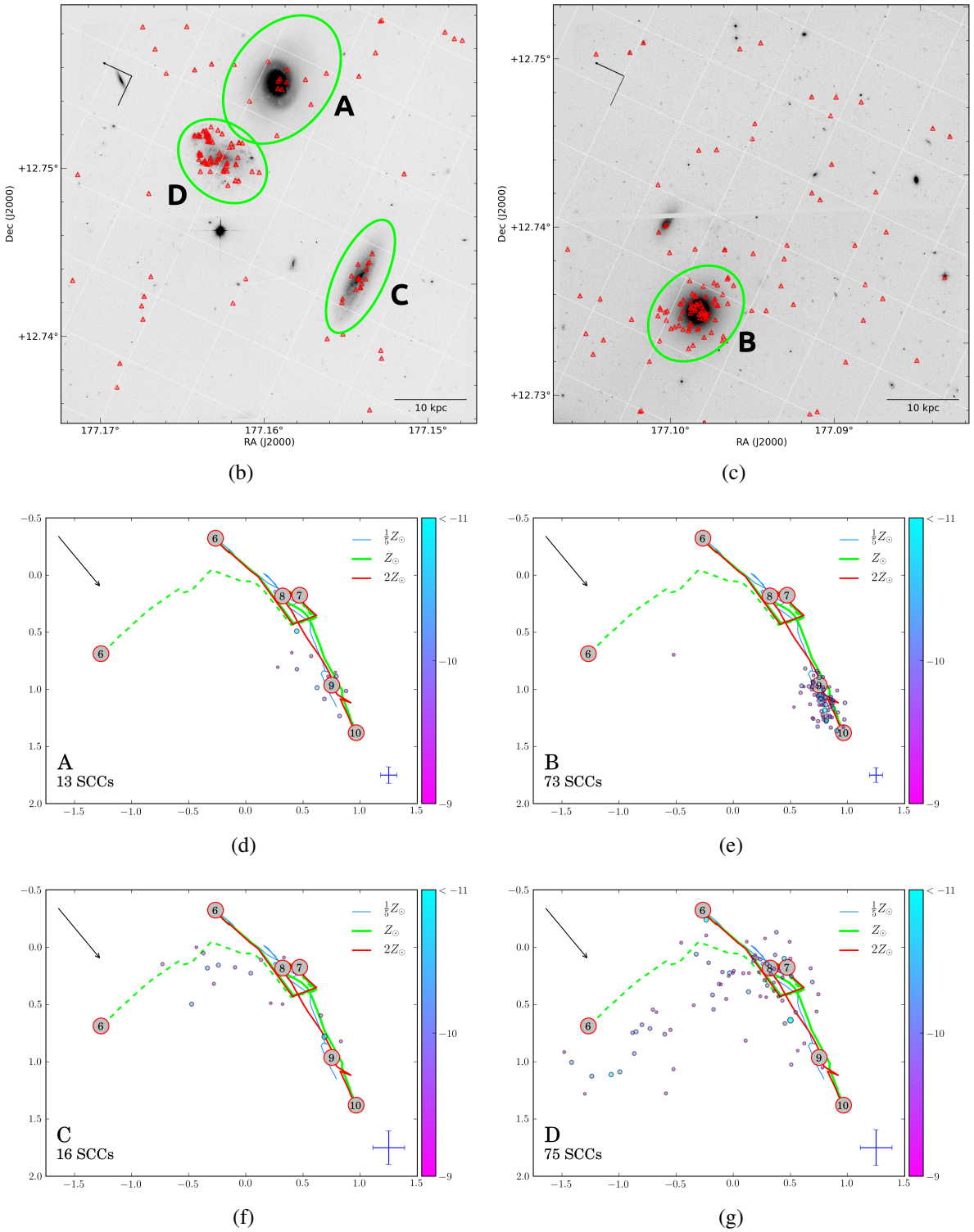

Figure 2.12: ... figure continued from the previous page. Panels (b) and (c) are inverted V_{606} images which show the SCC system extent as defined by a V_{606} brightness contour of $\sim 1.25\sigma$ above the background level. Panels (c)–(f) are colour-colour plots for individual galaxies in the HCG 59 group. The large irregular 59D has a large population of young clusters. 59A hosts both old and intermediate-aged clusters, while the elliptical 59B has only a globular cluster population. (A colour version of this figure is available in the online journal.)

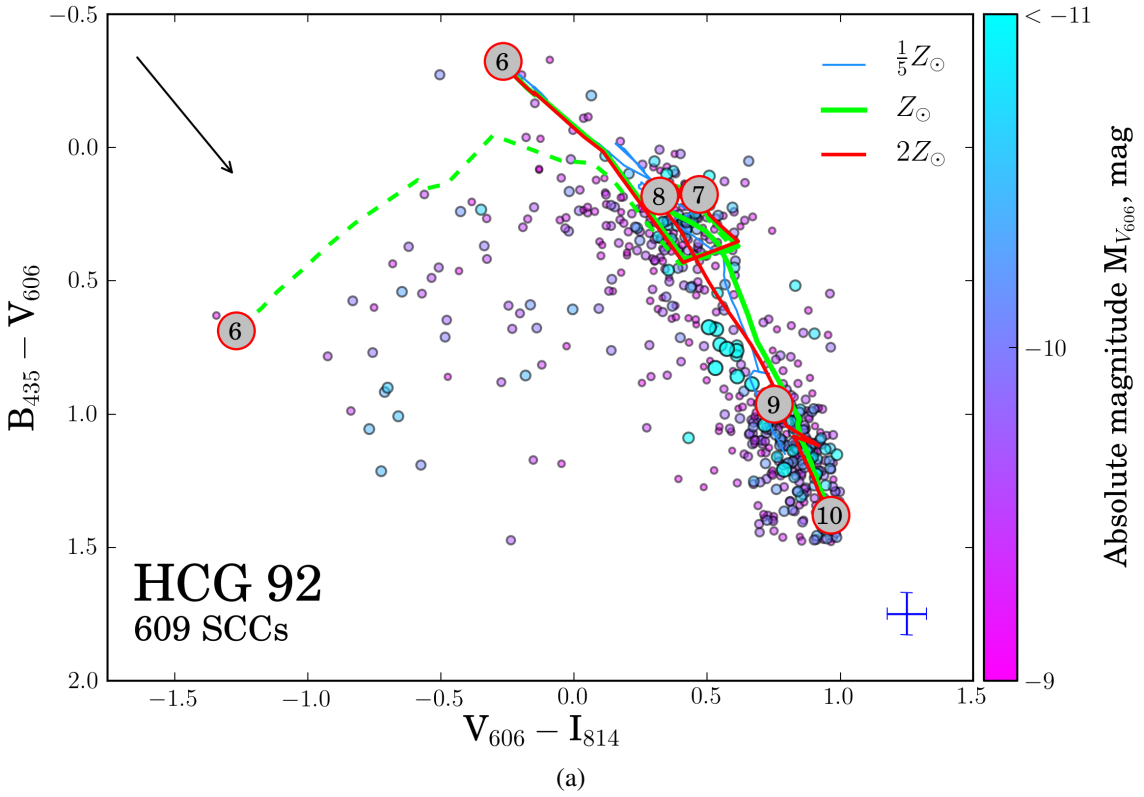

(a)

Figure 2.13: A colour-colour plot of all SCCs in HCG 92 (a), including clusters in the intergroup medium, and subplots for particular galaxies in that group (c)–(f) and (h)–(i), continued on the next pages. For more details see the caption for Fig. 2.9. (A colour version of this figure is available in the online journal.)

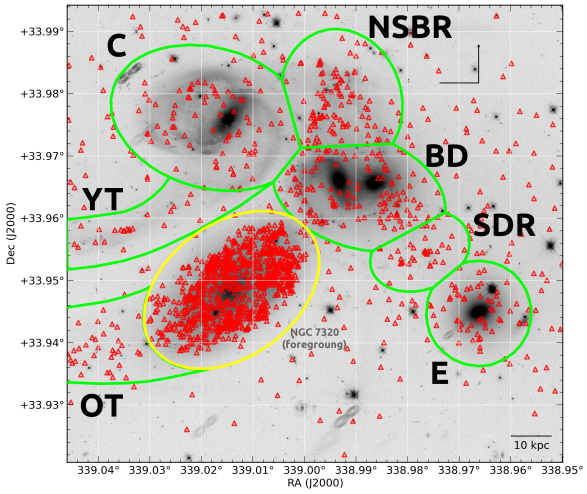

(b)

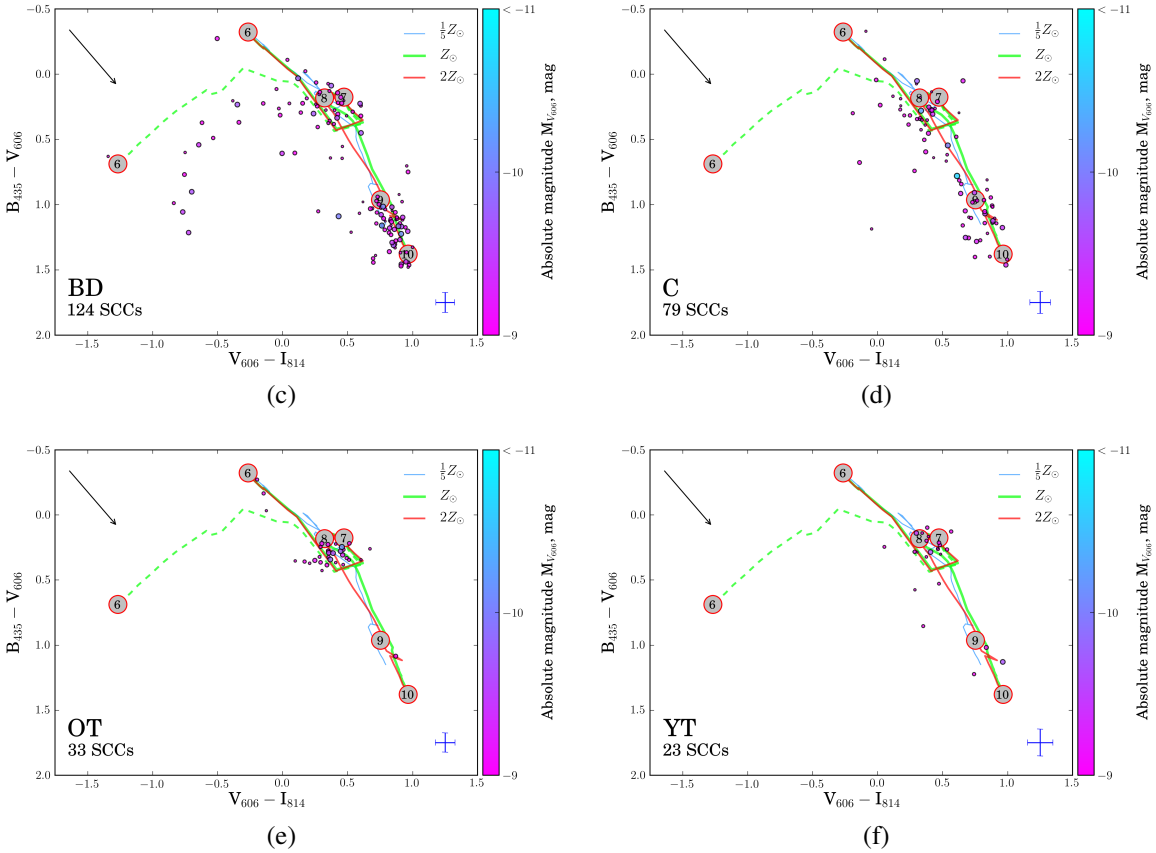

(c) (d) (e) (f)

Figure 2.13: Figure continued from the previous page. Panel (b) is the inverted V_{606} image which shows the SCC system extent as defined by the V_{606} brightness contour of $\sim 1.25\sigma$ above the background level. (The foreground galaxy 92A is outlined in yellow.) Panels (c)–(f) are colour-colour plots for particular galaxies and regions in the HCG 92 group. 92BD has a population of young clusters whose formation was triggered by the collision of 92B with the cold intragroup medium. 92C shows evidence for truncated star formation, with an intermediate (> 100 Myr) to old SC population. The Old Tail (OT) and Young Tail (YT) tidal features show a small populations of star clusters with well-defined colours, tracers of short bursts of star formation in these features. The 8-shape objects observed in the panel (b), also in panel (c) in Fig. 2.18, are ghost images caused by reflections off the CCD and return reflections from the CCD housing entrance window in WFC3. (A colour version of this figure is available in the online journal.)

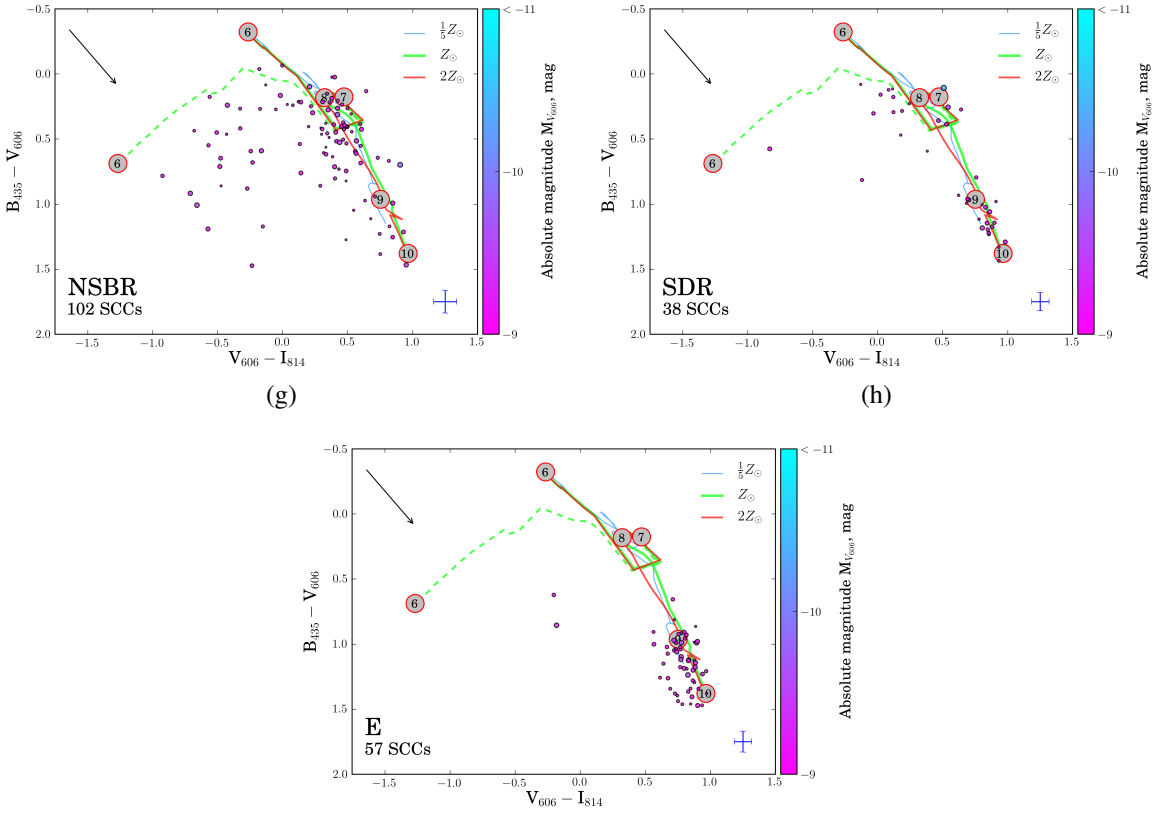

Figure 2.13: ... Figure continued from the previous page. Panels (g)–(i) are colour-colour plots for particular galaxies and regions in the HCG 92 group. The Northern Starburst Region (NSBR) shows the largest concentration of young clusters within the whole group, the Southern Debris Region (SDR) has a slightly older population of star clusters, and the elliptical 92D has primarily old clusters as expected. (A colour version of this figure is available in the online journal.)

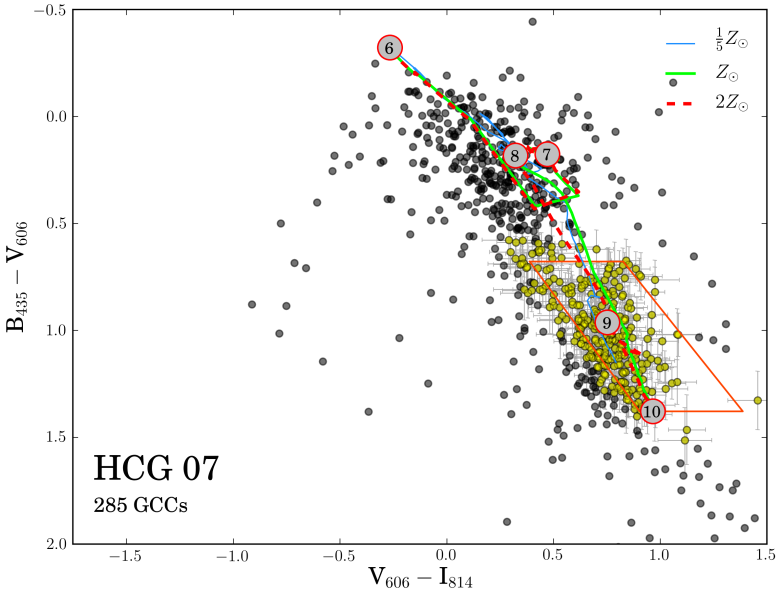

(a)

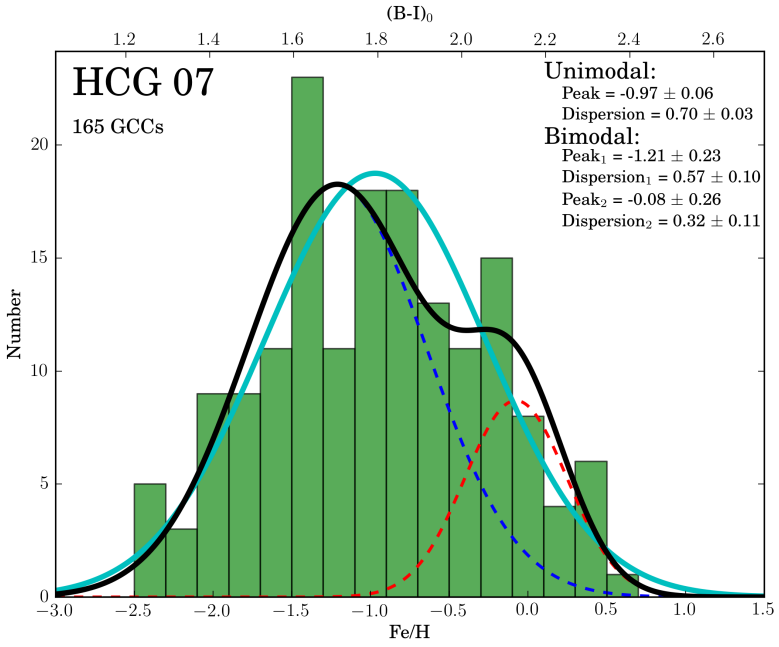

(b)

Figure 2.14: A colour-colour diagram of all detected GCCs in HCG 07 (a), including clusters located in the IGrM, and their metallicity distribution (b). The selection parallelogram in (a) is based on the colours of Milky Way Globular Clusters (Harris, 1996). The number of GCCs in the lower left corner is the number of clusters that are located inside the selection parallelogram or that overlap the selection region with their 1σ error bars. The thin solid line, solid line, and dashed line trace the evolution of SSP models of [0.2, 1.0, 2.0] $Z_\odot$ (Marigo et al., 2008). Note that the measured quantity for the panel (b), and for the rest of the plots of the same nature, is the colour index $B - I$. It was converted to Fe/H values according to prescription in Harris et al. (2013) and further analysis were carried out with those Fe/H values. Figure continued on the next page. (A colour version of this figure is available in the online journal.)

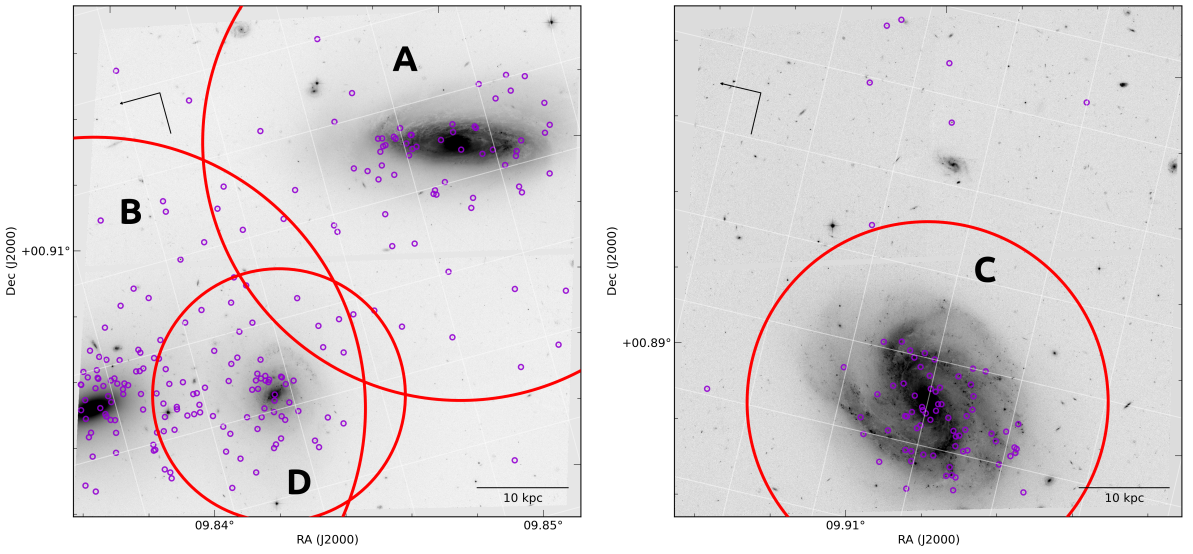

(c) (d)

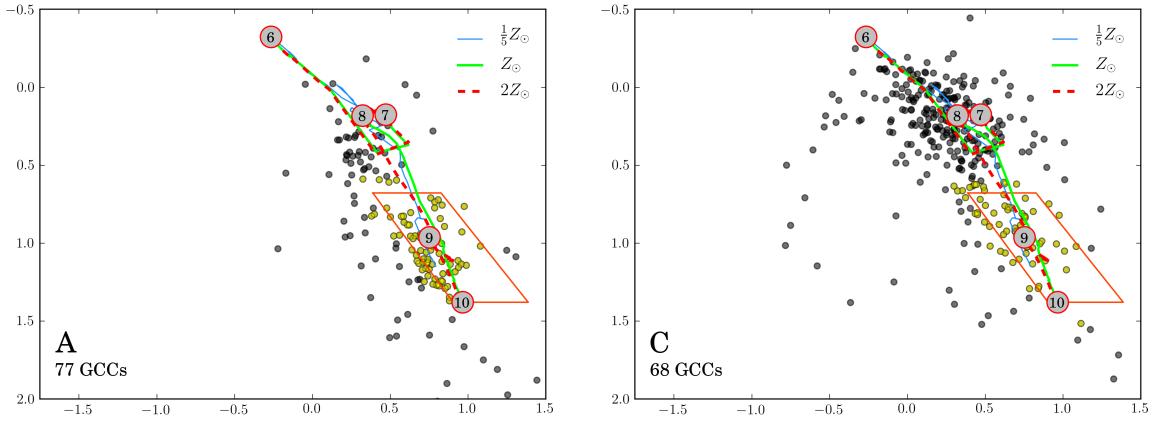

(e) (f)

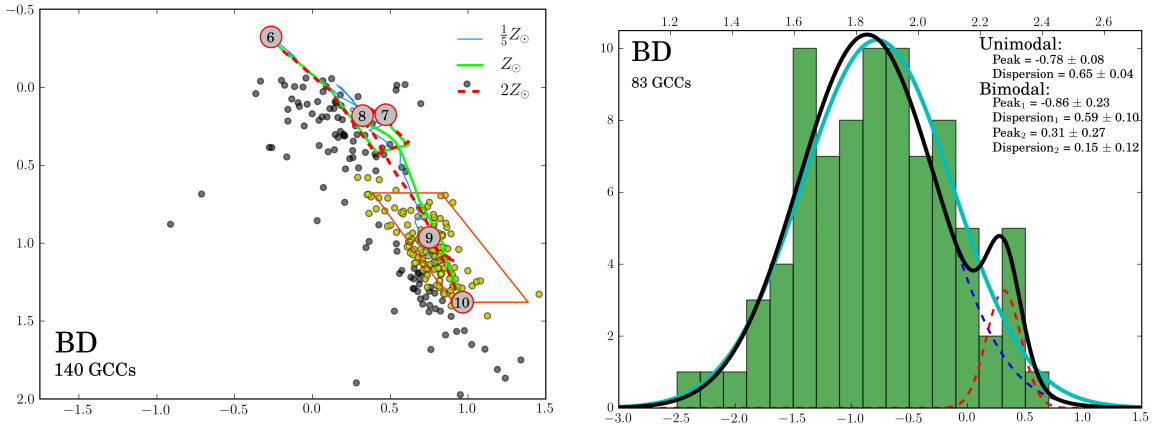

(g) (h)

Figure 2.14: ... Panels (c) and (d) are inverted V_{606} images which show the GCC system extent, with locations of GCCs overplotted as circles. GCCs found in the central regions and spiral arms of galaxies A and C could potentially be reddened young star clusters. Panels (e) and (g) are colour-colour plots for particular galaxies in the group. The systems of 7B and D are considered together because of the projected overlap of their expected GC system extents. Their metallicity distribution is consistent with a single-peaked Gaussian. (A colour version of this figure is available in the online journal.)

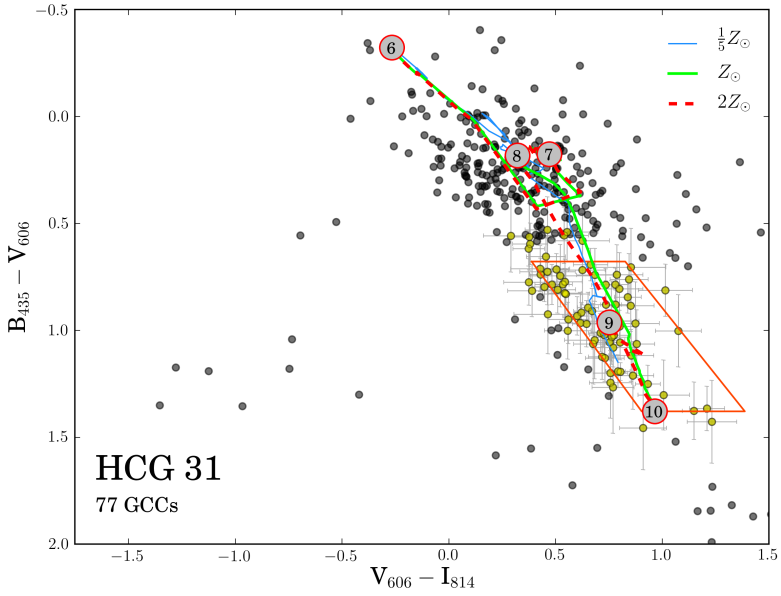

(a)

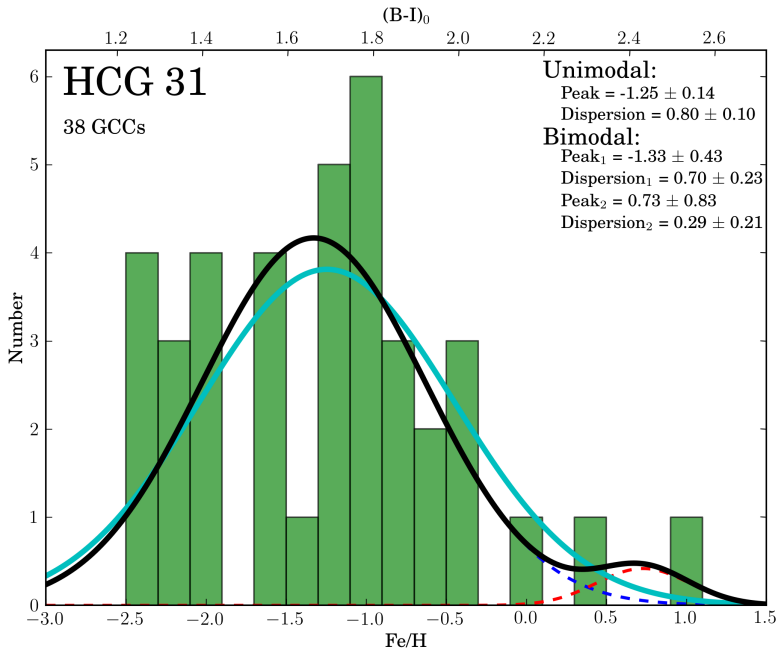

(b)

Figure 2.15: The GCC population of HCG 31 (a) and its metallicity distribution (b). For more details see caption for Fig. 2.14. Given the high rate of star formation in this group, the low masses of the individual galaxies, and the spatial distribution of GCCs, it is reasonable to assume that the majority of the star clusters labelled as GCCs are in fact reddened young clusters. Therefore, the metallicity distribution plot (b) should be considered with caution. (A colour version of this figure is available in the online journal.)

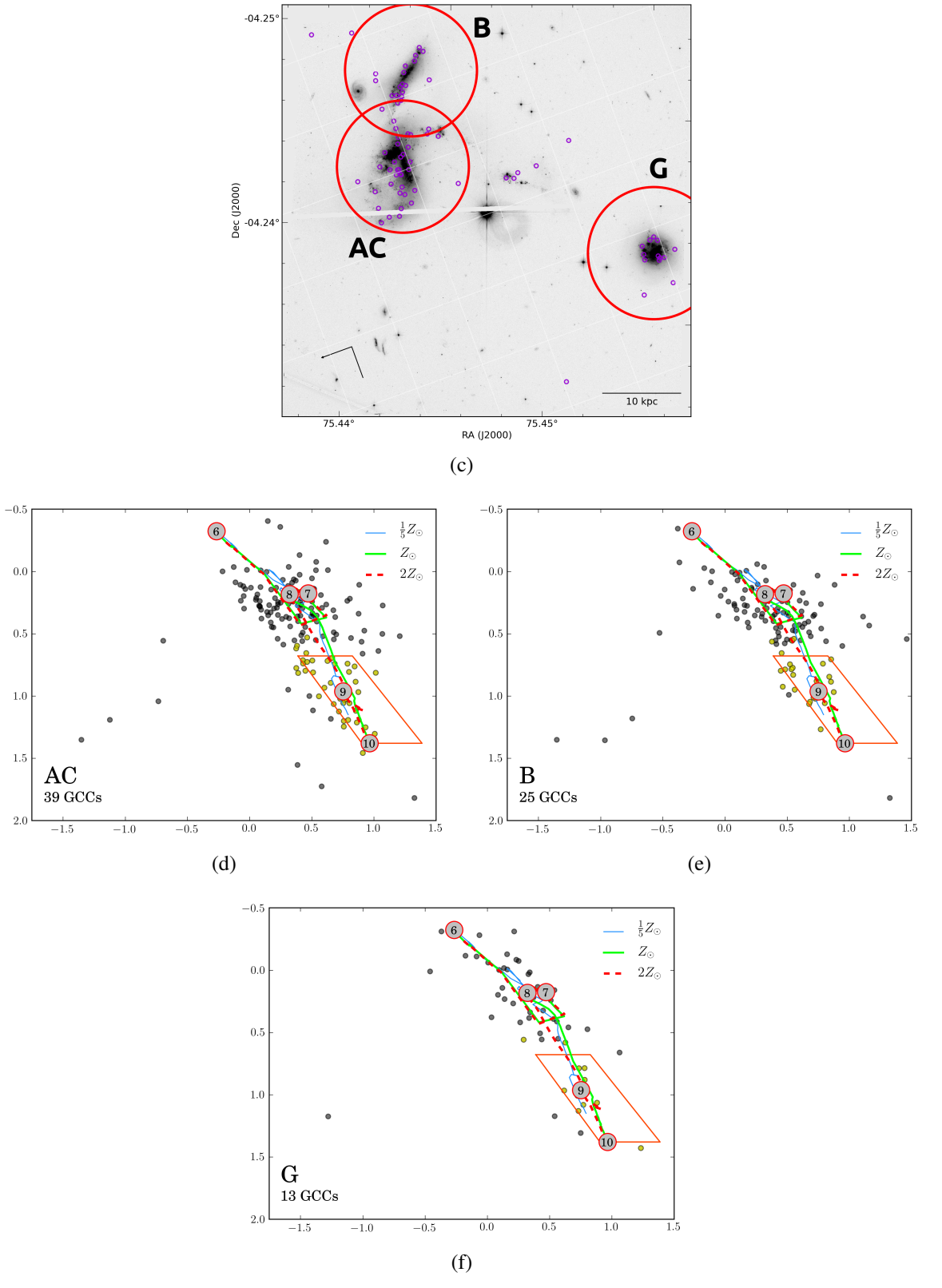

Figure 2.15: ... Panel (c) is an inverted V_{606} image which shows the GCC system extent, with locations of GCCs overplotted as circles. Panels (d)–(f) are colour-colour plots for particular galaxies/regions in that group. Most likely, the majority of the small population of GCCs are reddened young clusters. (A colour version of this figure is available in the online journal.)

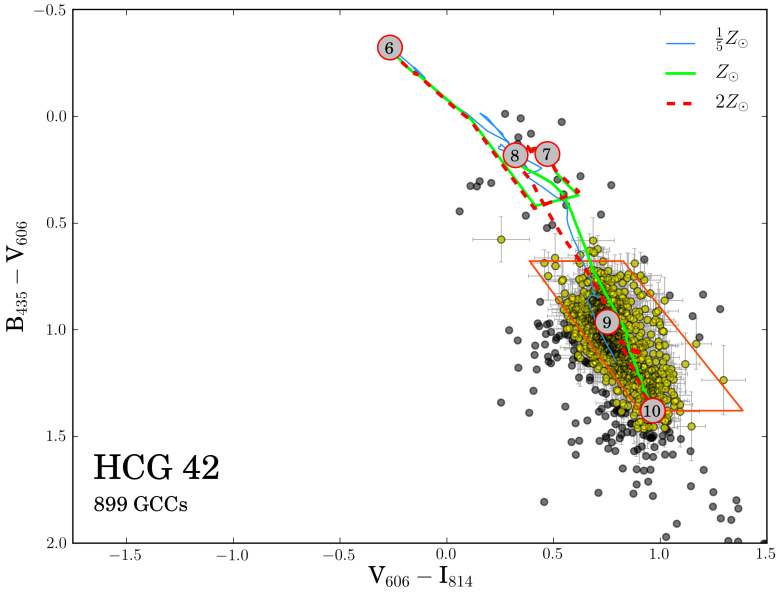

(a)

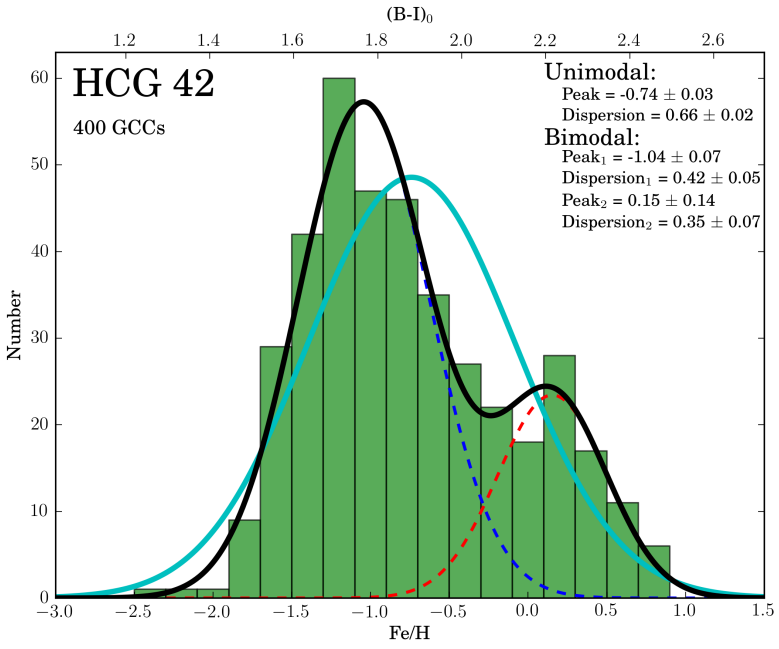

(b)

Figure 2.16: The GCCc population of HCG 42 (a) and its metallicity distribution (b). For more details see caption for Fig. 2.14. (A colour version of this figure is available in the online journal.)

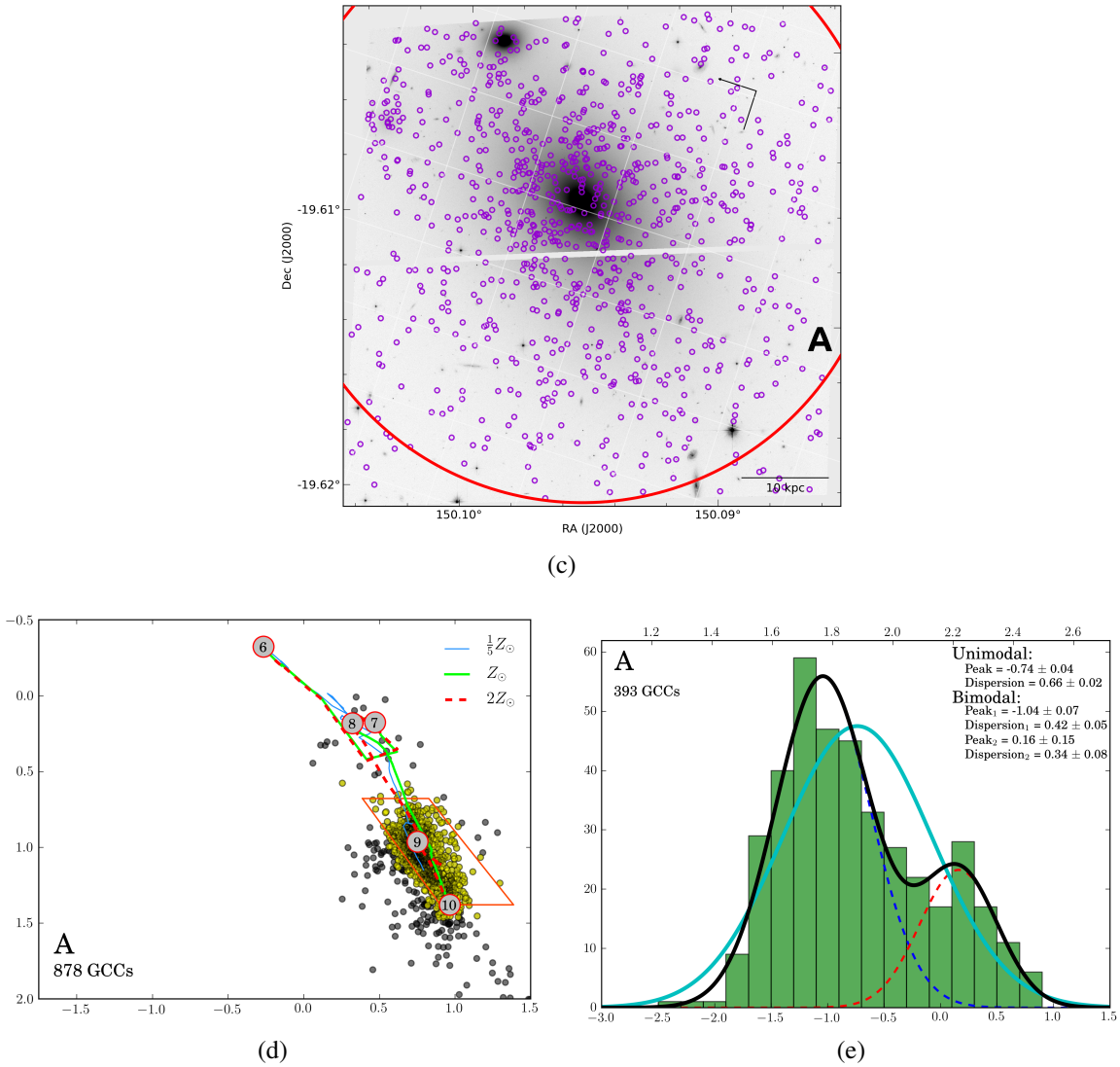

Figure 2.16: ... Panel (c) is an inverted V_{606} images which show the GCC system extent, with locations of detected GCCs overplotted as circles. Panel (d) is a colour-colour plot for galaxy HCG 42A. A slight overdensity of GCCs close to the left upper corner corresponds to the location of a dwarf galaxy, a member of HCG 42. Panel (e) is a plot of the metallicity distribution of GCCs in HCG 42A. The GMM results favour a bimodal distribution with the first peak at [Fe/H] = -1.04 ± 0.07 and the second peak at [Fe/H] = 0.16 ± 0.15. (A colour version of this figure is available in the online journal.)

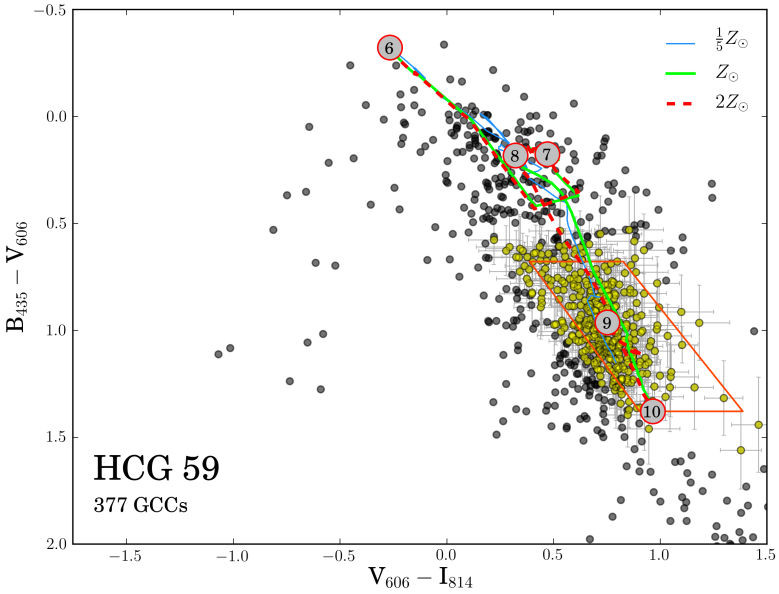

(a)

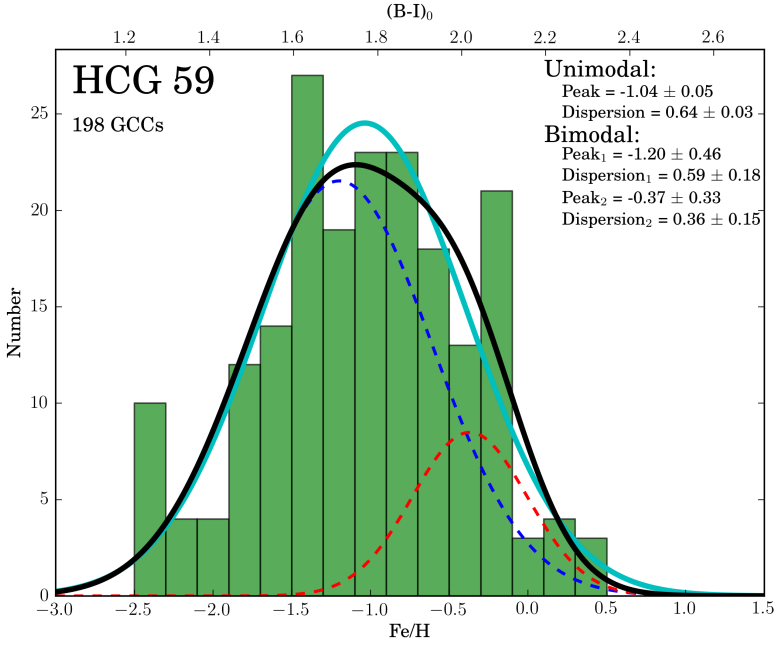

(b)

Figure 2.17: The GCC population of HCG 59 (a) and its metallicity distribution (b). See caption for Fig. 2.14. (A colour version of this figure is available in the online journal.)

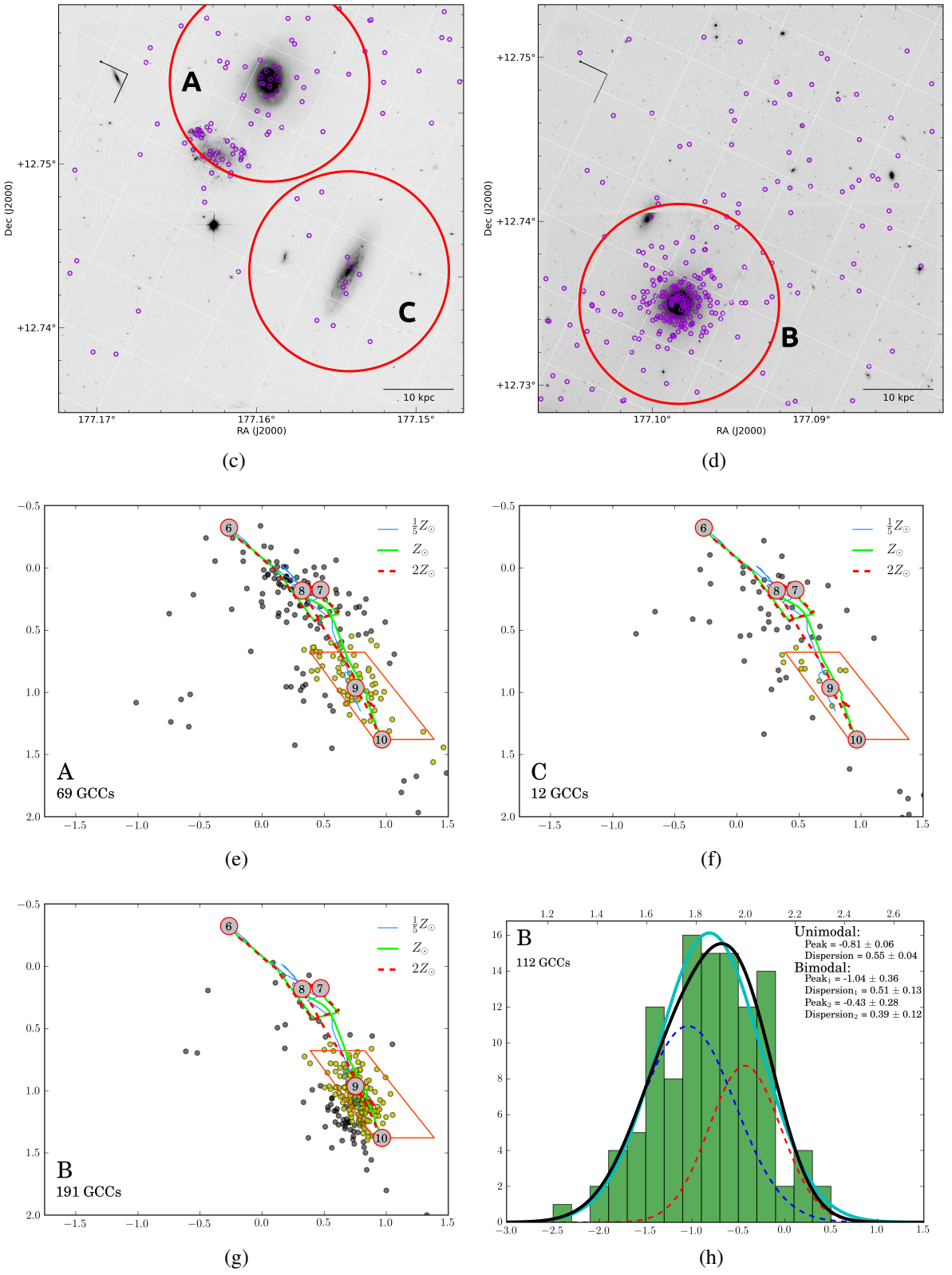

Figure 2.17: ... Panels (c) and (d) are inverted V_{606} images which show the GCC system extent, with locations of detected GCCs overplotted as circles. Panels (e)–(g) are colour-colour plots for particular galaxies in that group. Panel (h) represent metallicity distribution of the large population of GCCs in HCG 59B. The GMM results are inconclusive, and a single-peaked distribution is consistent with the data. (A colour version of this figure is available in the online journal.)

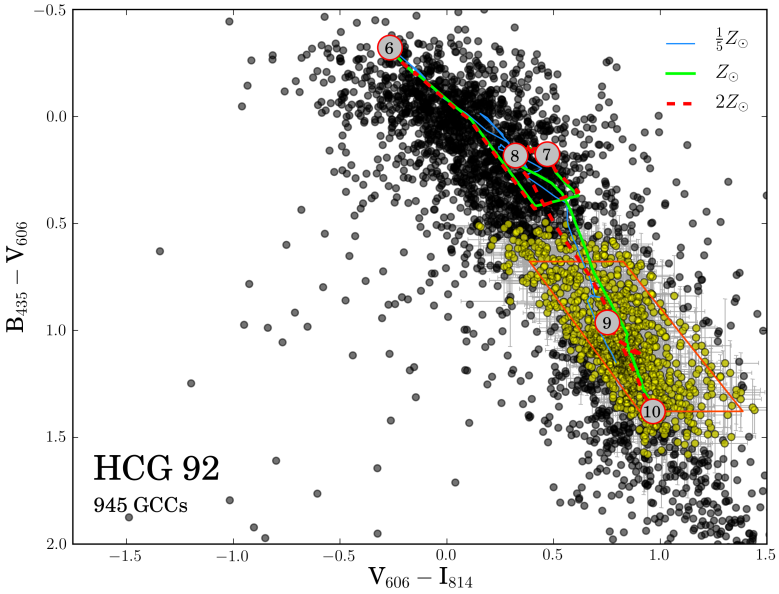

(a)

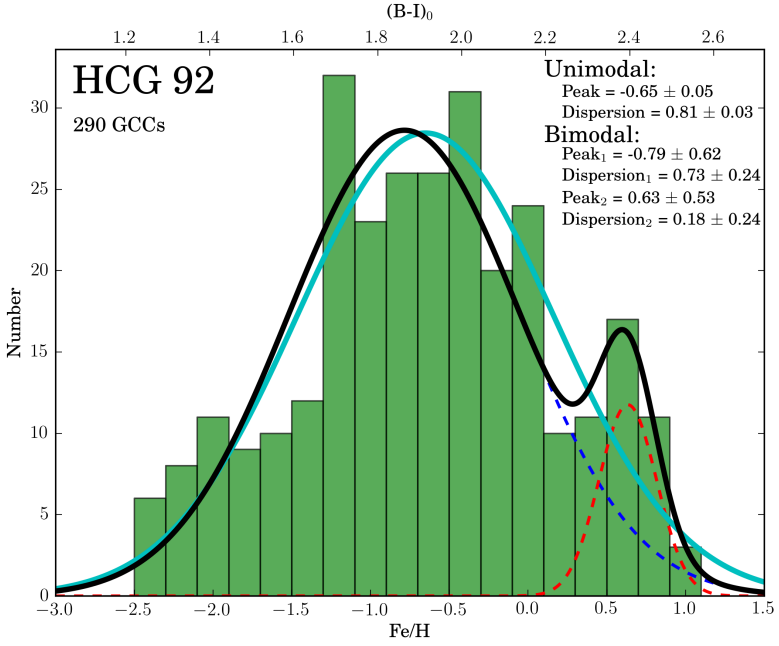

(b)

Figure 2.18: The GCCs population of HCG 92 (a) and its metallicity distribution (b). See caption for Fig. 2.14. (A colour version of this figure is available in the online journal.)

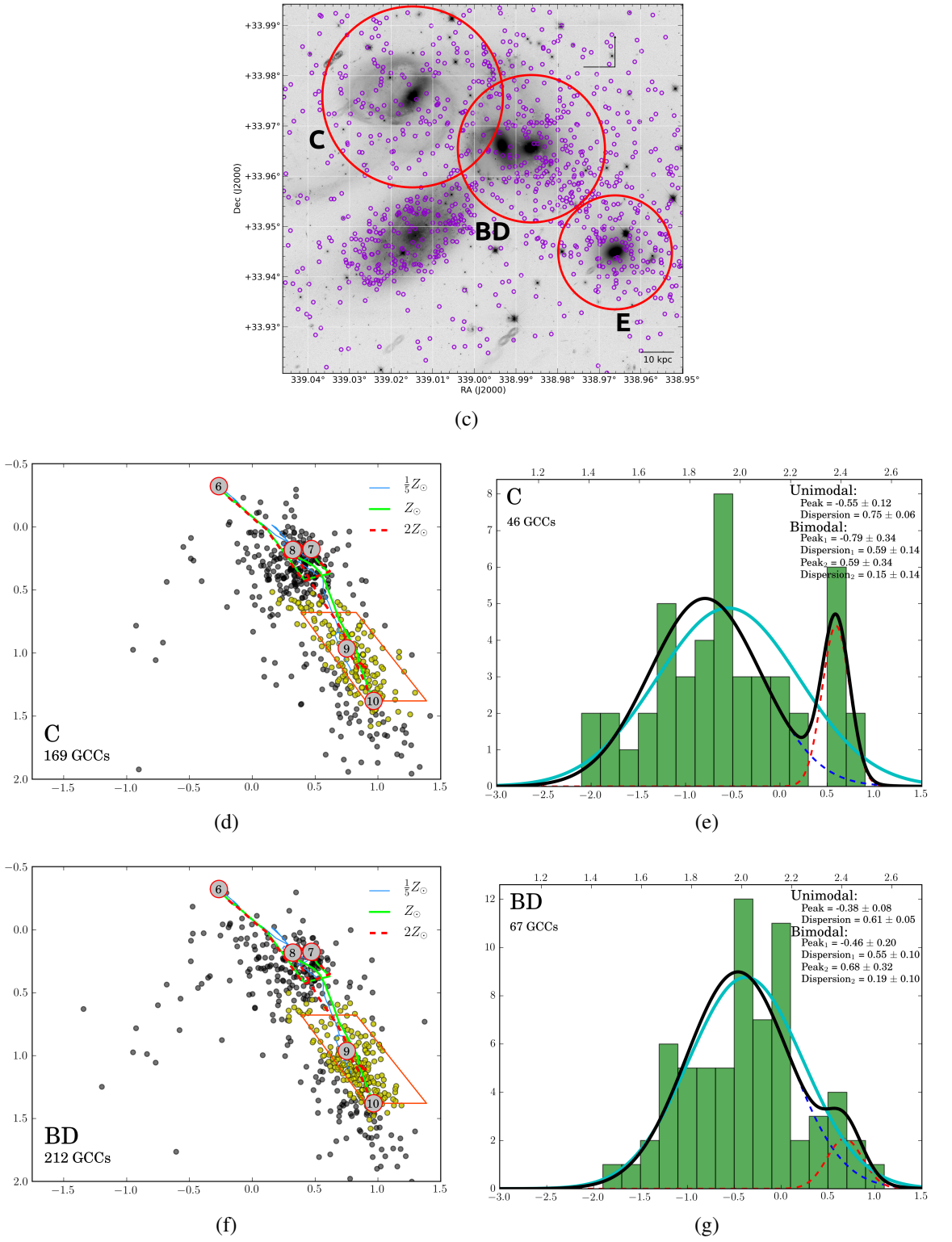

Figure 2.18: Panel (c) is the inverted V_{606} image which shows the GCC system extents, with locations of detected GCCs overplotted as circles. Panels (d) and (f) are colour-colour plots for particular galaxies and regions HCG 92. NGC 7319 (HCG 92C) is a face-on spiral and the GCC located in the central region, as well as in the spiral arms, could potentially be reddened young star clusters. The BD region contains the elliptical galaxy NGC 7318A (HCG 92D) and the spiral galaxy NGC 7318B (HCG 92B) in a field of debris, material left from current and previous interactions. Thus, it is likely that GCCs in the BD region are heavily contaminated by reddened young star clusters. Subfigures (e) and (g) are the metallicity distributions for C and BD, respectively. (A colour version of this figure is available in the online journal.)

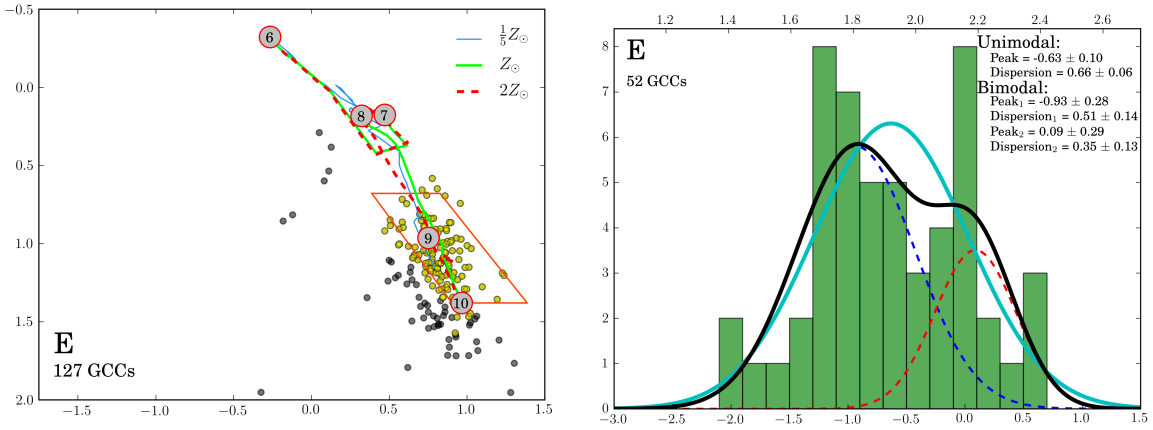

(h) (i)

Figure 2.18: ...Panel (h) is a colour-colour plot for galaxy E and panel (i) is a plot of its metallicity distribution. (A colour version of this figure is available in the online journal.)

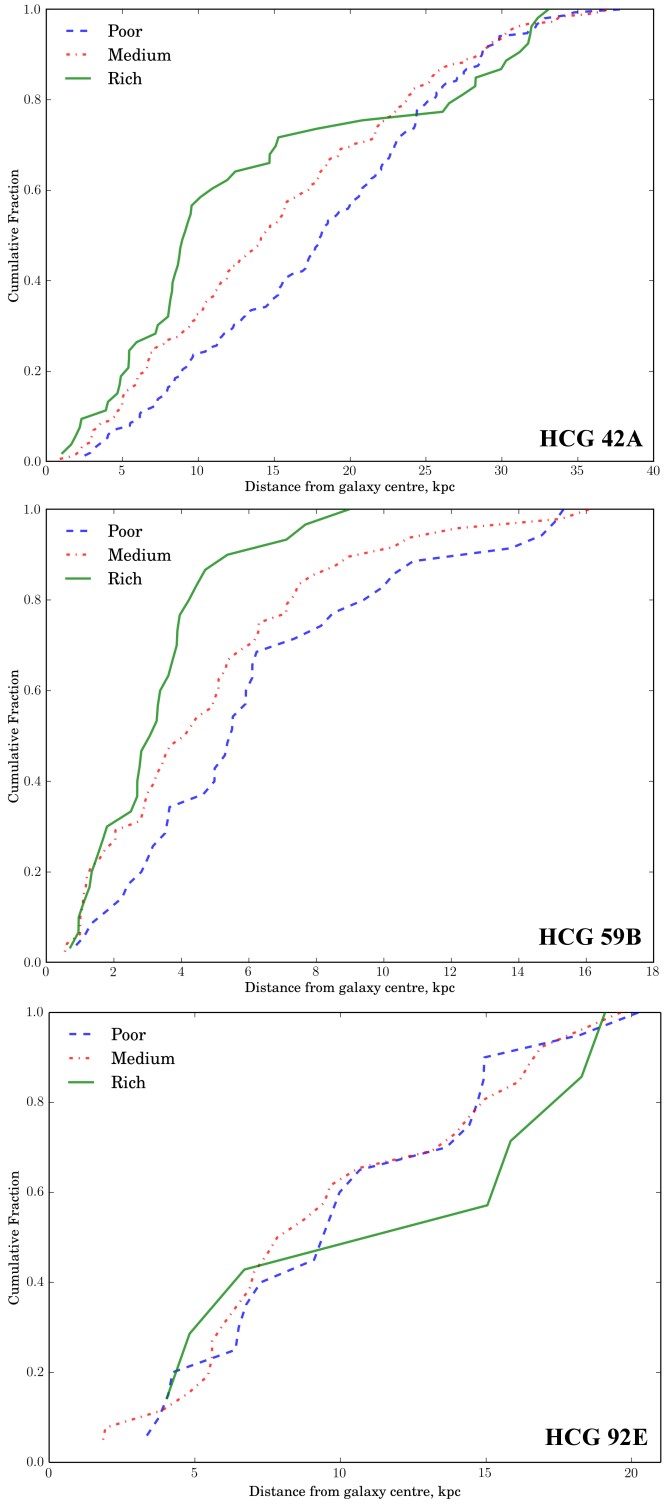

Figure 2.19: Cumulative function of radial distribution of clusters with different metallicities for galaxies HCG 42A, HCG 59B, and HCG 92E (top, middle, and bottom panels, respectively). The KS-test has shown that metal rich and metal poor populations of 42A and 59B are drawn from different distributions (with confidence of $> 99\%$). The GC populations in 92E appear to be well mixed throughout the galaxy. (A colour version of this figure is available in the online journal.)

Chapter 3

Star Cluster Formation in the Tidal Debris of Stephan's Quintet: Age and Mass Constraints

K. Fedotov, S. C. Gallagher, R. Chandar, T. D. Desjardins, N. Bastian, I. S. Konstantopoulos, P. Appleton, and J. Charlton.
Submitted to the Monthly Notices of the Royal Astronomical Society

Abstract

We use $UBV_{\rm m}VI$ images of Stephan's Quintet (Hickson Compact Group 92) taken with the Wide Field Camera 3 on the Hubble Space Telescope *(HST)* centred on NGC 7318B/A and the Northern Starburst Region (NSBR, a.k.a. SQ-A). We identify five regions of interest in our observations: the Left and Right tidal Arcs, NSBR, the Southern Debris Region (SDR), and an overdensity of star clusters between NGC 7318A and the SDR, which we dub the Upper SDR (USDR). We identify star clusters throughout these regions, and estimate their masses and ages by comparing their observed spectral energy distributions with predictions from population synthesis models. Comparing star clusters between the different regions, we find that the youngest clusters are very tightly clustered in all the regions, while clusters with older ages are more distributed. The population of old massive star clusters (age $> 10^9$ yr), presumably globular clusters, appear to be roughly centred on the elliptical galaxy NGC 7318A. We observe a shallow age gradient along the Left Arc, suggesting that intruder galaxy NGC 7318B is inclined such that its eastern spiral arm is the initial point of interaction. We also discuss the possible origin of young star clusters throughout the system. We construct the mass function for the youngest clusters in all the regions with age ranges between $10^6 < \tau < 10^7$ yr, and find that it can be described by a power law, $\mathrm{d}N/\mathrm{d}M \propto M^{\beta}$, where β ranges from -1.42 to -2.60. We find that the young population of SCs in all regions have surprisingly few high mass ($> 10^4 \mathrm{M}_{\odot}$) clusters. Based on the similarity of the age and mass distributions of their young clusters, Left Arc and SQ-A appear to be associated; the Right Arc and SDR appear to have had a long history of active star formation that started $\sim 10^8$ yr ago. The low numbers of clusters in the USDR make its association more ambiguous. The mass distribution of very young

$\leq 10^7$ yr clusters in the Left Arc, which coincides with the strong shock, shows a steeper cumulative distribution with fractionally fewer higher mass clusters. This may be a consequence of the suppression of star formation in a strong shock inferred in the literature.

3.1 Introduction

Most stars form in the cluster environment (Lada & Lada, 2003). Over time, the majority of clusters will disperse, contributing their stars to the surrounding stellar field, with the fraction of clusters disrupted every dex in log(age) ranging from 0.5 (Bastian, 2011) to 0.9 (Chandar et al., 2006). Studying the properties of star clusters (SCs), in particular their mass and age distributions, provides insights into the process of star cluster formation and disruption.

Previous studies of age and mass distributions of star clusters (e.g., Bastian et al., 2005b; Chandar et al., 2010b; Fall, 2004; Whitmore et al., 2010) have suggested that both distributions can be described by a single power law, with appropriate indices for each distribution. The recent work on this subject by Fall & Chandar (2012, hereafter FC12) used the observations of six galaxies with a wide range of galactic environments (dwarf, merging, quiescent and interacting galaxies) to determine these distributions. They found that for the systems in the sample, the mass distribution is well represented by $\mathrm{d}N/\mathrm{d}M \propto M^{\beta}$ with $\beta \approx -1.9$ (for the age range of $10^6 \lesssim \tau/\mathrm{yr} \lesssim 10^9$), and the age distribution can be described by $\mathrm{d}N/\mathrm{d}\tau \propto \tau^{\gamma}$ with $\gamma \approx -0.8$ (for the mass range of $10^2 \leq \mathrm{M/M_\odot} \leq 10^6$). The authors emphasized that they would not expect that the mass and age distributions would be exactly the same in all parts of all galaxies, especially considering the range of histories of cluster formation and/or disruption processes under different conditions, e.g., quiescent vs. actively star-forming. However, they argue that the minor differences in the exponents that might be present on small scales in galaxies will gradually diminish with increasing physical scale as local inhomogeneities are averaged out. On the galactic scale, the similarities of these distributions are such that the term "universal" can be applied to them. The results of FC12 appear to imply that the shapes of the age and mass distributions, on the galactic scale, are not heavily dependent on the large-scale environment. To test this possibility, a study of age and mass distributions in an environment significantly different from the previously studied ones is in order. That is, if cluster formation and disruption are sensitive to large-scale influences, then investigating an extreme environment is most likely to reveal differences. The extreme environment of a strong, large-scale shock is promising for such a study. We might expect a complicated relation between the shocked gas and cluster formation and/or disruption processes, particularly because the shock environment can assist star formation as well as impede it or alternatively speed up the disruption processes. Thus, looking for environments where "universality" breaks down might help us to understand the origin of so-called universal distributions.

The compact group of galaxies known as Stephan's Quintet (HCG 92; hereafter SQ) is a perfect system for our enquiries, considering that this system has both quiescent and interacting galaxies, tidal tails, star formation in the intra-group medium (IGM), and, most importantly for our case, a ~40 kpc long X-ray emitting shock region (first discovered by Allen & Hartsuiker 1972 as a radio emission ridge at 21 cm). The shock was created by a collision between the intruder galaxy NGC 7318A (blueshifted with respect to the group mean velocity by $\sim 900\ \mathrm{km\,s^{-1}}$) and approximately $10^{10}\ \mathrm{M_\odot}$ of material (O'Sullivan et al., 2009) deposited in that

region by previous interactions between the galaxies in the group (Moles et al., 1997; Sulentic et al., 2001).

In our previous work (Fedotov et al., 2011, hereafter F11), we studied the star cluster population of SQ, including the strong shock region. The work was based on Early Release Observations (ERO) obtained with the Wide Field Camera 3 (WFC3) on *Hubble Space Telescope* (*HST*). We showed that SCs can be used as tracers of star formation triggered by gravitational interactions and have confirmed intense star formation along the shock region (e.g., Xu et al., 2005) and the ages of newly formed SCs that in some cases are less than 10^7 yr old (e.g., Gallagher et al., 2001).

This paper utilizes the superb ERO data with the addition of new U_{336} and V_{547} observations, carried out with WFC3 in October of 2011 that cover the interacting pair NGC 7318B/A and the regions of extragalactic star formation that surround them. The addition of two more filters to the *BVI* photometry already in hand enables us to break the age-reddening degeneracy for age-dating star clusters and gives greater resolution to ages in the 10^7–10^8 yr range. That allows us to probe the age and mass distribution of star clusters to unprecedented sensitivity and photometric precision for a system such as SQ so that we may test the "universality" of these distributions in the unique setting present in SQ.

The outline for the remainder of the paper is as follows: in Section 3.2 we discuss the data and star cluster selection. In Section 3.3 we present the method that we use to determine the age and mass of star clusters. Section 3.4 is devoted to the presentation and discussion of our results, and in Section 3.5 we summarize our final conclusions. Throughout this paper, we adopt a Hubble constant of $H_0 = 70$ km s^{-1} Mpc^{-1}. The luminosity distance to SQ is 88.8 Mpc ((m-M) = 34.74 mag); 1″ at that distance corresponds to 0.43 kpc. The scale of the images is 0.″028 pixel^{-1} or 12 pc per pixel.

3.2 Observations and Cluster Selection

3.2.1 Data

For this paper, we used observations obtained with the *HST* Early Release Science data (ERS; proposal 11502, PI K. S. Noll). The observations were carried out with WFC3 in six filters of which we use F438W (B_{438}), F606W (V_{606}), F814W (I_{814}), and F665N ($H\alpha_{665}$) images. The exposure times were 13200, 5400, 7200, and 15600 seconds for the B_{438}, V_{606}, I_{814}, and $H\alpha_{665}$ filters, respectively. Additionally, we added observations in the F336W (U_{336}) and F547M (V_{547}) filters, which were obtained in October 2011 (proposal 12301, PI S. C. Gallagher), and had exposure times of 17280 and 5834 seconds, respectively. The F336W filter images are essential to resolve age ambiguities at young ages, by completing the *UBVI* photometric baseline (Anders et al., 2004). The medium-band imaging with the F547M filter provides images that are free from nebular contamination by Hβ, [O III] λ4959, 5007, Hα, [N II] λ6583 and [S II] λ6716, 6731, that is present in the very broad F606W filter images. This contamination was a limiting factor to our *BVI* age-dating process in our previous study of SQ (F11), because we used only the F606W filter images.

The twelve WFC3 images in each of the U_{336}, B_{438}, V_{606}, $H\alpha_{665}$, and I_{814} filters, and the four images in the V_{547} filter were combined into deep, cosmic-ray cleaned, geometric-

distortion corrected mosaics using `Multidrizzle` version 3.3.8. We did not use the drizzled products available for ERS data from the archive due to pointing errors that can result in a non-optimal point spread function (PSF). Instead, we obtained the calibrated (i.e., bias and dark-subtracted, flat-fielded) images from the archive, and reprocessed them with the latest version of `Multidrizzle` and the most recent distortion corrections available.

As previously stated, small shifts between images are caused by telescope pointing errors ($\lesssim 1''$). To correct these shifts, we measured the centroids of non-saturated point sources (e.g., stars in the broad band filters, as well as galaxy nuclei in $H\alpha_{665}$) in each of the pointings and then computed the residual offsets between frames after an initial run of `Multidrizzle`. These offsets were then resupplied to the software in the form of a shift file in an effort to minimize the offsets. This ensures the shape of the PSF is well-behaved and its width is minimized in the final output image.

Following the procedure outlined in Fruchter et al. (2009), we changed the values of the *final_pixfrac* and *final_scale* parameters to achieve improved spatial resolution. The mosaics each have a pixel scale of $0\farcs028$ pixel^{-1}. To correct the astrometry of the final mosaic products, we registered the images with the USNO B-1.0 all-sky astrometric catalogue. This catalogue was chosen for its completeness ($\sim 10^9$ objects down to $V = 21$ mag) in addition to its astrometric accuracy of $0\farcs2$. Corrections to the world coordinate system (WCS) were made using the `IMWCS` task in WCSTools version 3.8.1.

3.2.2 Source Detection and Photometry

With a distance of 88.8 Mpc to SQ, one pixel on the WFC3 image corresponds to $0\farcs028$ or $\sim$ 12 pc. With the average size of a star cluster of 3–6 pc (Barmby et al., 2006; Scheepmaker et al., 2007; Whitmore et al., 1997), most of the SCs in SQ will appear as point sources. Even the massive young clusters, which could reach sizes of $\sim$ 10 pc (e.g., Bastian et al., 2005a; Whitmore et al., 1999, though both studies caution that the sizes larger than 10–15 pc are likely due to crowding), are not expected to be resolved. Hence, our finding algorithm was tuned for point-source detection.

The detection of point sources was carried out with the `DAOFIND` task (Stetson, 1987) in `IRAF`[1] in the V_{606} because it is the deepest image available. We used the coordinate list of detected sources to derive the PSF magnitudes of these sources in each filter. The PSF was constructed from bright, isolated and unsaturated stars with point-like radial curves of growth. There were 18, 60, 27, 86, and 89 such stars in the U_{336}, B_{438}, V_{547}, V_{606}, and I_{814} filters, respectively.

We convert the instrumental magnitudes to the VEGAMAG magnitude system by applying the following zeropoints: 23.484 mag for U_{336}, 24.974 mag for B_{438}, 24.748 mag for V_{547}, 25.987 mag for V_{606}, and 24.680 mag for I_{814}, which are provided by the STScI. [2]

The photometry in the F336W, F438W, F606W, and F814W wide filters was corrected for foreground extinction calculated using data from Schlafly & Finkbeiner (2011), with resulting values of $A_{336} = 0.353$ mag, $A_{438} = 0.288$ mag, $A_{606} = 0.197$ mag, and $A_{814} = 0.122$ mag. The

[1]IRAF is distributed by the National Optical Astronomy Observatory, which is operated by the Association of Universities for Research in Astronomy (AURA) under cooperative agreement with the National Science Foundation.

[2]Space Telescope Science Institute: `http://www.stsci.edu/hst/wfc3/phot_zp_lbn`

correction for the medium F547M filter was interpolated, based on the wide filter correction, to have a value of $A_{547} = 0.226$ mag. The aperture corrections were determined in a similar manner as in Fedotov et al., 2014, and have the following values: 0.790, 0.724, 0.641, 0.600, and 0.599, for U_{336}, B_{438}, V_{547}, V_{606}, and I_{814} filters, respectively.

In addition to the already mentioned shifts between pointings in one filter, there are also shifts between resulting images for different filters. Since the U_{336} and V_{547} observations were carried out separately from ERS, with a smaller field of view and a different roll angle (220° for ERS and 82° for later observations, the shifts between these observations are particularly large. Additionally, it appears that in our *HST* images the point sources that are further from the central point on the image have higher shift values. To address these issues we divided the resulting image in V_{606} into 16 regions (in a 4×4 matrix) and calculated shifts between frames for each region with the `MATCH` [3] software written by Michael Richmond.

Approximately 6,000 point sources were detected in all 5 filters (U_{336}, B_{438}, V_{547}, V_{606}, and I_{814}) and constitute our initial SC candidate catalogue. Table 3.1 gives an example of our catalogue and the full version of it is available in on-line version of this paper.

3.2.3 Cluster Selection

Throughout the analyses, we will be using two catalogues. The first catalogue represents the unfiltered list of all detected sources (N=5996; Fig. 3.1), and the second one consists of the high confidence star cluster candidates (SCCs). The latter has 1588 objects in it and was created by applying the following criteria to the initially detected sources:

- **Colour cuts**

  To minimize the contamination from the foreground stars, we keep only objects that satisfied the following color restrictions: $B - V < 1.5$ or $V - I < 1.0$. This values were chosen based on spectroscopic study of sources in SQ by Trancho et al. (2012) (see their fig. 8).

- **Photometric error σ < 0.3 mag in all five filters**

  For an object to be considered a SCC, its photometric errors should be less than 0.3 in all filters. This requirement reduces the uncertainty in our age and mass estimations calculated subsequently.

- **Sharpness between −2 and 2 in all bands**

  The sharpness parameter is set to weed out non-astronomical objects and brightness enhancements that are elongated in x or y directions. Sharpness is measured as the difference between the square of the width of the object and the square of the width of the PSF. A truly round object will have sharpness=0, and with that in mind, we set our interval in sharpness between −2 and 2. We have to note, however, that the brightest objects in our list are rarely round, i.e., they have high sharpness values. Thus, a number of extremely large star clusters and star cluster complexes can potentially be filtered out by the application of the sharpness criterion.

[3] `http://spiff.rit.edu/match/`

Table 3.1: A sample table of the UBV_mVI catalogue for star clusters in Stephan's Quintet. The full catalogue is available online.

RA	Dec	F336W			F438W			F457M			F606W			F814W			χ_I	S1	S2	S3	S4	SCC	χ	$E(B-V)$	A_V	age	mass	Region
deg	deg	mag	err	sharp	mag	err	sharp	mag	err	sharp	mag	err	sharp	mag	err	sharp									mag	yr	$M_\odot$	
(1)	(2)	(3)	(4)	(5)	(6)	(7)	(8)	(9)	(10)	(11)	(12)	(13)	(14)	(15)	(16)	(17)	(18)	(19)	(20)	(21)	(22)	(23)	(24)	(25)	(26)	(27)	(28)	(29)
338.98535	33.971085	20.875	0.026	0.401	21.966	0.074	0.446	21.841	0.033	0.499	21.822	0.036	0.234	21.453	0.065	0.992	10.959	1	1	0	1	–	0.0	0.32	0.99	4570881.89	395086.9	RightArc
338.99658	33.959503	21.358	0.073	2.421	22.753	0.07	1.229	22.786	0.076	1.678	21.938	0.097	1.401	22.625	0.107	2.446	7.401	1	0	0	1	–	0.1	0.28	0.86	1047128.54	186987.0	LeftArc
339.00162	33.96772	21.362	0.041	1.103	22.36	0.065	0.894	22.301	0.052	0.898	22.13	0.043	0.6	21.748	0.051	1.232	7.942	1	1	0	1	–	0.2	0.0	0.0	34673685.0	649639.6	LeftArc
338.98199	33.962109	21.69	0.069	1.859	22.942	0.087	0.569	22.923	0.056	1.011	22.744	0.053	0.655	22.285	0.08	1.904	10.69	1	1	0	1	–	0.1	0.16	0.49	6309573.44	145276.7	USDR
339.00006	33.962971	21.901	0.05	1.41	22.918	0.038	0.537	22.839	0.035	0.597	22.695	0.046	0.509	22.222	0.057	1.345	7.962	1	1	0	1	–	0.3	0.02	0.06	32359365.6	400436.2	LeftArc
338.99704	33.970909	21.957	0.035	0.93	22.742	0.042	0.548	22.656	0.037	0.701	22.549	0.035	0.558	22.227	0.055	1.155	7.736	1	1	0	1	–	0.3	0.0	0.0	57543993.7	591600.8	LeftArc
338.99677	33.967438	21.975	0.077	2.085	23.387	0.072	1.224	23.663	0.079	1.649	23.236	0.072	1.127	23.538	0.095	2.215	7.561	1	0	0	1	–	2.1	0.0	0.0	5248074.60	33687.7	Other
338.98584	33.971863	21.975	0.065	1.836	23.43	0.063	0.878	23.507	0.071	1.521	23.166	0.065	1.04	23.544	0.089	2.125	7.744	1	0	0	1	–	0.0	0.18	0.55	2398832.91	49094.8	RightArc
338.99652	33.959476	22.137	0.108	2.846	23.156	0.082	1.417	23.101	0.089	2.053	22.545	0.091	1.41	23.111	0.145	2.641	10.963	1	0	0	1	–	1.2	0.26	0.80	3467368.50	75650.2	LeftArc
338.98175	33.962227	22.149	0.09	2.595	23.505	0.079	1.333	23.564	0.104	2.116	22.941	0.092	1.404	23.481	0.122	3.03	10.274	1	0	0	1	–	0.1	0.22	0.68	2754228.70	56570.4	USDR
338.9856	33.972649	22.247	0.057	1.731	23.638	0.074	1.127	23.783	0.068	1.548	23.483	0.09	1.172	23.887	0.082	1.716	6.116	1	1	0	1	–	0.0	0.08	0.24	3019951.72	25987.8	RightArc
338.99448	33.959503	22.291	0.083	2.621	23.609	0.074	1.32	23.622	0.079	1.838	22.672	0.069	1.089	23.186	0.103	2.487	10.339	1	0	0	1	–	0.2	0.12	0.37	6025595.86	62003.2	LeftArc
338.99649	33.959515	22.314	0.08	2.482	23.838	0.086	1.412	24.007	0.08	1.583	23.13	0.101	1.577	23.66	0.19	2.702	6.41	1	0	0	1	–	1.5	0.0	0.0	6309573.44	33453.1	LeftArc
338.99432	33.981403	22.323	0.111	3.432	23.758	0.101	1.561	23.744	0.108	2.552	23.487	0.092	1.478	23.654	0.136	3.133	8.691	1	0	0	1	–	0.0	0.28	0.86	1000000.0	84011.6	SQ-A
338.99207	33.983459	22.35	0.084	2.542	23.652	0.078	1.252	23.525	0.089	2.206	23.108	0.071	1.086	23.534	0.11	2.428	10.083	1	0	0	1	–	1.4	0.22	0.68	3801893.96	54372.0	SQ-A
338.99606	33.980625	22.373	0.03	0.697	22.982	0.047	0.61	22.378	0.055	0.965	22.278	0.046	0.486	21.534	0.039	0.686	6.374	1	1	0	1	–	5.6	0.34	1.05	72443596.0	2325336.0	SQ-A
...																												

Notes. Columns list: (1) Right Ascension (J2000); (2) Declination (J2000); (3)–(5) Magnitude, error in magnitude, and sharpness values for U-band (F336W); (6)–(8) Magnitude, error in magnitude, and sharpness values for B-band (F435W); (9)–(11) Magnitude, error in magnitude, and sharpness values for V_m-band (F547M); (12)–(14) Magnitude, error in magnitude, and sharpness values for V-band (F606W); (15)–(17) Magnitude, error in magnitude, and sharpness values for I-band (F814W); (18) Goodness of fit factor χ from PSF-fitting in I-band; (19)–(22) Star cluster candidates selection criteria: 1 means that given criterion is satisfied; (23) Star cluster candidate flag. If 'yes', all SCC criteria are satisfied; (24) Goodness of fit factor to the SSP model; (25) $E(B-V)$ values; (26) Extiction values; (27) Age in years; (28) Mass in $M_\odot$; (29) Region.

- **Goodness of fit χ in I-band**

  The I-band was chosen for the goodness of fit criterion because the PSF model is best determined in that band and there is no expected contamination from emission lines. Thus, this band will give a more realistic result in the determination of the goodness of the PSF fitting. For this condition we require $\chi < 3$.

- **Magnitude cut at $M_{V_{606}} < -9$ mag**

  To eliminate contamination from individual luminous supergiants, which can reach $M_{V_{606}} \simeq -8$ mag, we considered only sources with $M_{V_{606}} < -9$ mag.

3.2.4 The Use of Two Catalogues

As was mentioned above, throughout the paper we are going to use two catalogues: all detected sources and the high confidence SCCs. The idea is to both obtain a general "feel" for the entirety of the population and to perform quantitative analysis with a more restricted, higher photometric-quality dataset. The plots created with all detected sources give us the more general view to reveal possible trends. It is more likely that there will be some contamination but, at the same time, there also will be genuine sources that would otherwise be filtered out with our stricter SCC criteria. On the other hand, the SCC catalogue has fewer sources but there is a very high probability that most of those sources are actual star clusters. Studying plots that were produced with the SCC catalogue should give us a more refined view of the star cluster properties. One additional thing to note is that for the SCC catalogue, sources that are plotted not only satisfy all 4 conditions required to be considered as SCCs, but we also apply one additional condition: the goodness of fit to the simple stellar population (SSP) model must be less than 3 (analogous to the condition for the I- band χ from PSF-fitting; see §3.3).

3.3 Age and Mass Determination

In order to constrain the mass distribution of young clusters along the strong shock and other regions in SQ, it is essential to have reliable age and mass constraints for the young cluster population. Accurate ages and masses are obtained from our WFC3 photometry via simple stellar population synthesis models after correcting for intrinsic extinction. Extinction (assumed to be Galactic; Fitzpatrick 1999) causes spectral curvature that can be detected unambiguously with multiple bandpasses in a broad enough wavelength range ($\sim 300 - 800$ nm).

With only BVI photometry in our previous analysis of the cluster population in Stephan's Quintet, we were able to estimate coarse age distributions for the clusters in different regions. The addition of U_{336} and medium V_{547}-band (as opposed to V_{606}) photometry, offers the wavelength coverage and resolution to both break the age-reddening degeneracy that can plague BVI colour-colour age estimates and avoid the effect of strong Hα contamination in the broad V_{606}-band filter. The age, mass and extinction (up to $A_V \leq 1.5$) of each cluster are estimated from the photometry in the five filters (UBV_mVI) as described and implemented by Chandar et al. (2010b). In particular, the age and extinction for each cluster are found by performing a least χ^2 fit for best combination of age and extinction. During the fit the observed magnitudes in five

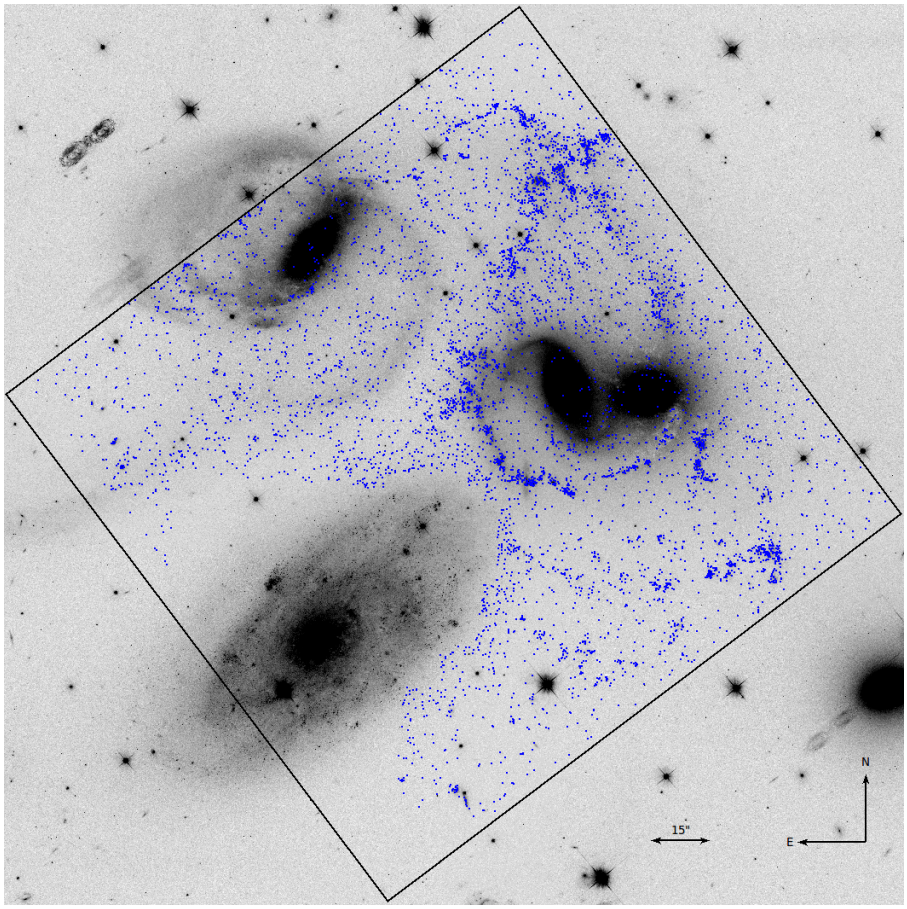

Figure 3.1: Field-of-view (black square) of the new *HST* images (U_{336} and V_{547} filters) with all 5996 detected objects plotted over the inverted *V*-band image from the original ERS observations. Tidal features hosting the youngest star clusters are clearly seen as concentrations of sources.

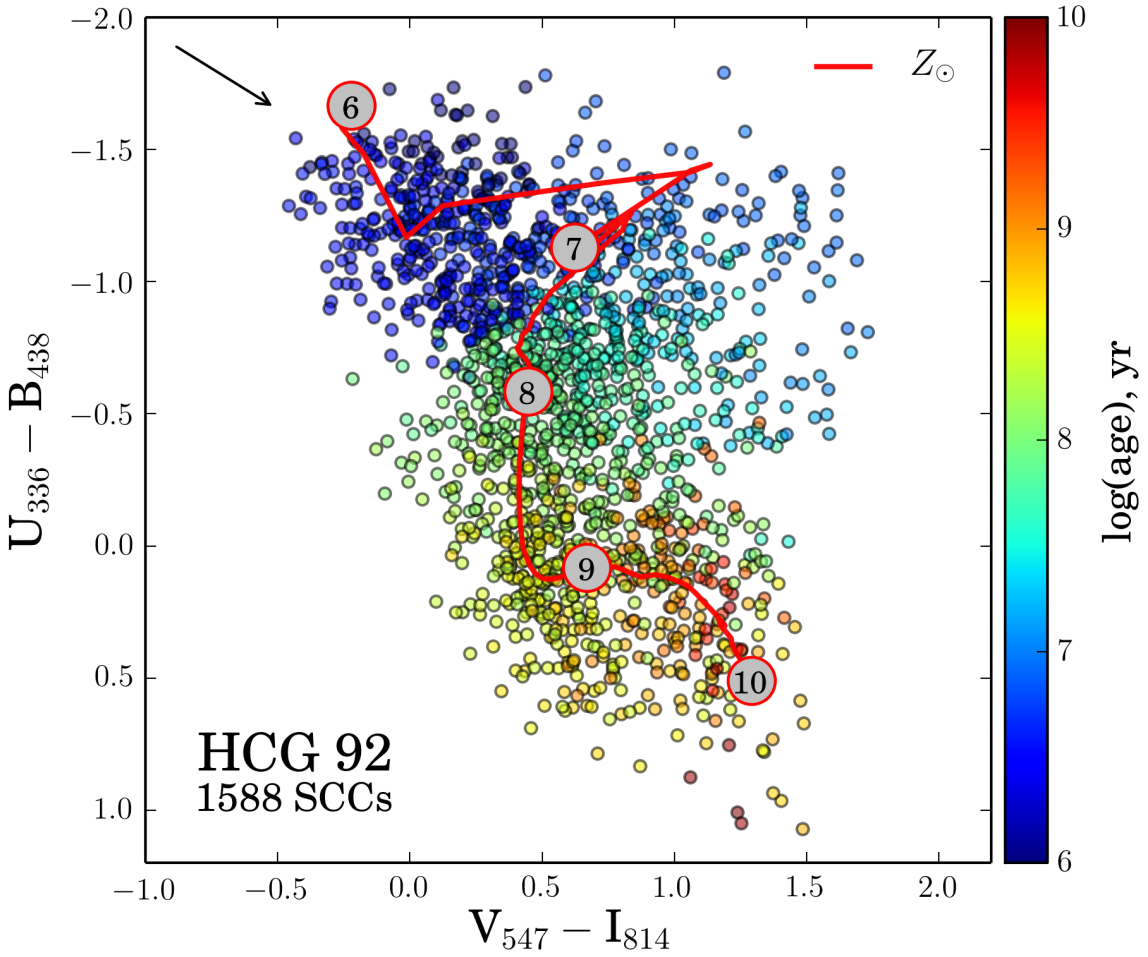

Figure 3.2: Colour-colour plot of $U - B$ vs $V_m - I$ of the star cluster candidates detected in HCG 92 colour-coded according to the age values obtained by SED fitting. Overplotted is an evolutionary track based on the SSP model of Marigo et al. (2008) (identical to one used in Fedotov et al. 2014). In the upper left corner a reddening vector with length equivalent to V_{606} = 1 mag is shown. The SED-fitting ages of star-cluster candidates are consistent with the expectation from the colours. Note that the use of V_m-band minimizes the effect of H_α emission on the colours of the youngest clusters.

Table 3.2: Completeness levels in the five UBV_mVI filters for different background brightness levels (Fig. 3.3).

Background	U_{336}		B_{438}		V_{547}		V_{606}		I_{814}	
level	90%	50%	90%	50%	90%	50%	90%	50%	90%	50%
Bright	25.97	27.05	25.96	27.11	26.25	27.19	26.42	27.29	26.29	27.16
Medium	25.52	27.52	26.98	27.71	26.55	27.72	27.04	27.87	26.72	27.75
Dark	27.01	27.77	27.15	28.02	27.22	28.04	27.42	28.20	27.18	27.96

*`http://ned.ipac.caltech.edu/ngi/`

filters (UBV_mVI) are compared with predictions from the 2009 update to the Bruzual G. A. & Charlot (2003) simple stellar population models (with a Chabrier (2003) initial mass function). The extinction evaluated based on a Galactic extinction law (Fitzpatrick, 1999). The masses are then estimated from the extinction-corrected V_{606}-band magnitudes and the mass-to-light ratio predicted by the models, assuming the adopted distance modulus to SQ. As a quick check of the obtained values, we compare the ages of clusters determined by aforementioned method with the evolutionary track of a hypothetical cluster in $U - B$ vs. $V_m - I$ colour- colour plot (Fig. 3.2). As we can see, predicted ages for star cluster correlate well with the evolutionary track.

3.3.1 Completeness

The completeness levels were calculated in three regions corresponding to dark, moderate, and bright background levels (Figure 3.3). For each region we used `ADDSTAR` to add 1500 artificial stars in the apparent magnitude range 24–28 mag, i.e., absolute magnitudes ranging between –10.74 mag and –6.74 mag (given the distance modulus to HCG 92 of 34.74 mag). We applied the same point source detection algorithm (as described in §3.2.2) to determine the recovery rates. The results are presented in Table 3.2.

3.3.2 Regions

We divide the field into five regions, according to star cluster overdensities (Fig. 3.4). The Left Arc represents the eastern tidal arc, which includes the strong shock region (Allen & Hartsuiker, 1972; Xu et al., 2003), and the Right Arc represents the western tidal arc. The Northern Starburst Region (NSBR, a.k.a. SQ-A) represents a region where the two tidal arcs intersect. It has strong H_α emission (Xu et al., 1999) and hosts many young star clusters (Gallagher et al., 2001, F11). The Southern Debris Region, originally detected by Shostak et al. (1984), has approximately $3.1 \times 10^9\,M_\odot$ of H I (Shostak et al., 1984) and a number of young star clusters (F11). The Upper Southern Debris Region is a small overdensity of star clusters that are likely of tidal nature as well. Figures 3.6 to 3.9 show age and mass distributions for the SCC populations, as well as for all detected sources, for all the regions.

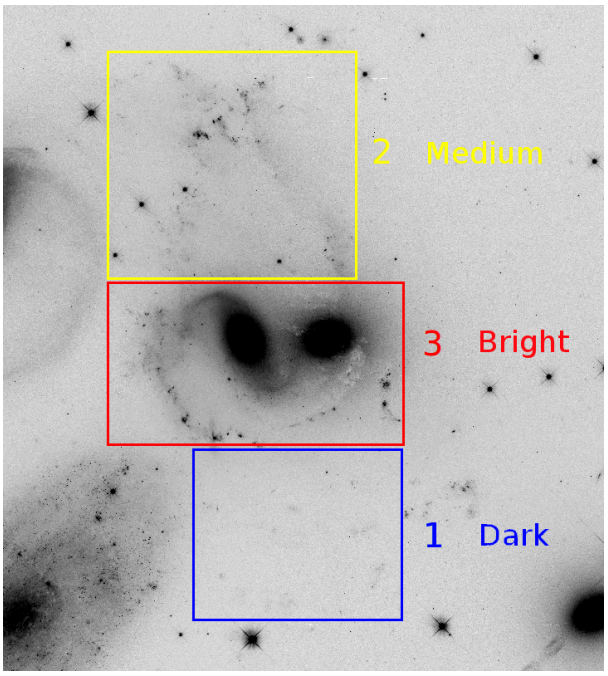

Figure 3.3: Inverted *V*-band image of the interacting pair NGC 7318B/A with square regions indicating the parts of the images designated as (1) dark, (2) medium, and (3) bright background for the completeness determination. Completeness levels were calculated separately for each background type.

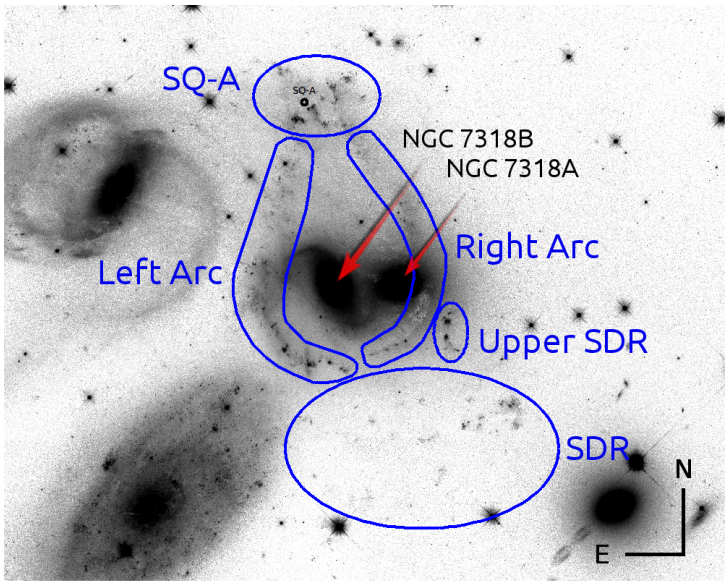

Figure 3.4: Labelled regions plotted over the inverted *V*-band image. SQ-A is also known as the Northern Starburst Region (NSBR). The Right Arc and Upper Southern Debris Region (SDR) are defined here for the first time. The Left Arc and SQ-A are most directly associated with the strong shock region; the Right Arc, Upper SDR and SDR are not spatially coincident with the X-ray emitting shock.

3.4 Results and discussion

3.4.1 Logarithmic Age Versus Mass Diagram

Fig. 3.5 shows the logarithmic age versus mass diagram with additional plots representing individual regions. Even a quick visual review of the plot reveals a few interesting features. First, there is a lack of massive young star clusters. Most of the clusters with masses over $10^5 M_\odot$ are older than 10^8 yr. Second, there is an absence of old clusters (between ages of 10^9 and 10^10 yr) in the Left Arc, SQ-A, and USDR regions. The presence of the aforementioned clusters in the Right Arc and SDR can be explained by their proximity to NGC 7318A, which is classified as elliptical (Konstantopoulos et al., 2014) and as such is expected to have a significant population of older clusters. Additionally, we observe the recent star formation episode at $\sim 10^{6.5}$ yr in all five regions, as an overdensity of clusters at that age. The regions Left Arc and SQ-A had more-or-less continuous star formation starting from 10^9 yr up to the present, with an additional noticeable peak at around 10^8 yr. There is a hint of that in the Right Arc region as well, although it is less pronounced. In both SDR and especially Right Arc region a reduction in star formation between 10^7 and $10^{7.5}$ yrs is observed. The USDR region has the smallest number of SCCs detected and because of that not many conclusions can be drawn about this region.

Below, we investigate the spatial maps of age and mass distributions, along with the age and mass functions of SCCs in all regions. In the cases for which we need to boost our statistics, we are going to use catalogues of all detected sources, following the approach outlined in § 3.2.4.

3.4.2 Maps of Age and Mass Distributions

We bin SCCs in all five regions into four bins according to their ages ($\tau < 10^7$, $10^7 < \tau < 10^8$, $10^8 < \tau < 10^9$, and $\tau > 10^9$; all ages in years) and plot them superimposed on the image of SQ (Figs. 3.6 and 3.7, for the catalogues of SCCs and all sources). We notice that the young star clusters ($\tau < 10^7$ yr) are tightly concentrated along the tidal features and, as was pointed out earlier, have relatively low masses $M < 10^4$ $M_\odot$.

The SCCs with ages $10^7 < \tau < 10^8$ yrs have a bit wider spatial distribution, albeit still concentrated along tidal features. They are also a bit more massive than clusters in the previous bin, with masses reaching $M \sim 10^5$ $M_\odot$ and an average mass of $M = 10^{4.3}$ $M_\odot$. The fact that they still follow the tidal features could mean that the interaction-triggered star formation in the arcs has been going on for rather a long time (~ a few tens Myr).

The SCCs with ages between 10^8 and 10^9 yrs are distributed over the whole area. Their masses range between 10^4 $M_\odot$ and $10^{5.5}$ $M_\odot$, with very few objects outside of that range. More massive objects tend to be situated inside the galaxies. A relatively even cluster distribution about the whole area suggests that the clusters were deposited there rather than formed there.

The SCCs in the last bin (with ages over 10^9 yr) most likely represent globular clusters predominantly concentrated around the elliptical NGC 7813A. The estimated extent for the globular cluster system of NGC 7813A has a diameter of ~ 30 kpc and effectively covers all of NGC 7318B, the majority of the Left Arc, all of the Right Arc and Upper SDR, and most of the SDR (Fedotov et al. 2014; panel (c) of fig. 18). These are the most massive star clusters overall, with masses ranging from 10^5 $M_\odot$ to 10^6 $M_\odot$. A similar picture is observed on the plots of the age distributions of clusters separated by mass (Figs. 3.6 and 3.7).

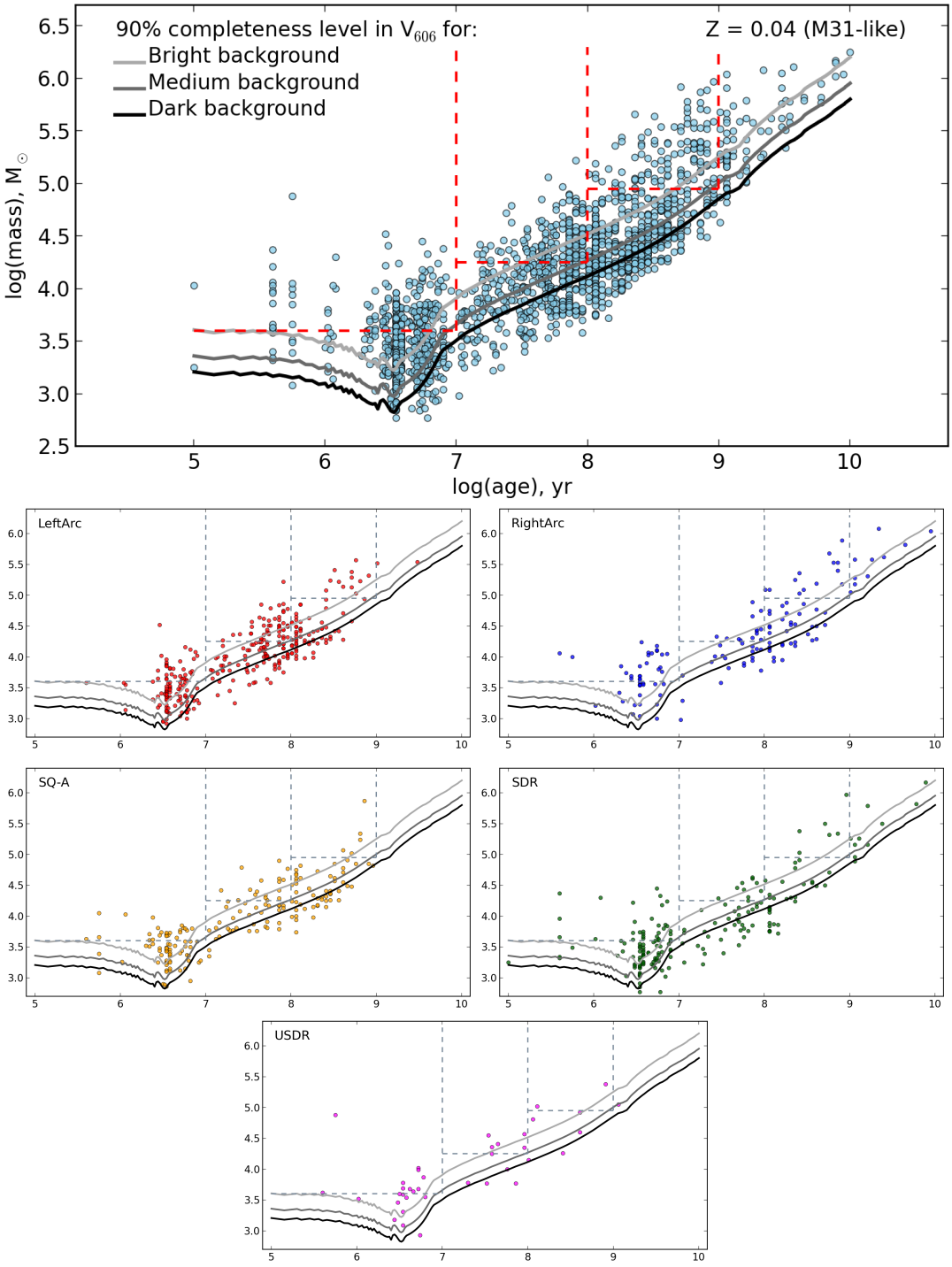

Figure 3.5: **Top:** A plot of log(mass) vs. log(age) for all the SCCs. The grey curves show the 90% completeness levels for bright (light grey), medium (grey) and dark (black) backgrounds as a function of age and mass. While the sensitivity to lower mass clusters decreases with age, up to 10^9 yr clusters with masses $\gtrsim 10^5$ $M_\odot$ are detectable. For the mass distribution, the bins are defined by the dashed lines. The limiting mass for the clusters younger than 10^7 yr is $10^{3.6}$ $M_\odot$; for the clusters with ages between 10^7 and 10^8 yr the limiting mass is $\sim 10^{4.3}$ $M_\odot$, and for the last bin of SCCs with ages between 10^8 and 10^9 yr the limiting mass is $\sim 10^5$ $M_\odot$, as shown by the dashed red lines. The rest of the plots are similar to the top one except that clusters for only one region are plotted. Here, and thereafter, the colours of points are intent to distinguish the different regions as labelled in the top left corner of each panel.

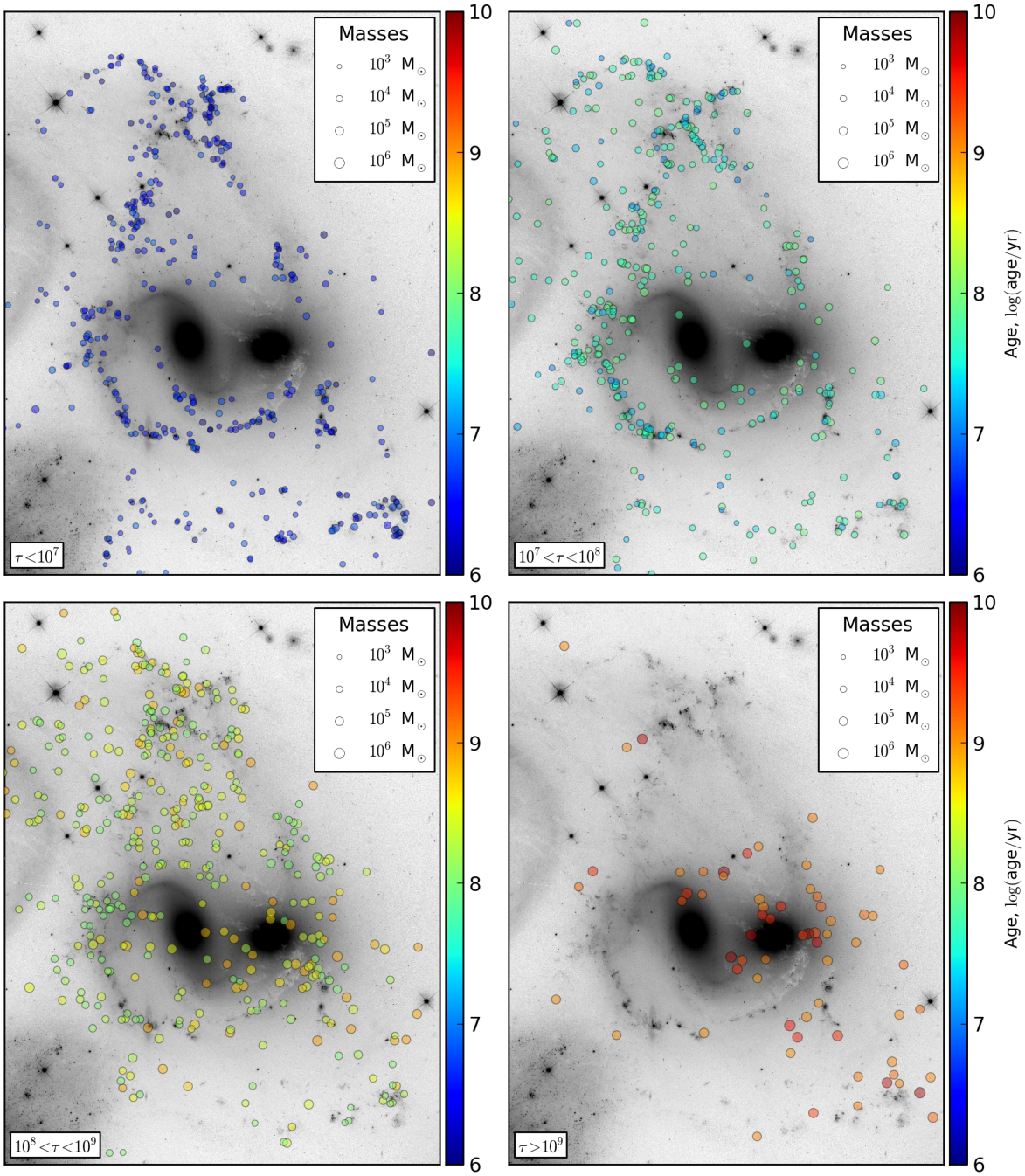

Figure 3.6: Plots of the spatial distribution of SCCs divided according to age bins, with the age bin ranges displayed in the lower left corner of each plot. The marker sizes are mass indicative, concordant with the legend in the upper right corner. The markers are colour coded according to their age, represented by colour bars on the right hand side of each plot. As in Fig. 3.5 we can clearly see how the mass of detected SCCs increases with age. However, in the first two age bins (top row of figures) only one SCC over $10^5 M_\odot$ is observed. On the images the north is up and the east is left.

A strong correlation between masses and ages is expected (see Fig. 3.5); star clusters dim as they age and only the brightest clusters, and hence the most massive ones, are detected, particularly at late ages. However, what is surprising is the complete lack of massive young star clusters. Moreover, given three different conditions of the regions where the young star clusters are detected (active star formation in the NSBR ($1.45\,M_{\odot}\,yr^{-1}$; Xu et al., 1999), the strong shock region along the middle part of the Left Arc, and the lower part of the Left Arc that runs from East to West below NGC 7318B), it is rather remarkable how similar their distributions are in terms of ages and masses. It would appear that star formation is happening rather uniformly on a large scale in the tidal features around the two interacting galaxies. Similar large-scale star formation in the compact group environment is observed in HCG 31 (Gallagher et al., 2010), although in that group stars are forming not only in the tidal H I bridge connecting the interacting pair HCG 31AC and HCG 31B with HCG 31G, but also within the galaxies as well. In contrast however, HCG 31 is believed to be a set of four, gas-rich, low-mass galaxies that are coming together for the first time with relatively small radial velocity differences ($\Delta v_{\rm rad} \sim 60$ km s^{-1}). The picture of the NGC 7318B/A interaction is complicated by the presence of material (mostly dust and gas) that was deposited in the vicinity by previous interactions between the other members of the group (and likely by nearby galaxy NGC 7320C; Lisenfeld et al., 2002; Moles et al., 1997; O'Sullivan et al., 2009; Xu et al., 1999). In all likelihood, we are observing the complex outcome of an on-going three body interaction.

There are quite a few things still unclear about the tidal arcs in SQ. What is the origin of each of these features? How can star formation be happening simultaneously in regions that are seemingly independent from each other (e.g., the NSBR and the SDR)? Why are the young star cluster properties so similar in the different regions?

According to an H_{α} velocity map of H II regions located in the Left Arc (Konstantopoulos et al., 2014), the Arc has a velocity gradient starting from the SDR in the south with the velocity of intruder NGC 7318B; $v_{\rm R} \approx 5800$ km s^{-1} and ending with NSBR (SQ-A) with the IGM velocity of $v_{\rm R} \approx 6600$ km s^{-1}. Consistent velocities for the general regions of the NSBR and the SDR were observed by Williams et al. (2002) in their study of H I gas in SQ. Thus, it appears that the Left Arc is a single structure and not a combination of two different tidal features or a chance projection, which might otherwise explain the apparent gap in the line of young star clusters just above the eastern spiral arm of 7318B. But what is the origin of this ridge of gas? We look at the age distribution of the young SCCs along the Left Arc in detail to investigate this question. Given the assumption that the duration of the ongoing interaction between 7318A and B is a few tens of Myr (e.g., Renaud et al., 2010), we isolated clusters that are younger than 2×10^7 yr and located along the Left Arc. In order to boost the statistics we use all detected sources, not just SCCs. We assigned clusters to bins first by creating 10 equal bins along the y axis of the image, and also by creating 10 bins in the vertical direction with an equal number of clusters in each bin. The results are presented in Fig. 3.10. It would appear that there is a shallow age gradient; it starts with the youngest clusters at the northern part of the Arc and increasing due south, reaching the peak at the part of the arc that is located just below the center of NGC 7318B as observed along the y axis. There is also a suggestion that the age is getting smaller again as we go further along the Arc, but the observed age increase could be a projection effect, because a part of the cluster distribution is scattered perpendicular to the y axis. Based on these results, we conclude that the lower part of the eastern spiral arm of NGC 7318B was the first to interact with NGC 7318A and the material situated in that part

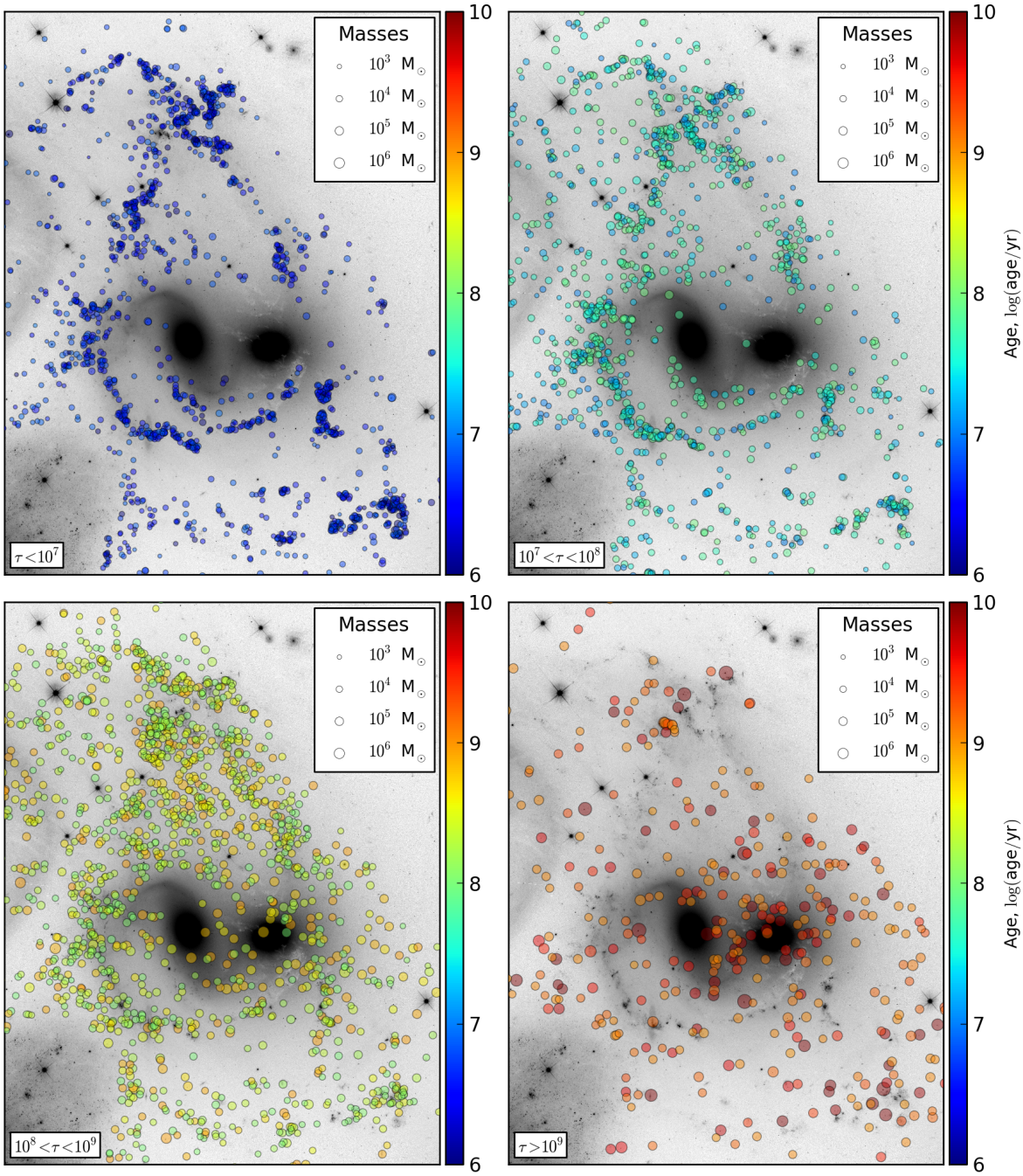

Figure 3.7: Plots of the spatial distribution of all detected sources divided according to age bins, with the age bin ranges displayed in the lower left corner of each plot. The marker sizes are mass indicative, concordant with the legend in the upper right corner. The markers are colour coded according to their age, represented by colour bars on the right hand side of each plot. For the spatial distributions of all sources we observe the same trend as for SCCs (the previous Fig. 3.6): there are virtually no sources with masses over $10^5 M_\odot$ that are younger than 10^8 yr. On the images the north is up and the east is left.

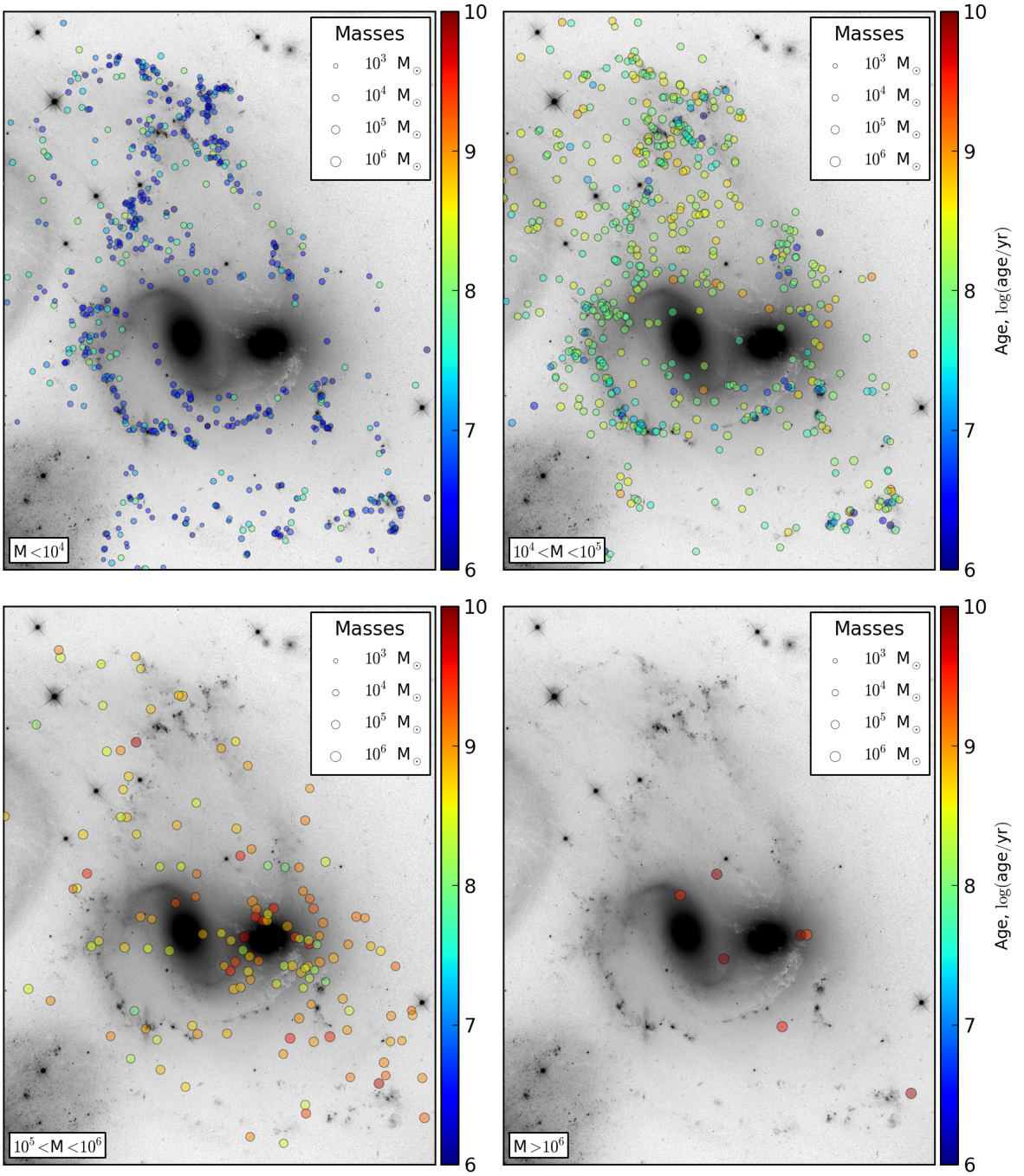

Figure 3.8: Plots of the spatial distribution of SCCs divided according to mass bins, with the mass bin ranges displayed in the lower left corner of each plot. The marker sizes are mass indicative, concordant with the legend in the upper right corner. The markers are colour coded according to their age, represented by colour bars on the right hand side of each plot. As we can see, the bottom row panels corroborates with the story presented in Fig. 3.7; there are no young SCCs ($< 10^7$ yr) with the masses above $10^5 M_\odot$. On the images the north is up and the east is left.

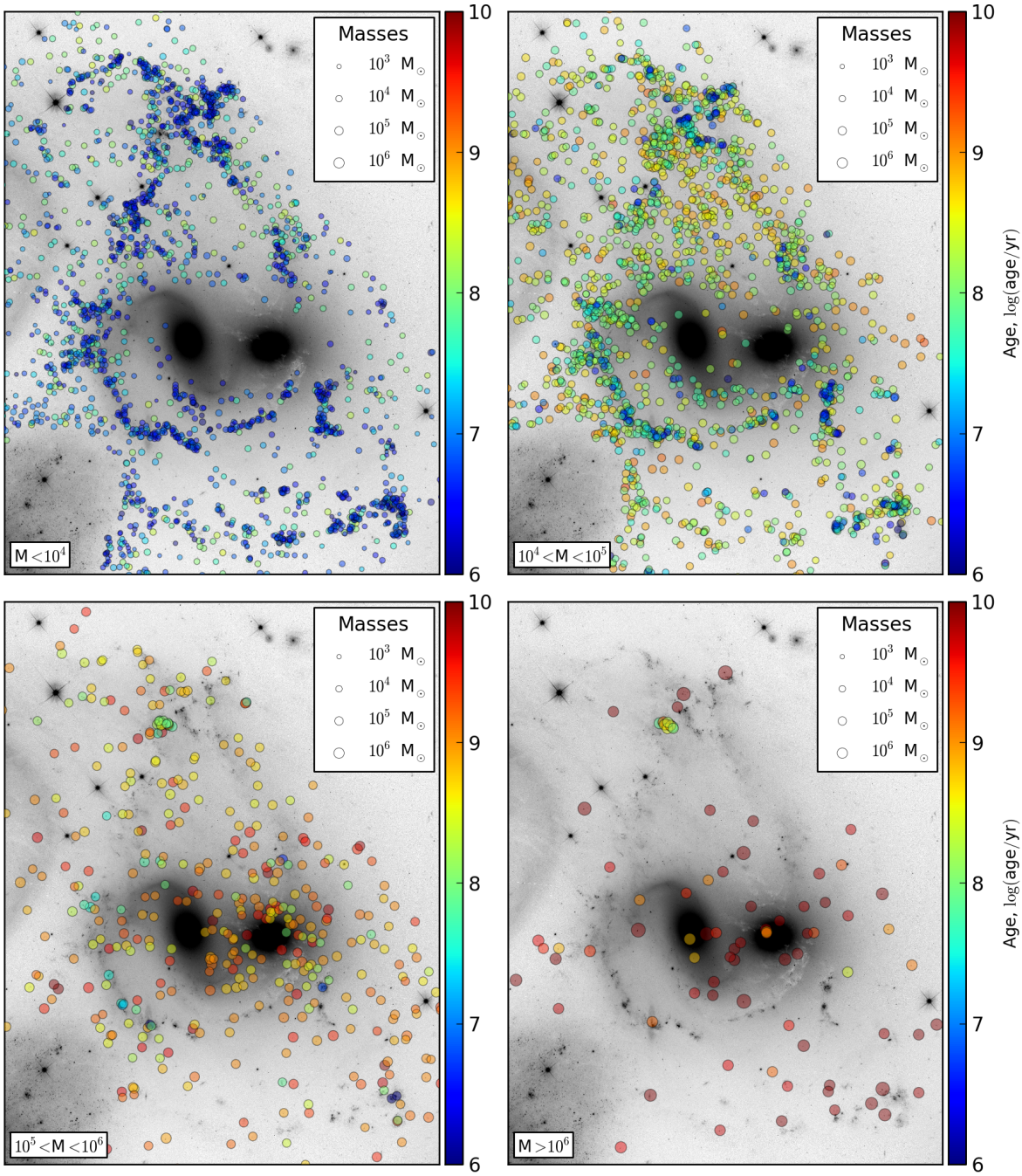

Figure 3.9: Plots of the spatial distribution of all detected sources divided according to mass bins, with the mass bin ranges displayed in the lower left corner of each plot. The marker sizes are mass indicative, concordant with the legend in the upper right corner. The markers are colour coded according to their age, represented by colour bars on the right hand side of each plot. Plots of all detected sources replicate the trend observed in the Fig. 3.8. On the images the north is up and the east is left.

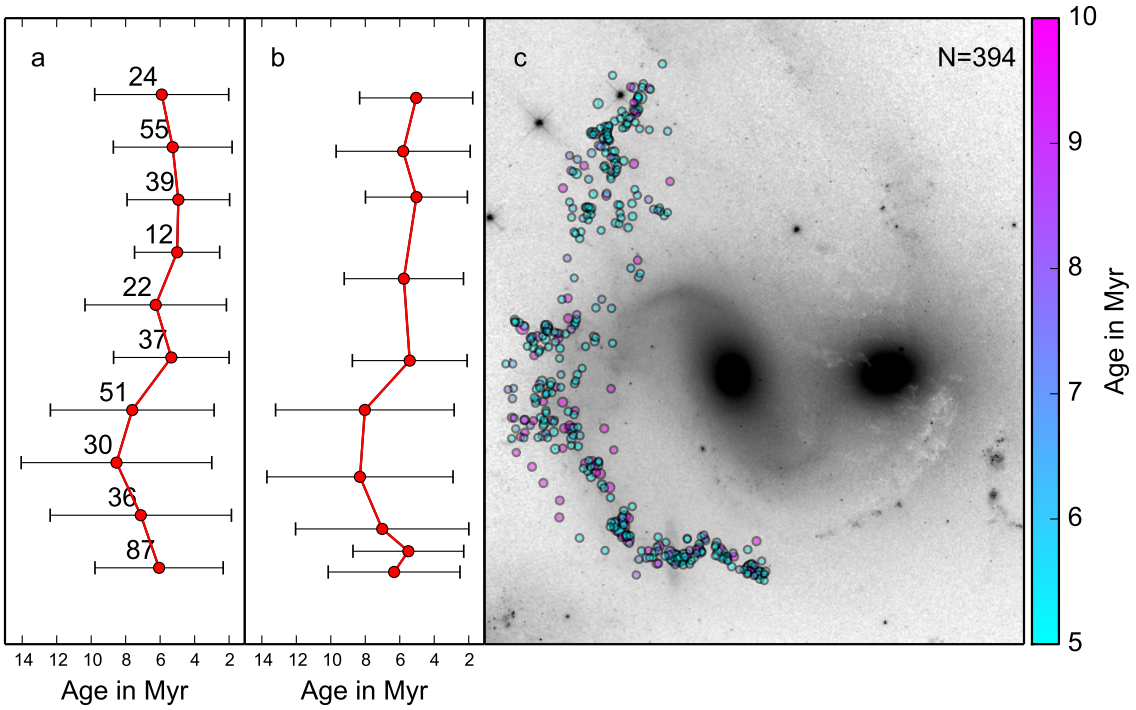

Figure 3.10: The spatial distribution of all detected sources in the Left Arc that are younger than 2×10^7 yr, plotted on top of the inverted V_{606} image of interacting pair 7318AB with the total number of such sources displayed in the upper right corner (panel c). The binning of the sources was carried out in two ways: with variable bin sizes, with an equal number of sources in each bin (panel b), and with fixed bin sizes along the y axis (panel a). The total number of sources with a given age range is shown in the upper right corner of panel (c). The errors in panels (a) and (b) are the standard deviation of the sources in each bin. The north is up and the east is left. Based on the presented plot we conclude that there is no overwhelming evidence for an age-gradient along the Eastern arc.

of the group.

3.4.3 Age Distribution

We construct the age distribution of SCCs in each region with masses over $10^{3.6}M_\odot$ and with limiting age of 10^7 yr, shown in Fig. 3.11. Since the distributions are not well described by a power law, we do not perform linear fitting. We find the median mass of the clusters in the top and bottom quartiles, 25% of the youngest and the oldest clusters, respectively. What we discovered is that for the SQ-A region the top quartile is just slightly larger than the bottom quartile, and for the Left Arc region the top quartile is actually smaller than the bottom one. For the rest of the regions we see the top quartile being larger than the bottom one. Knowing that the Left Arc region could be influenced by strong shock that coincides with the region (Xu et al., 2001; Xu et al., 2003), the observed decrease in mass between clusters in the last 10^7 yr can, potentially, be result of that influence.

In order to compare age distributions between the regions, we construct a diagram with all

five distributions plotted against each other (Fig 3.12). It appears that the overall recent star formation history is approximately the same for all regions, with some discrepancies in the SDR: the region has a large fraction of clusters at $\sim 10^{6.9}$ yr, as compared to other regions.

So, it looks like at $10^{6.9}$ yr the SDR region has a large fraction of clusters at that age, as compared to other regions.

Due to the drop in the numbers of SCCs in the subsequent mass bins, the age distribution of star clusters by individual regions does not contribute to this study. Instead, we will analyse plots of age distributions for all detected sources plotted in comparison with each other.

For the age distributions of SCCs with masses over $10^{4.25}M_{\odot}$ and limiting age of 10^8 yr (Fig. 3.13, upper plot), it would appear that the USDR is the least active recent star-forming region. However, the USDR also has the least number of detected sources which makes any analysis of that region rather uncertain. For most of the rest of our analysis we are going to ignore the USDR region, unless we mention it specifically. The Left Arc region has the highest fraction of SCCs between ages $\sim 10^{6.75}$ and $\sim 10^{7.75}$ suggesting a more active star formation during that time. Similarly, there is a hint, to the best of our results' resolution, that the formation of SCs at $\sim 10^{7.75}$ was a bit lower in SQ-A, as compared to other regions.

For the next mass bin (over $\sim 10^5 M_{\odot}$ and under 10^9 yrs; Fig. 3.13, lower plot) we see a reversal of the roles: here, the Right Arc and SDR have larger fractions of old clusters. However, the observed distribution can be a result of proximity of the elliptical NGC 7318A, which is expected to have a large number of older clusters, as was mentioned earlier.

Summing up, it would appear that the star formation first started in the Right Arc and SDR, then SQ-A and the Left Arc outperformed the rest of the regions, and "currently" (in the last 10^7 yr), in terms of the mass distributions the clusters appear to be quite similar across all regions.

3.4.4 Mass Distribution

Analogously with age distribution, we first construct cumulative mass distributions for the youngest SCCs ($< 10^7$ yr). According to log(mass) vs. log(age) (Fig. 3.5), which illustrates the completeness levels of our data in age and mass, the limiting mass for young clusters is approximately $10^{3.5}$ $M_{\odot}$. We plot the mass distribution of SCCs for each of our five regions: the Left Arc, Right Arc, Southern Debris Region, USDR, and SQ-A (Fig. 3.14). With the SCC catalogue the numbers of clusters per region with this age and mass range are rather small. In this case, determining the slopes of the distributions will be influenced by small number statistics particularly at the higher mass end, where the handful of clusters translate into large uncertainties. Nevertheless, based on the slopes we can split our regions into two groups: the Left Arc, SQ-A and the Right Arc, SDR. The later group has shallower slopes indicative of the presence of clusters with larger masses. Again, to boost our statistics we turn to the all sources catalogue and plot mass distributions for all regions against each other (Fig. 3.15). The distributions for all five regions appear to be grossly consistent with each other, supporting the idea of uniform recent star cluster formation in all regions. This is particularly true for log(mass) < 3.7, where the distributions overlap.

As was mentioned earlier, there is some evidence that star formation in the tidal features started earlier than in the last 10^7 yr (see upper right panels in Figs. 3.6 and 3.7). Then, for clusters with ages between 10^7 and 10^8 yr the limiting mass will be 10^4 $M_{\odot}$ (Fig. 3.5), and

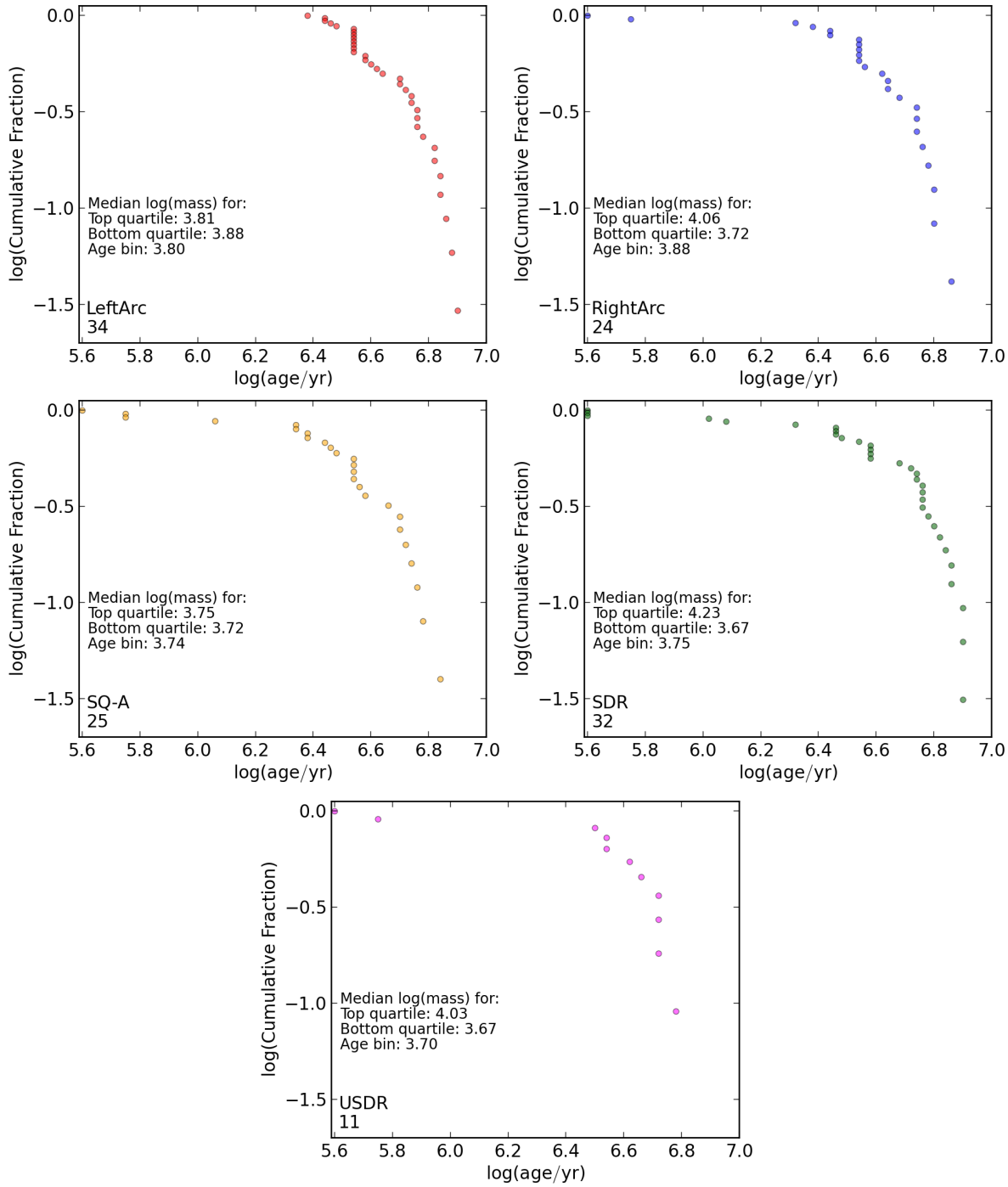

Figure 3.11: Age distribution for each of the five regions. In the lower left corner of each panel is the name of the region and the number of SCCs with log(mass) > $10^{3.6}$ and limiting age of 10^7 yr is displayed. Due to the nature of the distributions a linear fit is not meaningful. We find the median mass for the top quartile (the youngest age), the bottom quartile (the oldest age), and the whole age bin. For the Left Arc and SQ-A the masses of star clusters approximately stay the same, whereas masses for rest of the regions are larger. This could indicate the influence of the strong shock environment in the Left Arc and SQ-A, in that such an environment suppresses the formation of the larger SCs.

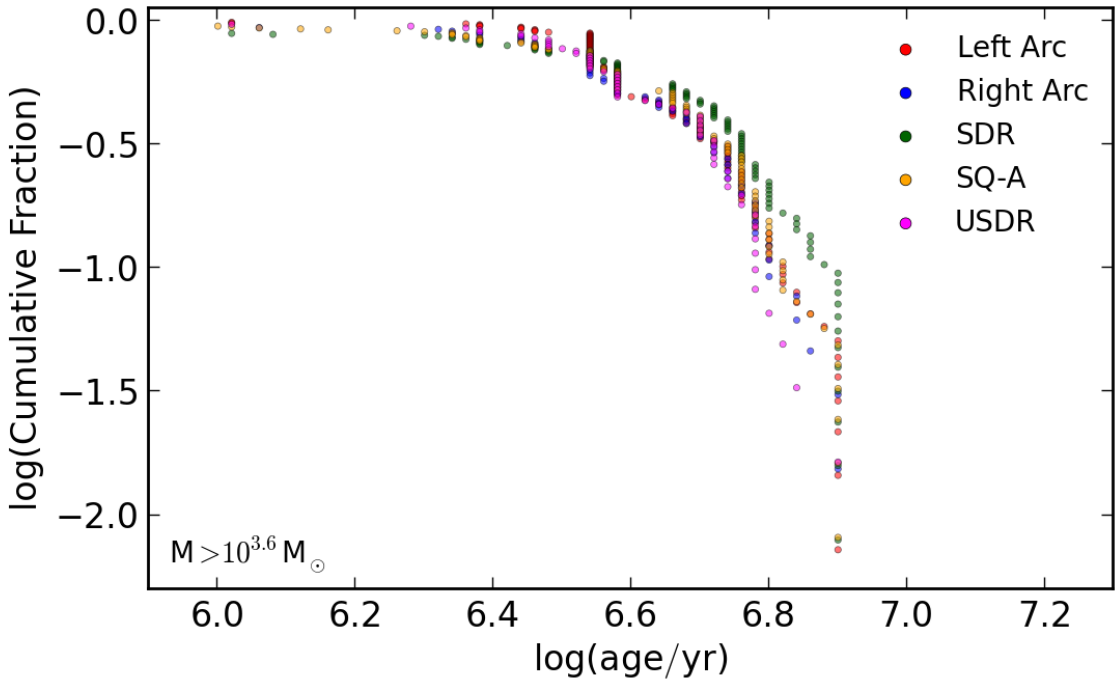

Figure 3.12: Comparison of cumulative age distributions for all five regions for all sources younger than 10^7 yr and with masses above $10^{3.6}M_\odot$. From this plot we observe that initially the SDR region had the largest internal fraction of sources with ages $\sim 10^{6.9}$ yr. As we move to the present time the internal fractions of young star clusters in all regions are quite similar.

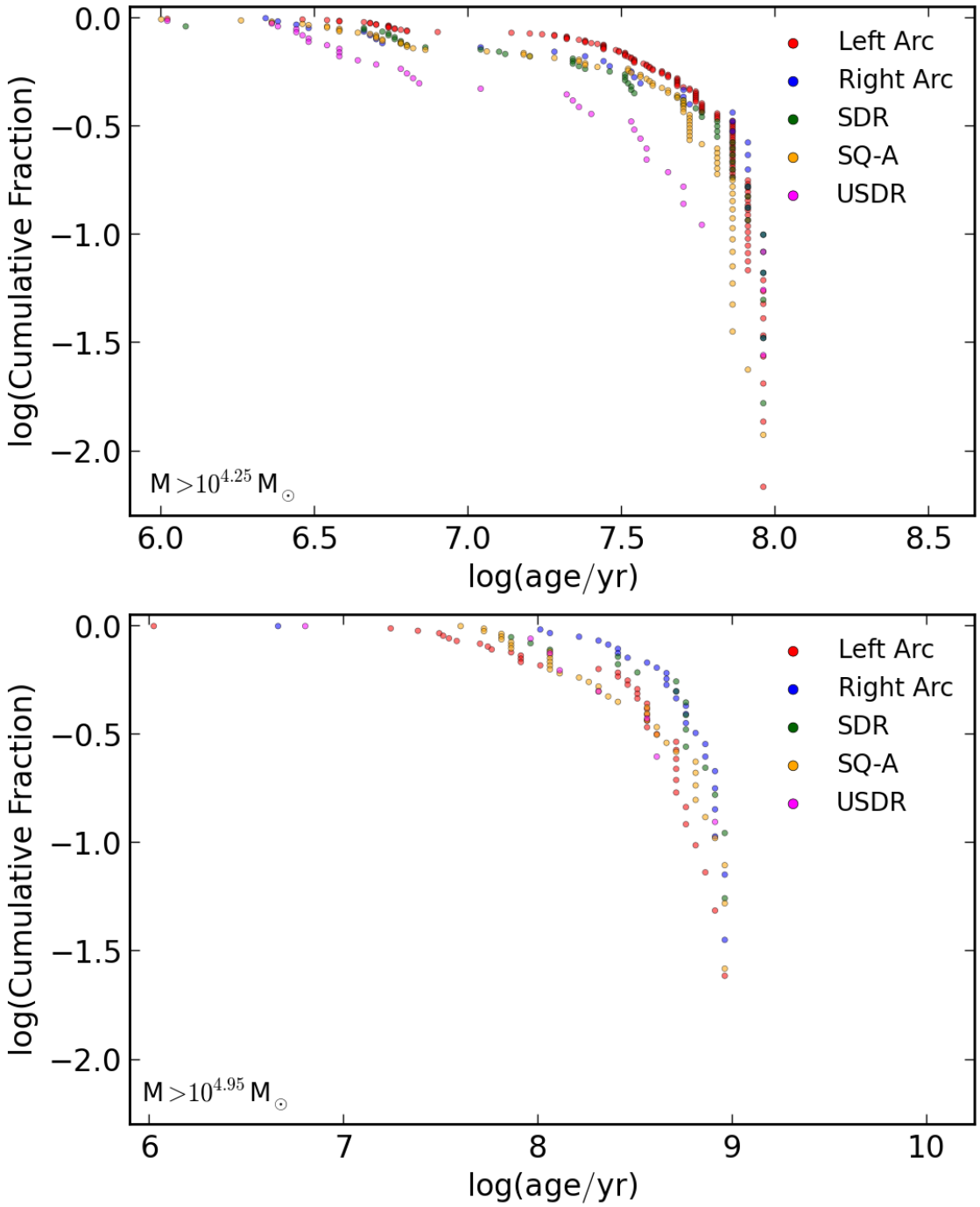

Figure 3.13: Comparison of the cumulative age distributions for all five regions for all sources younger than 10^7 yr and with masses above $10^{4.25}M_\odot$ (upper plot) and for sources younger than 10^9 yr and with masses above $10^{4.95}M_\odot$ (lower plot). Sources with ages $< 10^8$ yr have generally the same distribution, with the Left Arc region slightly above the rest, indicating that the internal fraction of sources with the ages between $\sim 10^{6.75}$ and $\sim 10^{7.75}$ is higher as compared to the rest of the regions. For the lower plot we observe that the the Right Arc and SRD regions have the higher fraction of the older sources. Most likely this is due to the proximity of elliptical NGC 7318A (Fig.3.9, lower right panel), which is expected to have higher number of older clusters. We exclude analysis of the USDR due to low source numbers.

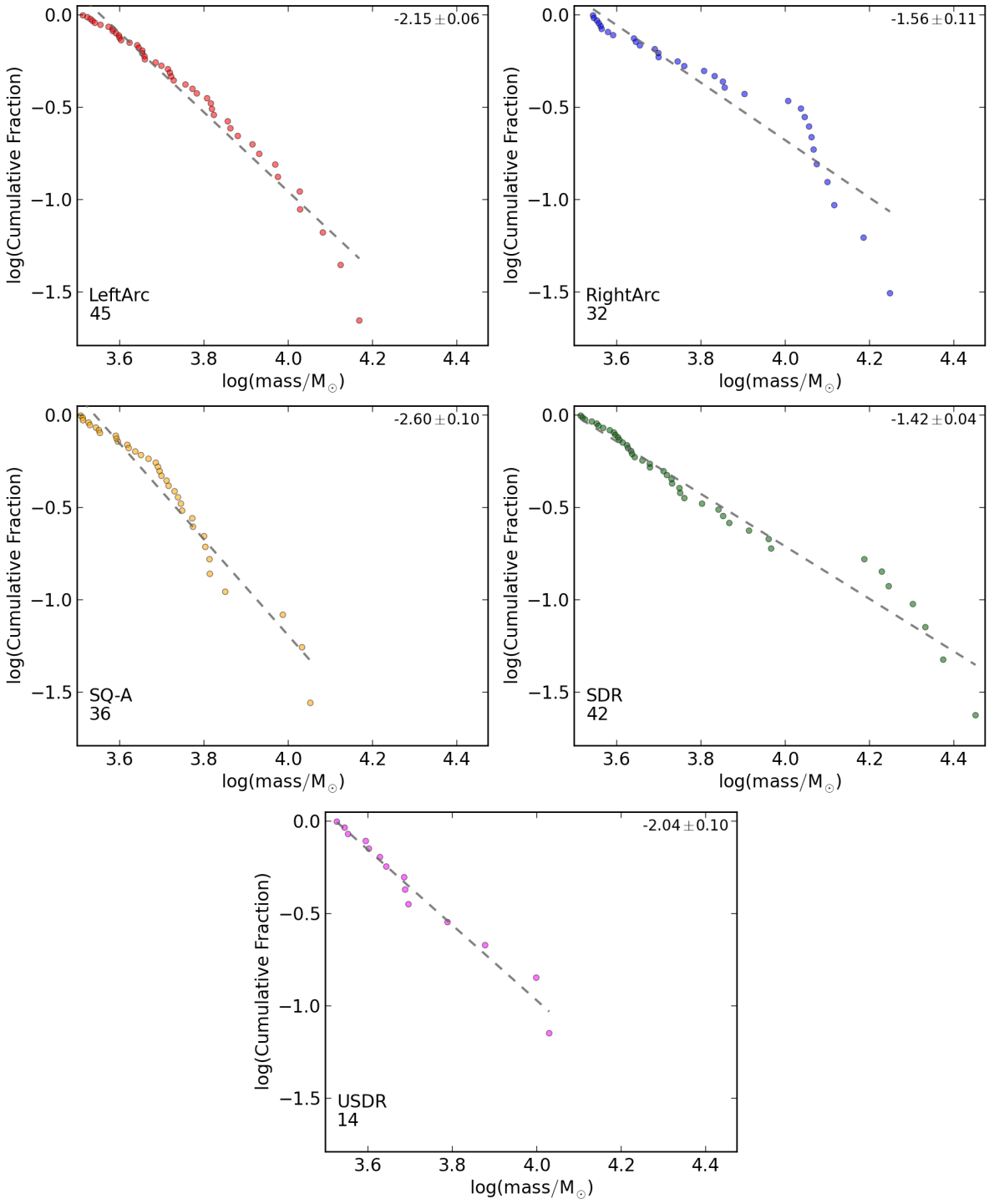

Figure 3.14: Mass distribution for each of the five regions. In the lower left corner of each panel the name of the region and the number of SCCs with ages less than 10^7 yr and with masses over $10^{3.5}$ $M_\odot$ are displayed. In the upper right corner is value of the slope, determined by the least squares fit over the whole mass range. Based on the slopes we see that regions can be separated into two groups: the Left Arc, SQ-A (with steeper slopes) and the Right Arc, SDR (with shallower slopes). Once again, the USDR is excluded from our analysis.

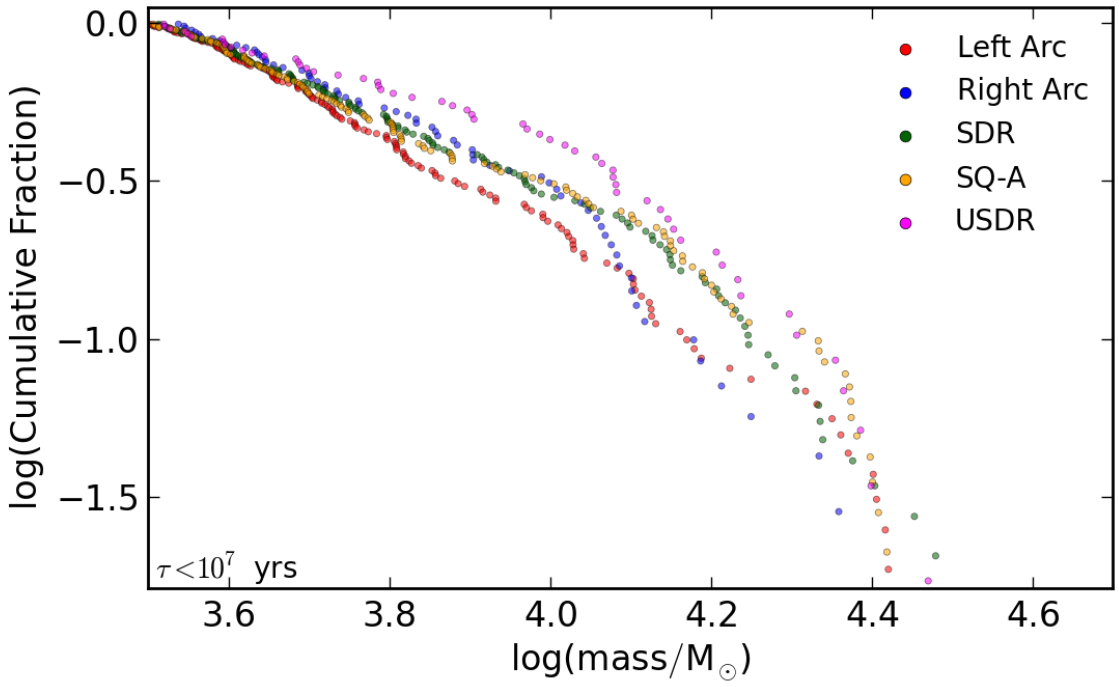

Figure 3.15: Comparison of cumulative mass distributions for all the five regions for clusters younger than 10^7 yr and with masses above $10^{3.5}M_\odot$. The distributions appear to be largely consistent with each other, particularly for clusters with log(mass)< 3.75. The Right Arc exhibits a similar bump at log(mass)$\sim 10^4$, which was also observed in Fig. 3.14. The SDR and SQ-A practically overlap over the whole age range, suggesting that their fractions between the sources with different ages are similar. The distribution of sources in the Left Arc region suggests a shortage of higher mass sources in this particular age bin.

we plot mass distributions of such clusters in all regions to see if there are any differences in the star formation in those regions (Fig. 3.16). We are in the small numbers statistical regime again, perhaps except for the Left Arc region, and so we use the all sources catalogue for this analysis (Fig. 3.17). Here we see that the distributions can be divided into two groups: Left Arc, USDR, and SQ-A regions appear to be able to form more massive clusters more frequently than Right Arc and SDR regions. This is rather interesting because one would naïvely think that the neighbouring USDR and SDR would more likely have similar star formation histories rather than the USDR and SQ- A, which are located $\sim$ 30 kpc from each other. However, this result must be taken with caution because even when we are using the all sources catalogue, the USDR has only 58 sources that satisfy the above conditions, still not a statistically large number. Nevertheless, from these plots we conclude that if we look at the star formation history in the last 10^8 yr, there appear to be some differences as to how star clusters formed between SQ-A, Left Arc regions and SDR, Right Arc regions.

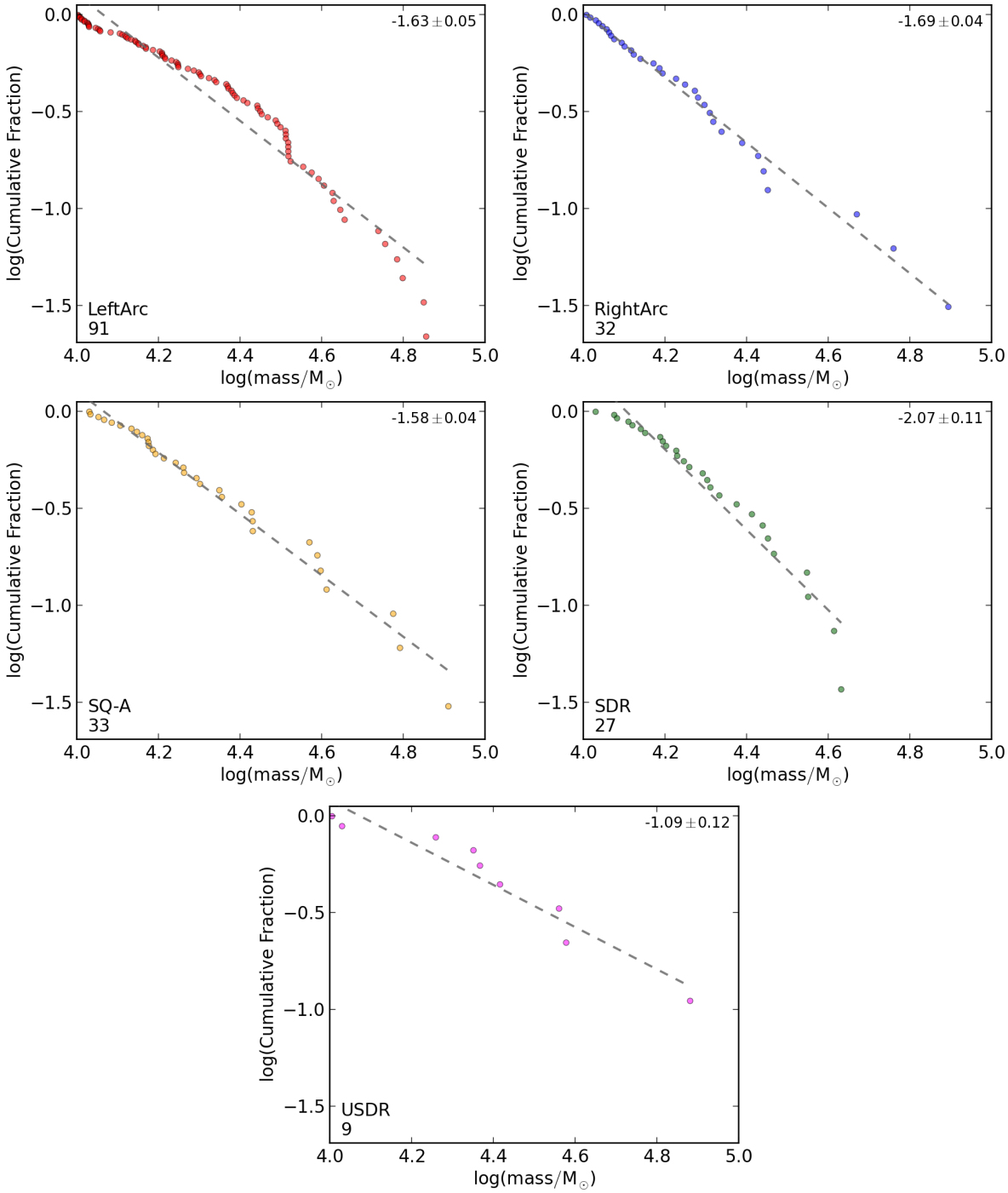

Figure 3.16: Mass distribution for each of the five regions. In the lower left corner of each panel the name of the region and the number of SCCs with ages less than 10^8 yr and with masses over $10^4 M_\odot$ are displayed. In the upper right corner is the value of the slope, determined by a least squares fit over the whole mass range. The Left and Right Arcs, SQ-A have similar slopes, with the Left Arc exhibiting a bump at $\sim 10^{4.4} M_\odot$, which, however, does not hold when distribution is plotted for all detected sources (Fig. 3.17). SDR has the steepest slope indicating a lack of the more massive sources. USDR is excluded from our analysis.

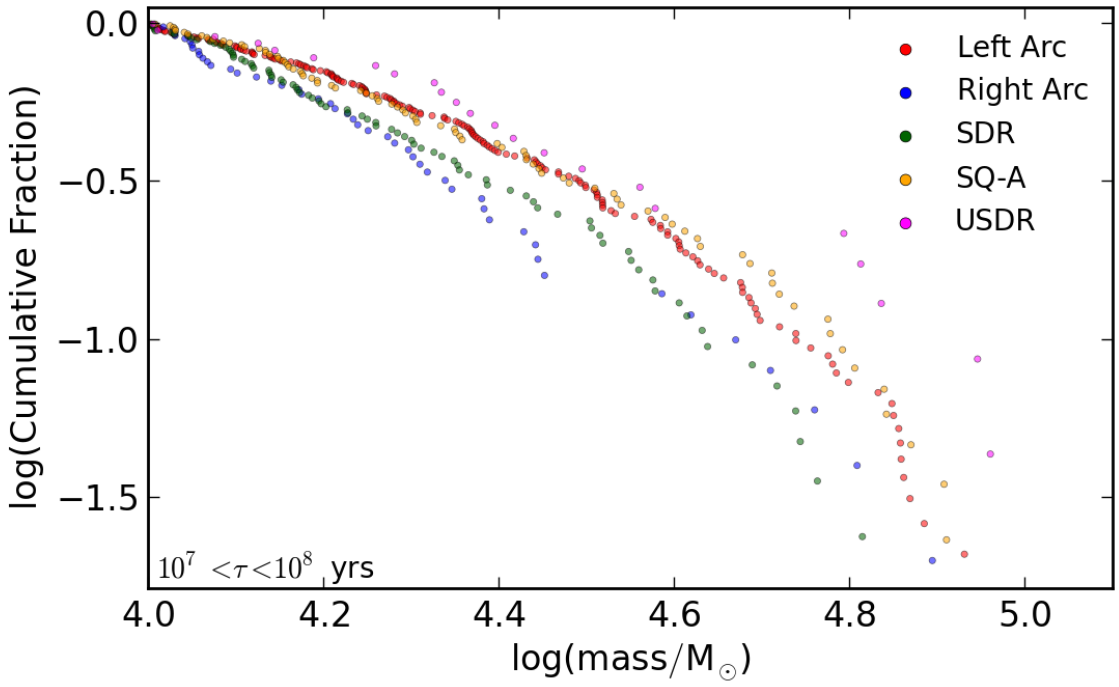

Figure 3.17: Comparison of cumulative mass distributions for all five regions for clusters with ages between 10^7 and 10^8. The distributions appear to be bunched into two groups, suggesting different star formation histories. Based on the plot, the two groups are: the Left Arc, SQ-A and the Right Arc, SDR. It would appear that the first group has larger fraction of massive clusters as the second.

3.5 Conclusions

Our goal at the outset of this project was to probe the apparent universality of the age and mass distributions of young clusters. In particular, the strong shock in SQ seemed like an excellent opportunity to see if these distributions remain "universal" even in such extreme conditions. Although interesting results were obtained from the separate regions in SQ that allowed us to reconstruct a likely scenario for the history of star formation in and around the interacting pair of NGC 7318AB for the last 10^8 yr, we find no strong evidence for a breakdown in universality. However, the small number of clusters available for analysis limits our ability to constrain the mass distribution sufficiently. Nonetheless, our speculative conclusion is that the effect of the strong shock on star cluster formation is minimal and is only revealed through the upper mass truncation of the recently formed star clusters. One of the reasons for the minimal impact of the shock on star formation may be that the strong shock and the young cluster regions are distinct and offset with respect to each other along our line of sight (Konstantopoulos et al., 2014), with the strong shock region being closer to us and with the young star clusters located behind it. Below, we discuss our results in more detail.

We used ages and masses of star cluster candidates derived from high resolution, deep HST WFC3 $UBV_{\rm m}VI$ photometry of Stephan's Quintet to characterize the history of star formation in the tidal debris around the interacting pair of galaxies NGC 7318A/B. We identify five regions of interest in our observations: the Left and Right tidal Arcs, the Northern Starburst Re-

gion (NSBR), the Southern Debris Region (SDR), and an overdensity of star clusters between NGC 7318A and the SDR, which we dub the Upper SDR (USDR). The large-scale shock from the collision of NGC 7318B with the intragroup medium is coincident with the Left Arc.

Our specific results are as follows:

- We investigate the age distribution of clusters in all five regions for different mass bins. For the clusters with masses down to $10^{3.6}M_{\odot}$, we are probing young clusters ($< 10^7$ yr), and we see that the regions have similar fractions of clusters for that time range. For the next mass bin (down to $10^{4.25}M_{\odot}$), we found that the Left Arc region appear to have an elevated fraction of the clusters between the ages of $10^{6.75}$ and $10^{7.75}$ yr. The rest of the regions have approximately the same fractions throughout that time interval. For the last mass bin (over $10^{4.95}M_{\odot}$) we see the Right Arc and SDR have a larger fraction of older clusters, possibly as a result of their proximity to the elliptical galaxy NGC 7318A.

- We examine the mass function of clusters in all regions for different age bins. The clusters are divided into two bins: clusters with ages $< 10^7$ yr and with limiting mass of $10^{3.6}M_{\odot}$ to study the recent star formation associated with the NGC 7318B interaction, and clusters with ages between 10^7 and 10^8 yr and with limiting mass of $10^4M_{\odot}$ to probe earlier star formation in the tidal features. We found that for sources younger than 10^7 yr the mass distributions are consistent with each other up to log(mass) $\sim 10^{3.7}M_{\odot}$. After that, the Left Arc region has a lower fraction of the sources with masses above $10^{3.7}M_{\odot}$, and the fraction of clusters with log(mass) above $\sim 10^{4.1}M_{\odot}$ drops for the Right Arc region. For the next age bin, we see regions splitting into two groups; the Right Arc and SDR having the lower frequency of sources virtually throughout the whole range of masses (from 10^4 to 10^5 $M_{\odot}$). We also compared slopes of our mass distributions with the ones from FC12. We found that our values are grossly consistent with FC12: for clusters with ages between 10^6 and 10^7 yr, the FC12 values are ranging from –1.7 to –2.14, whereas our values are between –1.42 and –2.60, and for cluster with $10^7 < \tau < 10^8$ yr, the FC12 values are between –1.86 and –2.03, and our values are from –1.58 to –2.07. (We exclude the USDR from this analysis due to low number counts.)

- We looked at maps of the age distribution of the star clusters in the Left Arc region, the site of the interaction between intruder galaxy NGC 7318B and the large cloud of cold gas in the intragroup medium located between the elliptical NGC 7318A and the spiral NGC 7319. We detect no strong evidence for an age gradient in the Left Arc region.

Based on our overall results, we conclude that the star formation in the debris regions started at $\leq 10^8$ yr ago, with the first star clusters being formed in the Right Arc and SDR, with star formation eventually spreading to all regions in our study. Initially, the clusters being formed in the Right Arc and SDR had masses less than $10^{4.8}M_{\odot}$. However, when star formation started in the Left Arc and SQ-A regions, it would appear that the formation was more intensive (judging by the absolute number of SCs) and the masses of the newly formed clusters were on average larger (reaching up to $10^5M_{\odot}$) than in the Right Arc and SDR. The formation rate of star clusters gradually diminished until the very recent on-set of new star formation within the last 10^7 yr. At this time, we observe star formation happening throughout and that is also similar region to region. Moreover, we see evidence that for all but one region, the masses of

the clusters increase as we move from the latest on-set of star formation to the present moment. The exception is the Left Arc region, the only one within the strong shock. The results suggest that the cluster masses in that region are getting smaller as we move to the present. We argue that this could be the effect of the strong shock on the star formation in this region.

One of the questions that has been raised during this study is the amount of star-forming material available in the different regions. While there are studies that looked at the amount of molecular gas in the upper part of the Left Arc and SQ-A (e.g., Cluver et al., 2010), we are not aware of work dedicated to the Right Arc, USDR, and SDR. For the future, a systematic high-resolution study of the molecular gas in all of the tidal features of SQ, similar to ALMA observations of the merging Antennae galaxies (Whitmore et al., 2014), would be powerful for connecting star cluster formation throughout this complex system to the fuel that enables it.

Acknowledgement

The authors would like to acknowledge the Queen Elizabeth II Graduate Scholarships in Science and Technology (Canada; K.F.) and the Natural Sciences and Engineering Research Council and the Ontario Early Researcher Award Program (Canada; S.C.G.). We thank Robert Corless, Gretchen Harris, John Landstreet, and Aaron Sigut for a careful read of the manuscript and their valuable suggestions that improved the paper.

Facilities: HST (WFC3)

Chapter 4

Conclusion

In chapter 1, I outlined the main ideas behind the use of star clusters to investigate events related to galaxy evolution/interaction. In particular, one of the environments of the local universe that can be used as an approximation of the earlier universe is of great interest to us. Compact groups of galaxies as selected by Hickson are defined in such a way that they have multiple prolonged interactions. Often, these interactions result in star clusters being formed. I showed that star clusters are reliable tools for age-dating epochs of star formation, and therefore can be used to evaluate large-scale galaxy interactions.

In chapter 2, I present a comprehensive catalogue of star clusters detected in five compact galaxy groups (HCGs 07, 31, 42, 59, and 92), based on deep, high-resolution multi-colour images from the Hubble Space Telescope Advanced Camera for Surveys and Wide Field Camera 3 (in the case of HCG 92) with the goal of examining the properties of the star cluster systems of compact group galaxies overall and further assisting researchers in star cluster related studies. The catalogue consists of 18,292 objects detected in the 16 galaxies of the sample, and after applying a number of criteria to identify the highest quality subset of objects, I narrow it to 1963 star cluster candidates and 1505 globular cluster candidates. The entirety of the photometric data from this catalogue is presented in Appendix A.

Detailed examination of the catalogue revealed the following:

- Star clusters are powerful tracers of episodes of star formation activity. Careful study of the distribution of cluster colours can lead to a better understanding of the evolutionary state of their hosts and can help to constrain (and in some cases to reconstruct) the sequence of events in the host groups (e.g. Fedotov et al., 2011; Gallagher et al., 2010; Konstantopoulos et al., 2010, 2012, 2013).

- The analysis of star cluster populations in CGs allowed to propose a reclassification of HCG 59 from a Type III to a Type II group. Most galaxies in Type III groups appear to be 'red' and 'dead' (e.g., HCG 42). However, the galaxy morphologies of HCG 59 do not comply with that statement. Moreover, its population of star clusters is more consistent with Type II groups.

- In general, the cluster luminosity functions of the CG spiral galaxies were consistent with spirals studied in the literature (e.g. Larsen, 2002; Whitmore et al., 2014). In particular, their CLF α-values ranged from -2.26 ± 0.05 to -2.54 ± 0.05. A notable exception were

the large negative α-values for the spirals HCG 07A and 07C with $\alpha = -2.65 \pm 0.06$ and $\alpha = -3.24 \pm 0.04$, respectively.

- I have examined the metallicity distributions of GCCs in the five groups overall and individually in the elliptical galaxies (nominally elliptical 07BD and 92BD, 42A, 59B, 92C, and 92E) with sufficient numbers of GCCs. Only in galaxy 42A do I detect a metallicity distribution with well-defined bimodality peaking at [Fe/H]= -1.04 ± 0.07 and [Fe/H]= -0.16 ± 0.15. The galaxy 92C may also host a bimodal distribution, but the statistical results were not conclusive.

- The number of GCs in each galaxy is proportional to the total stellar masses of galaxies (Fig. 2.4). Notably, I detect a rather large number GCs in 59B (and its immediate environs) and a small number of GCs in 59A. It is possible that these two galaxies have interacted before given their morphologies (59B is elliptical, 59A is lenticular) and apparent proximity; the GC population distribution may be the only record of that interaction. A low surface brightness stream of material between galaxies 59A and B, reported in Konstantopoulos et al. (2013), as well as their line-of-sight velocities (within 3% of each other) also support the idea of previous interactions.

- The number of "blue" clusters (with colour $V - I < 0.1$, representing the population of young star clusters) are well correlated with the star formation rate. Two spiral galaxies (92C and 59C) have a large number of "blue" clusters given their relatively lower star formation rates. That likely indicates that a recent bout of star formation triggered by interactions is coming to an end. However, the young star clusters have not been significantly age-dimmed yet, and so a large number of them are still detectable.

- For the three elliptical galaxies in the sample (42A, 59B, and 92E) I looked at the radial distribution of GCs of different metallicities. According to the KS-test, metal rich and metal poor populations of 42A and 59B are drawn from different distributions (with confidence of > 99%). The GCs of different metallicities in 92E appear to be well mixed throughout the galaxy. Dry mergers of galaxies with a similar mass could explain this last observation. However, the characteristic features for such a merger (such as shells and streams) are not detected.

The star cluster populations of Hickson Compact Group galaxies are particularly interesting given their potential to reveal the history of dynamical interactions that have clearly been so important in shaping the evolution of individual groups as a whole and the current state of their member galaxies. The deep *BVI* imaging and photometry presented in this catalogue illustrate this point. However, the advantage of adding U- band to photometric studies of star clusters is considerable. It breaks the age-extinction degeneracy of the *BVI* photometry and allows a shift from a qualitative description of cluster ages to a more quantitative analysis, along with determinations of intrinsic reddening and masses. This additional information adds considerably to the descriptive power of star cluster populations in specific environments.

For this reason, I embarked on a study of the star cluster populations of Stephan's Quintet (HCG 92) that incorporates U-band photometry. For chapter 3, I present ages and masses of SCCs derived from UBV_mVI observations of SQ, to study the tidal debris around the interacting

pair of galaxies NGC 7318AB. I have divided the field into five distinct regions to see if the pattern of star cluster formation in different environments within the compact group can be differentiated. The Left Arc region includes the strong shock present in the system from the high-speed collision of NGC 7318B with the intragroup medium. The peak of star formation in the group is found in the intragroup medium, home of the Northern Starburst Region (NSBR, also known as SQ-A). The Right Arc is a tidal feature extending to the north from the western side of NGC 7318A. The Southern Debris Region hosts clusters in a diffuse structure to the south of NGC 7318B/A, with a coherent feature closer to the galaxies, the Upper Southern Debris Region (USDR).

- I investigate the age function of clusters in all five regions for different mass bins. For the clusters with masses over $10^{3.6}M_{\odot}$ I probe young clusters ($< 10^7$ yr), and observe that the regions have similar fractions of clusters for that time range. For the next mass bin (over $10^{4.25}M_{\odot}$) I find that the Left Arc region appears to have elevated fraction of the clusters between the ages of $10^{6.75}$ and $10^{7.75}$ yr. The rest of the regions have approximately the same fractions throughout that time interval. For the last mass bin (over $10^{4.95}M_{\odot}$) I notice the Right Arc and SDR have larger fraction of older cluster, possibly the result of proximity of elliptical galaxy.

- I examine the mass function of clusters in all regions for different age bins. The clusters are divided into two bins: clusters with ages below 10^7 yr and with limiting log(mass) of $10^{3.5}M_{\odot}$ to study the recent star formation associated with the NGC 7318B interaction, and clusters with ages between 10^7 and 10^8 yr and with limiting log(mass) of $10^4M_{\odot}$ to probe earlier star formation in the tidal features. I find that for sources younger than 10^7 yr the mass distributions are consistent with each other up to log(mass)$\sim$ 3.7. After that the Left Arc region have lower fraction of the sources with log(mass) above $10^{3.7}$ $M_{\odot}$, and the fraction of clusters with log(mass) above $\sim 10^{4.1}M_{\odot}$ drops for the Right Arc region. For the next age bin, the regions split into two groups; the Right Arc and SDR have lower frequency of sources virtually throughout the whole range of log(mass) (from 10^4 to 10^5 $M_{\odot}$). I also compare slopes of the mass distributions with the ones from FC12. I find that the values are largely consistent with FC12: for clusters with ages between 10^6 and 10^7 yr FC12 values range from -1.7 to -2.14, whereas my values are between -1.42 and -2.60, and for cluster with $10^7 < \tau < 10^8$ FC12 values are between -1.86 and -2.03, and my values are from -1.58 to -2.07.

- I investigate the maps of the age distribution of the star clusters in the Left Arc region, the region most affected by the interaction between intruder galaxy NGC 7318B and the large cloud of gas in the intragroup medium located between NGC 7318A and NGC 7319. I detect no strong evidence for an age gradient in the Left Arc region.

Taking the specific results of this study and the history of interactions in Stephan's Quintet from the literature, I construct a possible narrative for the recent star formation in this group. I conclude that the star formation in the debris regions started $\leq 10^8$ yr ago, with the first star clusters being formed in the Right Arc and SDR, with star formation eventually spreading to all regions. Initially, the clusters formed in the Right Arc and SDR had masses less than $10^{4.8}M_{\odot}$. However, when star formation started in the Left Arc and the SQ-A region it would

appear that the formation was more intensive (judging by the large absolute number of SCs in those regions) and the masses of the newly formed clusters were on average larger (reaching up to $10^5 M_\odot$) than in the Right Arc and SDR. The formation of star clusters was gradually diminishing until the very recent on-set of new star formation (within the last 10^7 yr). This time, I observe the star formation that is happening in all of the regions and that is also comparable region to regions. Moreover, I see evidence that for all but one region the masses of the clusters are increasing with time: from the latest on-set of star formation to the present moment. The exception is the Left Arc region, the only one definitively within the strong shock. The results suggests that the cluster masses are getting smaller as the time move to the present. I argue that this could be the effect of the strong shock on the star formation in this region.

In chapter 3 I also investigate the apparent universality of the age and mass distributions of young clusters. In particular, the strong shock in SQ seemed like an excellent opportunity to see if these distributions remain "universal" even in such extreme conditions. However, I find no strong evidence for a breakdown in universality. The small number of clusters available for analysis limits the ability to constrain the mass distribution sufficiently. Nonetheless, a speculative conclusion is that the effect of the strong shock on star cluster formation is minimal and is only revealed through the upper mass truncation of the recently formed star clusters. One of the reasons for the minimal impact of the shock on star formation may be that the strong shock and the young cluster regions are distinct and offset with respect to each other along our line of sight (Konstantopoulos et al., 2014), with the strong shock region being closer to us and with the young star clusters located behind it.

One of the questions that has been raised during this study of Stephan's Quintet is the amount of star-forming material available in the different regions. This information is essential to judge the efficiency of star formation through its features. There are studies that looked at the amount of molecular gas in the upper part of the Left Arc and SQA, but author is not aware of any studies dedicated to the Right Arc, USDR, and SDR. Systematic, high-resolution studies of the spatial and velocity distribution of molecular gas in all of the tidal features of SQ, similar to ALMA observations of the merging Antennae galaxies (Whitmore et al., 2014), would be a powerful addition to the picture of star cluster formation in this interesting and complex environment. That would provide an additional handle on the large scale structure, and enable a study of the correspondence between the ionized and molecular gas.

Overall, I have demonstrated that star clusters are powerful probes of the gross patterns of epochs of star formation triggered by large-scale gravitational interactions. The broader picture of the relationship between star formation as probed by star cluster population studies and the presence and distribution of cold molecular gas, the fuel for star formation, in compact galaxy groups, is the obvious next issue to investigate.

Bibliography

Allen, R. J., & Hartsuiker, J. W. 1972, Nature, 239, 324

Ambartsumian, V. A. 1961, The Astronomical Journal, 66, 536

Anders, P., Bissantz, N., Fritze-v. Alvensleben, U., & de Grijs, R. 2004, Monthly Notices of the Royal Astronomical Society, 347, 196

Arp, H. 1965, Science (New York, N.Y.), 148, 363

Ashman, K. M., & Zepf, S. E. 1998, Globular Cluster Systems (Cambridge, U. K. ; New York: Cambridge University Press)

Baier, F. W., & Tiersch, H. 1979, Astrofizika, 15, 33

Barmby, P., Huchra, J. P., Brodie, J. P., Forbes, D. A., Schroder, L. L., & Grillmair, C. J. 2000, The Astronomical Journal, 119, 727

Barmby, P., Kuntz, K. D., Huchra, J. P., & Brodie, J. P. 2006, The Astronomical Journal, 132, 883

Barnes, J. E. 1989, Nature, 338, 123

Baron, E., & White, S. D. M. 1987, The Astrophysical Journal, 322, 585

Barton, E., Geller, M., Ramella, M., Marzke, R. O., & da Costa, L. N. 1996, The Astronomical Journal, 112, 871

Barton Gillespie, E., Geller, M. J., & Kenyon, S. J. 2003, The Astrophysical Journal, 582, 668

Bastian, N. 2008, Monthly Notices of the Royal Astronomical Society, 390, 759

Bastian, N. 2011, in Stellar Clusters & Associations: A RIA Workshop on Gaia, 85–97

Bastian, N., Covey, K. R., & Meyer, M. R. 2010, Annual Review of Astronomy and Astrophysics, 48, 339

Bastian, N., Emsellem, E., Kissler-Patig, M., & Maraston, C. 2006, Astronomy and Astrophysics, 445, 471

Bastian, N., Gieles, M., Lamers, H. J. G. L. M., Scheepmaker, R. A., & de Grijs, R. 2005a, Astronomy and Astrophysics, 431, 905

Bastian, N., Hempel, M., Kissler-Patig, M., Homeier, N. L., & Trancho, G. 2005b, Astronomy and Astrophysics, 435, 65

Bastian, N., Trancho, G., Konstantopoulos, I. S., & Miller, B. W. 2009, The Astrophysical Journal, 701, 607

Baumgardt, H., & Makino, J. 2003, Monthly Notices of the Royal Astronomical Society, 340, 227

Beasley, M. A., Baugh, C. M., Forbes, D. A., Sharples, R. M., & Frenk, C. S. 2002, Monthly Notices of the Royal Astronomical Society, 333, 383

Becker, R. H., White, R. L., & Edwards, A. L. 1991, The Astrophysical Journal Supplement Series, 75, 1

Bell, E. F. 2003, The Astrophysical Journal, 586, 794

Bergvall, N., Laurikainen, E., & Aalto, S. 2003, Astronomy and Astrophysics, 405, 31

Bik, A., Lamers, H. J. G. L. M., Bastian, N., Panagia, N., & Romaniello, M. 2003, Astronomy and Astrophysics, 397, 473

Binggeli, B., Tammann, G. A., & Sandage, A. 1987, The Astronomical Journal, 94, 251

Bitsakis, T., Charmandaris, V., Appleton, P. N., Díaz-Santos, T., Le Floc'h, E., da Cunha, E., Alatalo, K., & Cluver, M. 2014, Astronomy and Astrophysics, 565, A25

Blakeslee, J. P., Cho, H., Peng, E. W., Ferrarese, L., Jordán, A., & Martel, A. R. 2012, The Astrophysical Journal, 746, 88

Boutloukos, S. G., & Lamers, H. J. G. L. M. 2003, Monthly Notices of the Royal Astronomical Society, 338, 717

Brandner, W., Clark, J. S., Stolte, A., Waters, R., Negueruela, I., & Goodwin, S. P. 2008, Astronomy and Astrophysics, 478, 137

Bressert, E., et al. 2010, Monthly Notice of the Royal Astronomical Society, 409, L54

Bruzual G. A. 2010, Proceedings of the International Astronomical Union, 5, 55

Bruzual G. A., & Charlot, S. 2003, Monthly Notices of the Royal Astronomical Society, 344, 1000

Burbidge, E. M., Burbidge, G. R., & Hoyle, F. 1963, The Astrophysical Journal, 138, 873

Calzetti, D. 2008, in Astronomical Society of the Pacific Conference Series, Vol. 390, Pathways Through an Eclectic Universe, ed. J. H. Knapen, T. J. Mahoney, & A. Vazdekis, 121

Calzetti, D., & Harris, J. 2002, The Dynamics, Structure & History of Galaxies: A Workshop in Honour of Professor Ken Freeman. ASP Conference Proceedings, Vol. 273., 273

Calzetti, D., et al. 2007, The Astrophysical Journal, 666, 870

Caputo, F., Castellani, V., & Quarta, M. L. 1985, Astronomy and Astrophysics, 143, 8

Carrasco, E. R., Mendes de Oliveira, C., & Infante, L. 2006, The Astronomical Journal, 132, 1796

Chabrier, G. 2003, Publications of the Astronomical Society of the Pacific, 115, 763

Chandar, R., Fall, S. M., & Whitmore, B. C. 2006, The Astrophysical Journal, 650, L111

Chandar, R., Fall, S. M., & Whitmore, B. C. 2010a, The Astrophysical Journal, 711, 1263

Chandar, R., Whitmore, B., & Lee, M. G. 2004, The Astrophysical Journal, 611, 220

Chandar, R., Whitmore, B. C., Calzetti, D., Di Nino, D., Kennicutt, R. C., Regan, M., & Schinnerer, E. 2011, The Astrophysical Journal, 727, 88

Chandar, R., et al. 2010b, The Astrophysical Journal, 719, 966

Cluver, M. E., et al. 2010, The Astrophysical Journal, 710, 248

Conroy, C., Gunn, J. E., & White, M. 2009, The Astrophysical Journal, 699, 486

Conroy, C., White, M., & Gunn, J. E. 2010, The Astrophysical Journal, 708, 58

Conti, P. S., Leitherer, C., & Vacca, W. D. 1996, The Astrophysical Journal, 461, L87+

Cox, P., Lucas, R., Huggins, P. J., Forveille, T., Bachiller, R., Guilloteau, S., Maillard, J. P., & Omont, A. 2000, Astronomy and Astrophysics

Dahm, S. E., & Simon, T. 2005, The Astronomical Journal, 129, 829

de Grijs, R., & Anders, P. 2006, Monthly Notices of the Royal Astronomical Society, 366, 060118052800067

de Vaucouleurs, G., de Vaucouleurs, A., Corwin, Jr., H. G., Buta, R. J., Paturel, G., & Fouqué, P. 1991, Third Reference Catalogue of Bright Galaxies. Volume I: Explanations and references. Volume II: Data for galaxies between 0^h and 12^h. Volume III: Data for galaxies between 12^h and 24^h. (Springer)

de Wit, W. J., Testi, L., Palla, F., & Zinnecker, H. 2005, Astronomy and Astrophysics, 437, 247

Desjardins, T. D., et al. 2014, The Astrophysical Journal, 790, 132

Diaferio, A., Geller, M. J., & Ramella, M. 1994, The Astronomical Journal, 107, 868

Elmegreen, B. G., & Efremov, Y. N. 1997, The Astrophysical Journal, 480, 235

Elmegreen, B. G., Efremov, Y. N., Pudritz, R. E., & Zinnecker, H. 2000, Protostars and Planets IV (Book - Tucson: University of Arizona Press; eds Mannings

Elmegreen, B. G., & Hunter, D. A. 2010, The Astrophysical Journal, 712, 604

Fall, S. M. 2004, in The Formation and Evolution of Massive Young Star Clusters, Vol. 322, 10

Fall, S. M., & Chandar, R. 2012, The Astrophysical Journal, 752, 96

Fall, S. M., Chandar, R., & Whitmore, B. C. 2005, The Astrophysical Journal, 631, L133

Fall, S. M., Chandar, R., & Whitmore, B. C. 2009, The Astrophysical Journal, 704, 453

Fedotov, K., Gallagher, S. C., Konstantopoulos, I. S., Chandar, R., Bastian, N., Charlton, J. C., Whitmore, B. C., & Trancho, G. 2011, The Astronomical Journal, 142, 42

Fitzpatrick, E. L. 1999, Publications of the Astronomical Society of the Pacific, 111, 63

Friel, E. D., Janes, K. A., Tavarez, M., Scott, J., Katsanis, R., Lotz, J., Hong, L., & Miller, N. 2002, The Astronomical Journal, 124, 2693

Fruchter, A., Sosey, M., Hack, W., Dressel, L., Koekemoer, A. M., Mack, J., Mutchler, M., & Pirzkal, N. 2009, The MultiDrizzle Handbook, version 3.0 (Baltimore: STScI)

Gallagher, J. S., Hunter, D. A., & Bushouse, H. 1989, The Astronomical Journal, 97, 700

Gallagher, S. C., Charlton, J. C., Hunsberger, S. D., Zaritsky, D., & Whitmore, B. C. 2001, The Astronomical Journal, 122, 163

Gallagher, S. C., et al. 2010, The Astronomical Journal, 139, 545

Gieles, M., Lamers, H. J. G. L. M., & Portegies Zwart, S. F. 2007, The Astrophysical Journal, 668, 268

Gieles, M., Larsen, S. S., Bastian, N., & Stein, I. T. 2006a, Astronomy and Astrophysics, 450, 129

Gieles, M., Larsen, S. S., Scheepmaker, R. A., Bastian, N., Haas, M. R., & Lamers, H. J. G. L. M. 2006b, Astronomy and Astrophysics, 446, L9

Gies, D. R. 1987, The Astrophysical Journal Supplement Series, 64, 545

Goodwin, S. P., & Bastian, N. 2006, Monthly Notices of the Royal Astronomical Society, 373, 752

Goudfrooij, P., Strader, J., Brenneman, L., Kissler-Patig, M., Minniti, D., & Edwin Huizinga, J. 2003, Monthly Notice of the Royal Astronomical Society, 343, 665

Gunn, J. E., & Gott, J. R. 1972, The Astrophysical Journal, 176, 1

Harris, W. E. 1991, Annual Review of Astronomy and Astrophysics, 29, 543

Harris, W. E. 1996, The Astronomical Journal, 112, 1487

Harris, W. E. 2001, in Saas-Fee Advanced Course 28: Star Clusters, ed. L. Labhardt & B. Binggeli, 223

Harris, W. E. 2009, The Astrophysical Journal, 699, 254

Harris, W. E., Harris, G. L. H., & Alessi, M. 2013, The Astrophysical Journal, 772, 82

Harris, W. E., Whitmore, B. C., Karakla, D., OkoÅ, W., Baum, W. A., Hanes, D. A., & Kavelaars, J. J. 2006, The Astrophysical Journal, 636, 90

Herschel, W. 1789, Philosophical Transactions of the Royal Society of London, 79, 212

Hickson, P. 1982, The Astrophysical Journal, 255, 382

Hickson, P. 1997, Annual Review of Astronomy and Astrophysics, 35, 357

Hickson, P., Kindl, E., & Auman, J. 1989, The Astrophysical Journal Supplement Series, 70, 687

Hickson, P., Mendes de Oliveira, C., Huchra, J. P., & Palumbo, G. 1992, The Astrophysical Journal, 399, 353

Hunter, D. A., Elmegreen, B. G., Dupuy, T. J., & Mortonson, M. 2003, The Astronomical Journal, 126, 1836

Johnson, K. E., Hibbard, J. E., Gallagher, S. C., Charlton, J. C., Hornschemeier, A. E., Jarrett, T. H., & Reines, A. E. 2007, The Astronomical Journal, 134, 1522

Jones, L. R., Ponman, T. J., Horton, A., Babul, A., Ebeling, H., & Burke, D. J. 2003, Monthly Notice of the Royal Astronomical Society, 343, 627

Kennicutt, R. C. 1992, The Astrophysical Journal, 388, 310

Kennicutt, R. C. 1998, Annual Review of Astronomy and Astrophysics, 36, 189

Kennicutt, Jr., R. C., Roettiger, K. A., Keel, W. C., van der Hulst, J. M., & Hummel, E. 1987, The Astronomical Journal, 93, 1011

Kharchenko, N. V., Piskunov, A. E., Röser, S., Schilbach, E., & Scholz, R.-D. 2005, Astronomy and Astrophysics, 438, 1163

Klessen, R. S., Krumholz, M. R., & Heitsch, F. 2011, Advanced Science Letters, 4, 28

Konstantopoulos, I. S., et al. 2010, The Astrophysical Journal, 723, 197

Konstantopoulos, I. S., et al. 2012, The Astrophysical Journal, 745, 30

Konstantopoulos, I. S., et al. 2013, The Astrophysical Journal, 770, 114

Konstantopoulos, I. S., et al. 2014, The Astrophysical Journal, 784, 1

Kroupa, P. 2001, Monthly Notices of the Royal Astronomical Society, 322, 231

Kundu, A., & Whitmore, B. C. 2001, The Astronomical Journal, 122, 1251

Lada, C. J., & Lada, E. A. 2003, Annual Review of Astronomy and Astrophysics, 41, 57

Larsen, S. S. 2002, The Astronomical Journal, 124, 1393

Larsen, S. S. 2004, Astronomy and Astrophysics, 416, 537

Larsen, S. S. 2009, Astronomy and Astrophysics, 494, 539

Larsen, S. S. 2010, Philosophical transactions. Series A, Mathematical, physical, and engineering sciences, 368, 867

Larson, R. B. 1996, Proceedings of the 11th IAP Astrophysics Meeting

Leitherer, C., et al. 1999, The Astrophysical Journal Supplement Series, 123, 3

Li, Z., & Han, Z. 2008, The Astrophysical Journal, 685, 225

Lisenfeld, U., Braine, J., Duc, P.-A., Leon, S., Charmandaris, V., & Brinks, E. 2002, Astronomy and Astrophysics, 394, 823

Mamon, G. 1996, Third Paris Cosmology Colloquium within the framework of the International School of Astrophysics 'Daniel Chalonge'

Mamon, G. A. 1986, The Astrophysical Journal, 307, 426

Mamon, G. A. 1987, The Astrophysical Journal, 321, 622

Mamon, G. A. 2000, Dynamics of Galaxies: from the Early Universe to the Present, 197

Mamon, G. A. 2007, Groups of Galaxies in the Nearby Universe, ESO ASTROPHYSICS SYMPOSIA (Berlin, Heidelberg: Springer Berlin Heidelberg)

Marigo, P., Girardi, L., Bressan, A., Groenewegen, M. A. T., Silva, L., & Granato, G. L. 2008, Astronomy and Astrophysics, 482, 883

Marín-Franch, A., et al. 2009, The Astrophysical Journal, 694, 1498

Martín-Hernández, N. L., Vermeij, R., Tielens, A. G. G. M., van der Hulst, J. M., & Peeters, E. 2002, Astronomy and Astrophysics, 389, 286

McConnachie, A. W., Ellison, S. L., & Patton, D. R. 2008, Monthly Notice of the Royal Astronomical Society, 387, 1281

Mendes de Oliveira, C. L., Temporin, S., Cypriano, E. S., Plana, H., Amram, P., Sodré, Jr., L., & Balkowski, C. 2006, The Astronomical Journal, 132, 570

Meurer, G. R., et al. 2009, The Astrophysical Journal, 695, 765

Mihos, J. C., & Hernquist, L. 1996, The Astrophysical Journal, 464, 641

Misgeld, I., & Hilker, M. 2011, Monthly Notice of the Royal Astronomical Society, 414, 3699

Moles, M., Marquez, I., & Sulentic, J. W. 1998, Astronomy & Astrophysics, 334, 8

Moles, M., Sulentic, J. W., & Márquez, I. 1997, The Astrophysical Journal, 485, L69

Moore, B., Katz, N., & Lake, G. 1996, The Astrophysical Journal, 457, 455

Mould, J. R., et al. 2000, The Astrophysical Journal, 529, 786

Mulchaey, J. S., & Zabludoff, A. I. 1999, The Astrophysical Journal, 514, 133

Muratov, A. L., & Gnedin, O. Y. 2010, The Astrophysical Journal, 718, 1266

Murdin, P. 2001, Encyclopedia of astronomy and astrophysics (Bristol: Nature Publishing)

Neff, S. G., & Ulvestad, J. S. 2000, The Astronomical Journal, 120, 670

Nishiura, S., Shimada, M., Ohyama, Y., Murayama, T., & Taniguchi, Y. 2000, The Astronomical Journal, 120, 1691

Oleak, H., Stoll, D., Tiersch, H., & MacGillivray, H. T. 1995, The Astronomical Journal, 109, 1485

Ostriker, E. C. 2006, Proceedings of the International Astronomical Union, 2, 70

Ostriker, J. P., Spitzer, L., & Chevalier, R. A. 1972, The Astrophysical Journal, 176, L51

O'Sullivan, E., Giacintucci, S., Vrtilek, J. M., Raychaudhury, S., & David, L. P. 2009, The Astrophysical Journal, 701, 1560

Padmanabhan, T. 2002, Theoretical astrophysics: Galaxies and cosmology (Cambridge: Cambridge University Press), 638

Peng, E. W., et al. 2006, The Astrophysical Journal, 639, 95

Peterson, R. C., Rees, R. F., & Cudworth, K. M. 1995, The Astrophysical Journal, 443, 124

Piotto, G., et al. 2007, The Astrophysical Journal, 661, L53

Pompei, E., & Iovino, A. 2010, Galaxies in Isolation: Exploring Nature Versus Nurture

Portegies Zwart, S. F., McMillan, S. L., & Gieles, M. 2010, Annual Review of Astronomy and Astrophysics, 48, 431

Price, D. J., & Bate, M. R. 2008, Monthly Notices of the Royal Astronomical Society, 385, 1820

Purcell, C. W., Bullock, J. S., Tollerud, E. J., Rocha, M., & Chakrabarti, S. 2011, Nature, 477, 301

Ranalli, P., Comastri, A., & Setti, G. 2003, Astronomy and Astrophysics, 399, 39

Rejkuba, M., Greggio, L., Harris, W. E., Harris, G. L. H., & Peng, E. W. 2005, The Astrophysical Journal, 631, 262

Renaud, F., Appleton, P. N., & Xu, C. K. 2010, The Astrophysical Journal, 724, 80

Rhode, K. L., Zepf, S. E., Kundu, A., & Larner, A. N. 2007, The Astronomical Journal, 134, 1403

Robin, A. C., Reylé, C., Derrière, S., & Picaud, S. 2003, Astronomy and Astrophysics, 409, 523

Rosa-González, D., Terlevich, E., & Terlevich, R. 2002, Monthly Notices of the Royal Astronomical Society, 332, 283

Rose, J. A. 1977, The Astrophysical Journal, 211, 311

Rubin, V. C., & Ford, W. K. 1970, The Astrophysical Journal, 159, 379

Rudick, C. S., Mihos, J. C., & McBride, C. 2006, The Astrophysical Journal, 648, 936

Ryon, J. E., et al. 2014, The Astronomical Journal, 148, 33

Sabater, J., Verdes-Montenegro, L., Leon, S., Best, P., & Sulentic, J. 2012, Astronomy and Astrophysics, 545, A15

Salpeter, E. E. 1955, The Astrophysical Journal, 121, 161

Sandage, A. R., & Miller, W. C. 1964, Science (New York, N.Y.), 144, 405

Sanders, D. B., Soifer, B. T., Elias, J. H., Madore, B. F., Matthews, K., Neugebauer, G., & Scoville, N. Z. 1988, The Astrophysical Journal, 325, 74

Sastry, K. S., Singh, T. M., & Ramamani, N. 1988, Astrophysics and Space Science, 150, 1

Scheepmaker, R. A., Haas, M. R., Gieles, M., Bastian, N., Larsen, S. S., & Lamers, H. J. G. L. M. 2007, Astronomy and Astrophysics, 469, 925

Schlafly, E. F., & Finkbeiner, D. P. 2011, The Astrophysical Journal, 737, 103

Schlegel, D. J., Finkbeiner, D. P., & Davis, M. 1998, The Astrophysical Journal, 500, 525

Schweizer, F., et al. 2008, The Astronomical Journal, 136, 1482

Selman, F. J., & Melnick, J. 2008, The Astrophysical Journal, 689, 816

Shakhbazyan, R. K. 1973, Astrofizika, 9, 495

Shakhbazyan, R. K., & Petrosyan, M. B. 1974, Astrofizika

Shapley, H. 1916, Contributions of the Mount Wilson Solar Observatory

Shostak, G. S., Allen, R. J., & Sullivan III, W. T. 1984, Astronomy and Astrophysics, 139, 15

Sirianni, M., et al. 2005, Publications of the Astronomical Society of the Pacific, 117, 1049

Spitzer, L. 1987, Dynamical evolution of globular clusters (Princeton, NJ: Princeton University Press), 191

Springel, V., Di Matteo, T., & Hernquist, L. 2005, Monthly Notice of the Royal Astronomical Society, 361, 776

Stetson, P. B. 1987, Publications of the Astronomical Society of the Pacific, 99, 191

Sulentic, J. W. 1983, The Astrophysical Journal, 270, 417

Sulentic, J. W., Rosado, M., Dultzin-Hacyan, D., Verdes-Montenegro, L., Trinchieri, G., Xu, C. K., & Pietsch, W. 2001, The Astronomical Journal, 122, 2993

Tadross, A. L., Osman, A. I., Marie, M. A., & Hassan, S. M. 2003, eprint arXiv:astro-ph/0308156

Tago, E., Einasto, J., Saar, E., Tempel, E., Einasto, M., Vennik, J., & Müller, V. 2008, Astronomy and Astrophysics, 479, 927

Temporin, S., Staveley-Smith, L., & Kerber, F. 2005, Monthly Notice of the Royal Astronomical Society, 356, 343

Teyssier, R., Chapon, D., & Bournaud, F. 2010, The Astrophysical Journal, 720, L149

The, L. S., & White, S. D. M. 1986, The Astronomical Journal, 92, 1248

Toomre, A., & Toomre, J. 1972, The Astrophysical Journal, 178, 623

Trancho, G., Konstantopoulos, I. S., Bastian, N., Fedotov, K., Gallagher, S., Mullan, B., & Charlton, J. C. 2012, The Astrophysical Journal, 748, 102

Tzanavaris, P., et al. 2010, The Astrophysical Journal, 716, 556

Vacca, W. D., & Conti, P. S. 1992, The Astrophysical Journal, 401, 543

Van Dokkum, P. G., & Conroy, C. 2010, Nature, 468, 940

VanDalfsen, M. L., & Harris, W. E. 2004, The Astronomical Journal, 127, 368

Verdes-Montenegro, L., Yun, M. S., Williams, B. A., Huchtmeier, W. K., Del Olmo, A., & Perea, J. 2001, Astronomy and Astrophysics, 377, 812

Walterbos, R. A. M., & Greenawalt, B. 1996, The Astrophysical Journal, 460, 696

White, P. M., Bothun, G., Guerrero, M. A., West, M. J., & Barkhouse, W. A. 2003, The Astrophysical Journal, 585, 739

Whitmore, B. C., Chandar, R., Bowers, A. S., Larsen, S., Lindsay, K., Ansari, A., & Evans, J. 2014, The Astronomical Journal, 147, 78

Whitmore, B. C., Chandar, R., & Fall, S. M. 2007, The Astronomical Journal, 133, 1067

Whitmore, B. C., Miller, B. W., Schweizer, F., & Fall, S. M. 1997, The Astronomical Journal, 114, 1797

Whitmore, B. C., & Zhang, Q. 2002, The Astronomical Journal, 124, 1418

Whitmore, B. C., Zhang, Q., Leitherer, C., Fall, S. M., Schweizer, F., & Miller, B. W. 1999, The Astronomical Journal, 118, 1551

Whitmore, B. C., et al. 2010, The Astronomical Journal, 140, 75

Whitmore, B. C., et al. 2014, eprint arXiv:astro-ph/1410.4473, 39

Wielen, R. 1971, Astronomy and Astrophysics, 13

Williams, B. A., Yun, M. S., & Verdes-Montenegro, L. 2002, The Astronomical Journal, 123, 2417

Williams, J. P., & McKee, C. F. 1997, The Astrophysical Journal, 476, 166

Wilson, C. D., Harris, W. E., Longden, R., & Scoville, N. Z. 2006, The Astrophysical Journal, 641, 763

Xu, C., Gao, Y., Lu, N., & Condon, J. J. 2001, in Astronomical Society of the Pacific Conference Series, Vol. 240, Gas and Galaxy Evolution, ed. J. E. Hibbard, M. Rupen, & J. H. van Gorkom, 594

Xu, C. K., Lu, N., Condon, J. J., Dopita, M., & Tuffs, R. J. 2003, The Astrophysical Journal, 595, 665

Xu, C. K., Sulentic, J. W., & Tuffs, R. 1999, The Astrophysical Journal, 512, 178

Xu, C. K., et al. 2005, The Astrophysical Journal, 619, L95

York, D. G., et al. 2005, in IAU Colloq. 199: Probing Galaxies through Quasar Absorption Lines, ed. P. Williams, C.-G. Shu, & B. Menard, 58–64

Zhang, Q., & Fall, S. M. 1999, The Astrophysical Journal, 527, L81

Zinn, R. 1985, The Astrophysical Journal, 293, 424

Zwicky, F. 1933, Helvetica Physica Acta, 6, 110

Appendix A

Possible Supernova Detection

The observations that were used for Chapter 2 have been carried out with a two year interval (2009 and 2011). A new object, possibly a supernova, was detected in our new observations from October 2011. The 4 pixel aperture photometry gave the magnitude values of m_{336} = 21.218 ± 0.003 mag and m_{547} = 22.544 ± 0.005 mag. Figure A1 shows cut-outs from all filters with the same region in the first epoch of observations (B_{438}, V_{606}, and I_{814} filters) and in new observations (U_{336} and V_{547} filters). The coordinates of the object are RA(2000) = $22^h\,35^m\,58\overset{s}{.}38$, Dec(2000) = $+33^d\,58^m\,51\overset{s}{.}38$, and it is located approximately $5\overset{''}{.}4$ from the center (RA(2000) = $22^h\,35^m\,58\overset{s}{.}7$, Dec(2000) = $+33^d\,58^m\,55\overset{s}{.}0$) of star-burst region SQ- A (Xu et al., 1999).

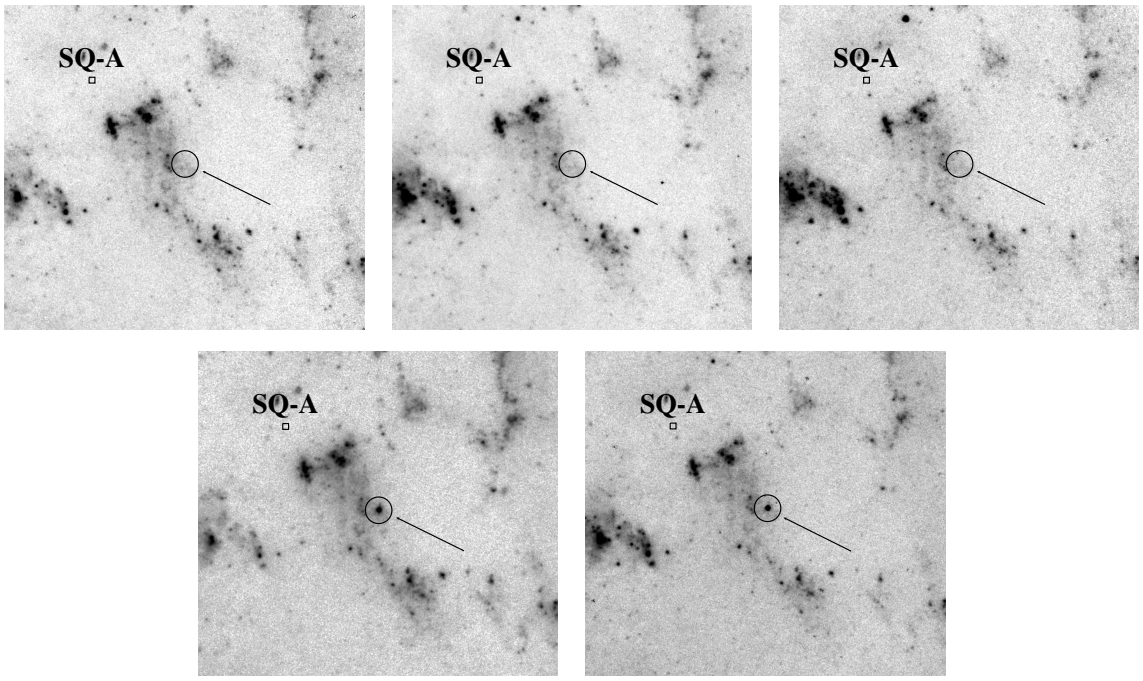

Figure A1: Possible SN detection. 2009 epoch observations on the top row (left to right): B_{438}, V_{606}, and I_{814} filters. 2011 epoch observations on the bottom row (left to right): U_{336} and V_{547} filters. The center of SQ-A star-burst region (Xu et al. 1999) is denoted by black square.

Curriculum Vitae

EDUCATION

The University of Western Ontario, London, ON — 2010 – 2014
Ph. D., Astronomy, expected December 2014
Star Cluster Populations in Compact Groups of Galaxies

The University of Western Ontario, London, ON — 2008 – 2010
M. Sc., Astronomy
Star Clusters as Tracers of Interactions in Stephan's Quintet

The University of Victoria, Victoria, BC — 2003 – 2008
B. Sc., Co-op Combined Honours in Physics and in Astronomy

RESEARCH EXPERIENCE

Graduate Research — 2008 – 2014
The University of Western Ontario, London, ON
Supervisor: Dr. Sarah C. Gallagher
Galaxy Interactions, Compact Groups, Star Clusters

Co-op Research Assistant — Fall 2007
The University of Victoria, Victoria, BC — Summer 2008
Supervisor: Dr. Kim Venn
Behaviour of Optical Spectral Lines of RGB Stars in M31

Co-op Research Assistant — Summer 2007
Dominion Radio Astrophysical Observatory, Penticton, BC
Supervisor: Dr. Roland Kothes
Multi-Frequency Radio Studies of Four Supernova Remnants

Co-op Research Assistant — Summer 2005
Herzberg Institute of Astrophysics, Victoria, BC
Supervisor: Dr. Eric Peng
HST Photometry of RGB Stars in a Tidal Stream of NGC 5128

Co-op Research Assistant — Winter 2005
Dominion Radio Astrophysical Observatory, Penticton, BC
Supervisor: Dr. Roland Kothes
Fundamental Properties of Supernova Remnants in the Canadian Galactic Plane Survey

TEACHING EXPERIENCE

Teaching Assistant 2008 – 2014
The University of Western Ontario, London, ON
1st year Physics lab instructor
1st year Astronomy project coordinator
1st & 2nd year Physics and Astronomy classes
Guest Lecturer

OBSERVING EXPERIENCE

Near-infrared imaging with WIRCam on the CFHT, Mauna Kea, HI	2009
CO(2-1) observations on the Caltech Submillimeter Telescope, Mauna Kea, HI	2011
Phase 2 for *HST* Wide Field Camera 3 proposal	2011
Hα imaging on NOAO 4-meter Telescope, Kitt Peak, AR	2013

ACCEPTED CO-I PROPOSALS

18 orbits, *Hubble Space Telescope*, COS, *"COS Spectroscopy Of The Stephan's Quintet Giant Shock"*, PI: P. Guillard, 2013

8 hours, Gemini South, GMOS, *"What Are Tidal Tails Made Of?"*, PI: I. S. Konstantopoulos, 2013A

3.5 nights, Kitt Peak National Observatory, Mayall 4-meter, MOSAIC, *"Mapping Star Formation in Dense Environments: Hα Imaging of Compact Galaxy Groups"*, PI: T. D. Desjardins, 2012B

20.4 hours, Canada France Hawaii Telescope, MegaCam, *"Tracing Interaction Histories In Compact Galaxy Groups"*, PI: T. D. Desjardins, 2012B

8 orbits, *Hubble Space Telescope*, WFC3, *"Precision Age-Dating of Star Clusters in Stephan's Quintet"*, PI: S. C. Gallagher, 2010

8 hours, Canada France Hawaii Telescope, WIRCam, *"Constructing K-band Galaxy Luminosity Functions For 13 Hickson Compact Groups"*, PI: S. C. Gallagher, 2009B

SCHOLARSHIPS

Queen Elizabeth II Scholarship, 2013–2014

Queen Elizabeth II Scholarship, 2011–2012

PROFESSIONAL MEMBERSHIP

Member of Canadian Astronomical Society (2008 – present)

ORAL PRESENTATIONS

"Star Clusters As Tracers Of Interactions In Stephan's Quintet", Canadian Astronomical Society Conference, London, ON, 2011

"HST Photometry Of Star Clusters In HCGs", HCG Team Meeting, State College, PA, 2010

"Galaxy Evolution In Compact Groups: HCG 7 As A Dry Merger Precursor" Herzberg Institute of Astrophysics, Victoria, BC, 2010

"Fundamental Properties Of SNRs In The CGPS", Canadian Undergraduate Physics Conference, London, ON, 2005

POSTERS

Fedotov, K., Gallagher, S. C., Chandar, R., Bastian, N., Konstantopoulos, I. S., Appleton, P., & Desjardins, T. D., *"Shockingly Few Massive Young Star Clusters In Stephans Quintet"*, Massive Young Star Clusters Near and Far: From the Milky Way to Re-ionization Conference, Pueblo, México, 2013

Fedotov, K., Gallagher, S. C., Chandar, R., Bastian, N., Konstantopoulos, I. S., & Appleton, P., *"Star Formation In The Strong Shock Of Stephans Quintet"*, Canadian Astronomical Society Conference, Vancouver, BC, 2013

Maybhate, A., **Fedotov, K.**, Konstantopoulos, I. S., Charlton, J. C., Zabludoff, A., Chandar, R., Durrell, P., Gallagher, S. C., & Tzanavaris, P., *"The Star Cluster Populations In The Evolutionary Sequence Of Hickson Compact Groups"*, American Astronomical Society Meeting #217, Seattle, WA, 2011

Fedotov, K., Gallagher, S. C., Chandar, R., Bastian, N., Konstantopoulos, I. S., Trancho, G., Charlton, J. C., & Whitmore, B., *"Star Cluster Populations As Tracers Of The History Of Interactions In Stephan's Quintet"*, Stellar population in the Cosmological Context Symposium, Baltimore, MD, 2010

Lee, K., Konstantopoulos, I. S., Charlton, J. C., Gallagher, S. C., **Fedotov, K.**, HCG Team, *"Star Formation In Hickson Compact Group 7: U-band Studies Of A Future Dry Merger"*, American Astronomical Society Meeting #215, Washington, DC, 2010

Konstantopoulos, I. S., Trancho, G., Bastian, N., Gallagher, S., C., **Fedotov, K.**, Charlton, J. C., HCG Team, *"Star Formation And Galaxy Evolution In A Compact Group Environment: A Multi-wavelength Study Of Stephan's Quintet"*, American Astronomical Society, AAS Meeting #215, Washington, DC, 2010

Kothes, R., Safi-Harb, S., Matheson, H., & **Fedotov, K.**, *"A Multi-wavelength Study Of The Mysterious PWN G63.7+1.1"*, 38th COSPAR Scientific Assembly, Germany, 2010

Fedotov, K., Gallagher, S. C., Chandar, R., Charlton, J. C., Durrell, P. R., Elmegreen, D. M., English, J., & Gronwall, C., *"Star Clusters In The Galaxies of Hickson Compact Group 7"*, Canadian Astronomical Society Conference, Toronto, ON, 2009

Fedotov, K., Kothes, R., *"MultiFrequency Radio Studies Of Supernova Remnants To Determine Their Spectral And Magnetic Field Characteristics"*, Summer School on the ISM, Naramata, BC, 2007 and Canadian Undergraduate Physics Conference, Vancouver, BC, 2007

Fedotov, K., Kothes, R., Foster, T. J., Uyaniker B., *"Fundamental Properties Of SNRs In The CGPS"*, Canadian Undergraduate Physics Conference, London, ON, 2005

REFEREED JOURNAL PUBLICATIONS

Konstantopoulos, I. S., Appleton, P., Guillard, P., Trancho, G., Cluver M., Bastian, N., Charlton, J. C., **Fedotov, K.**, Gallagher, S. C., Smith L., & Struck C., *"Shocks and Star Formation in Stephan's Quintet. I. Gemini Spectroscopy of Hα-bright knots"*, 2014. Astrophysical Journal, 784, 1, article id. 1, 15 pp.

Tzanavaris, P., Gallagher, S. C., Hornschemeier, A. E., **Fedotov, K.**, Eracleous, M., Brandt, W. N., Desjardins, T. D., Charlton, J. C., & Gronwall, C., *"A Chandra-Swift view of point sources in Hickson Compact Groups: High AGN fraction but a dearth of strong AGNs"*, 2014. Astrophysical Journal Supplement, 212, 9.

Konstantopoulos, I. S., Maybhate, A., Charlton, J. C., **Fedotov, K.**, Durrell, P. R., Mulchaey, J. S., English, J., Desjardins, T. D., Gallagher, S. C., Walker, L. M., Johnson, K. E., Tzanavaris, P., Gronwall, C., *"Stellar Populations in Compact Galaxy Groups: a Multi-Wavelength Study of HCGs 16, 22, and 42, their Star Clusters and Dwarf Galaxies"*, 2013. Astrophysical Journal, 770, 2, article id. 114, 18 pp.

Konstantopoulos I. S., Gallagher, S. C., **Fedotov, K.**, Durrell, P. R., Tzanavaris, P., Hill, A. R., Zabludoff, A. E., Maier, M. L., Elmegreen, D. M., Charlton, J. C., Johnson, K. E., Brandt, W. N., Walker, L. M., Eracleous, M., Maybhate, A., Gronwall, C., English, J., Hornschemeier, A. E., & Mulchaey, J. S., *"The Merger History, AGN and Dwarf Galaxies of Hickson Compact Group 59"*, 2012. Astrophysical Journal, Volume 745, Issue 1, article id. 30, 22 pp.

Trancho, G., Konstantopoulos, I. S., Bastian, N., **Fedotov, K.**, Gallagher, S. C., Mullan, B., & Charlton, J. C., *"Gemini Spectroscopic Survey of Young Star Clusters in Merging/Interacting Galaxies. IV. Stephan's Quintet"*, 2012. Astrophysical Journal, Volume 748, Issue 2, article id. 102, 14 pp.

Fedotov, K., Gallagher, S. C., Konstantopoulos, I. S., Chandar, R., Bastian, N., Charlton, J. C., Whitmore, B., & Trancho, G., *"Star Clusters as Tracers of Interactions in Stephan's Quintet (HCG 92)"*, 2011. Astronomical Journal, 142, 2, 42

Konstantopoulos, I. S., Gallagher, S. C., **Fedotov, K.**, Durrell, P. R., Elmegreen, D. M., Charlton, J. C., Tzanavaris, P., Chandar, R., Johnson, K. E., Maybhate, A., Gronwall, C., Zabludoff, A. E., Hornschemeier, A. E., English, J., & Whitmore, B., *"Galaxy evolution in compact groups: HCG 7 as a dry merger precursor"*, 2010, Astrophysical Journal, 723: 197-217

Kothes, R., **Fedotov, K.**, Foster, T. J., & Uyaniker, B., *"A catalogue of Galactic supernova remnants from the Canadian Galactic plane survey. I. Flux densities, spectra, and polarization characteristics"*, 2006, Astronomy & Astrophysics, 457, 1081

OTHER PUBLICATIONS

Konstantopoulos, I. S., **Fedotov, K.**, Gallagher, S. C., Maybhate, A., Durrell, P. R., Charlton, J. C., *"The Star Cluster Populations of Compact Galaxy Groups"*, Stellar Clusters & Associations: A RIA Workshop on Gaia. Proceedings. Granada, Spain, 2011